

CHALMERS



Transient Overvoltages in Cable Systems

Part 1 – Theoretical analysis of large cable systems

Master of Science Thesis

DANIEL MIREANU

MSc in Electric Power Engineering 60p (Degree of Civilingenjörsexamen, eq. 180p)

Department of Electric Power Engineering

Division of Energy and Environment

CHALMERS UNIVERSITY OF TECHNOLOGY

Göteborg, Sweden, 2007



Abstract

This thesis provides an analysis of transient overvoltages and their propagation in cable systems. This investigation is performed through the use of two systems: an industrial steel mill and a wind farm. Cables and vacuum circuit breakers, two essential components in any medium voltage cable system, are discussed in detail and modelled in PSCAD. The two systems are then simulated and, where available, the results are compared to measured data for validity.

The purpose of the wind farm section is to identify and analyze cases of interest, including energization, opening, and earth faulting of one of the feeders. The impact on the system is analyzed as well as ways to mitigate the negative effects of these transients. The impact of different wind farm topologies is also analyzed, and a discussion on protection against the negative effects of transients is ensued for both systems. One interesting finding was that common farm topologies used today (i.e. ring topology) may not necessarily be the best in terms of providing harmless transients.

Keywords: cables, vacuum circuit breakers, steel mill, industrial systems, wind farm, wind park, transients, overvoltages.



Preface

This thesis has definitely been one of the hardest and most elaborate projects I have ever been involved in. Delving so deep into a topic has never really been my strong suit, but I did it and I am glad because I learned a lot.

Coming to Sweden was not the easiest thing I have done in my life. The reason as to why it has worked out so well is because of the quality of people in Sweden. Especially then, I would like to thank Sweden for welcoming me and giving me a home, and for all the Swedes and international people I have met along the way that have made the transition easy and comfortable.

For that, I would like to especially thank the “young uns” at ABB that have been here throughout my time: Maialen, Johan, Mila, Oliver, Mikael, Michele and Mirko. Of course, thanks to everyone else at ABB for the working environment (i.e. “fika”) and for accepting the thesis workers as a party of the company.

Most importantly however are my bosses. Thanks to Ambra Sannino and Lars Liljestr nd for supporting my thesis work and giving me guidance along the way. It has been a tough 6 months, but I have something to show for it. Finally, thank you to Torbj rn Thiringer at Chalmers for being my examiner but most importantly for being a top-notch professor.

I finally have my Masters degree after a long 18 month journey. It’s been worth it, and I am happy to call Sweden my home now for the next few years as I start the next chapter in my life: train design with Bombardier.



TABLE OF CONTENTS

| | | |
|----------|---|-----------|
| 1 | INTRODUCTION | 6 |
| 1.1 | PURPOSE..... | 7 |
| 1.2 | DEFINITIONS | 7 |
| 2 | CABLE MODELLING IN PSCAD/EMTDC | 8 |
| 2.1 | INTRODUCTION | 8 |
| 2.2 | SELECTING THE CABLE PARAMETERS FOR STEADY STATE | 8 |
| 2.2.1 | Matching the cable capacitance | 10 |
| 2.2.2 | Skin effect | 11 |
| 2.2.3 | Matching the DC resistance of the cable | 11 |
| 2.2.4 | Matching the inductance of the cable | 12 |
| 2.2.5 | Determining the remaining parameters | 12 |
| 2.3 | COMPARISON OF RESULTS | 13 |
| 2.4 | HIGH FREQUENCY EFFECTS..... | 15 |
| 2.4.1 | Description of the test circuit..... | 15 |
| 2.4.2 | Coupling coefficients..... | 15 |
| 2.5 | CONCLUSION | 17 |
| 3 | THE VCB AND MODELLING IN PSCAD/EMTDC | 18 |
| 3.1 | INTRODUCTION | 18 |
| 3.2 | THE PHYSICALLY COMPLETE MODEL | 18 |
| 3.2.1 | The main phenomena | 18 |
| 3.2.2 | Feasibility of accurate simulation | 20 |
| 3.3 | DESCRIPTION OF THE MAIN PHENOMENA | 20 |
| 3.3.1 | Vacuum gap breakdown | 20 |
| 3.3.2 | High frequency arc interruption..... | 23 |
| 3.3.3 | Current chopping and importance of it | 24 |
| 3.4 | THE TEST CIRCUIT | 24 |
| 3.5 | THE PSCAD/EMTDC MODEL | 27 |
| 3.5.1 | Introduction | 27 |
| 3.5.2 | Results of simulation..... | 27 |
| 3.5.3 | Problems with the model | 33 |
| 3.6 | OPERATION OF VCB WITH FULL CABLE MODEL (REFLECTIONS)..... | 34 |
| 3.7 | OPERATION OF VCB IN A 3-PHASE SYSTEM..... | 38 |
| 3.8 | CONCLUSION | 41 |
| 4 | INDUSTRIAL SYSTEM | 42 |
| 4.1 | INTRODUCTION | 42 |
| 4.2 | DESCRIPTION AND ANALYSIS OF THE INDUSTRIAL SYSTEM CIRCUIT | 42 |
| 4.2.1 | Introduction | 42 |
| 4.2.2 | Modelling the system | 44 |
| 4.2.3 | The purpose of RC protection..... | 44 |
| 4.2.4 | Frequency response | 49 |
| 4.2.5 | Coupling between phases | 52 |
| 4.3 | RESULTS AND COMPARISON..... | 55 |
| 4.3.1 | Purpose..... | 55 |
| 4.3.2 | Normal opening operation | 55 |
| 4.3.3 | Opening operation with multiple re-ignitions..... | 58 |
| 4.4 | CONCLUSION | 60 |
| 5 | WIND FARM | 61 |
| 5.1 | INTRODUCTION | 61 |
| 5.2 | THE WIND FARM CIRCUIT | 61 |
| 5.3 | OPENING A FEEDER | 63 |
| 5.3.1 | Current chopping and necessity of simulation..... | 63 |
| 5.3.2 | Opening one of the feeders | 65 |



| | | |
|----------|--|-----------|
| 5.4 | ENERGIZATION OF THE WIND FARM | 67 |
| 5.4.1 | Energization of the 1 st feeder..... | 67 |
| 5.4.2 | Energization of the 5 th feeder..... | 70 |
| 5.4.3 | Energization of the 5 th feeder under different topologies..... | 73 |
| 5.5 | SLG FAULT AND CLEARING FAULT AT THE FEEDER | 77 |
| 5.5.1 | Application of the SLG fault | 78 |
| 5.5.2 | Clearing of the fault with the feeder breaker..... | 80 |
| 5.6 | DLG FAULT AND CLEARING FAULT AT THE FEEDER..... | 82 |
| 5.7 | FAULT CLEARING WITH A FUSE..... | 83 |
| 5.7.1 | Modelling the fuse..... | 83 |
| 5.7.2 | Clearing an actual fault | 84 |
| 5.8 | WIND FARM PROTECTION | 90 |
| 5.8.1 | Passive protection schemes | 90 |
| 5.8.2 | Active protection schemes..... | 92 |
| 5.9 | CONCLUSION | 92 |
| 6 | CONCLUSIONS..... | 94 |
| 7 | FUTURE WORK | 95 |
| 8 | REFERENCES..... | 96 |



1 INTRODUCTION

Generally speaking, designers of power systems are mainly concerned with steady-state frequency design, or at least up to several orders of harmonics as required by standards. The high frequencies that will be discussed in this work deal with very small time scales, so small in fact that the interest is in the cable reflections. Frequency brackets can be defined loosely as follows in Fig 1. The brackets simply imply a relative ordering, whereby transient oscillations due to system components occur on the lower frequency spectrum (TRV oscillations), while cable reflections occur relatively at very high frequencies. In this report the goal is to look at and analyze re-strikes, breakdowns, and cable reflections. TRV oscillations are ignored only because these are well known and easily handled by the system designer.

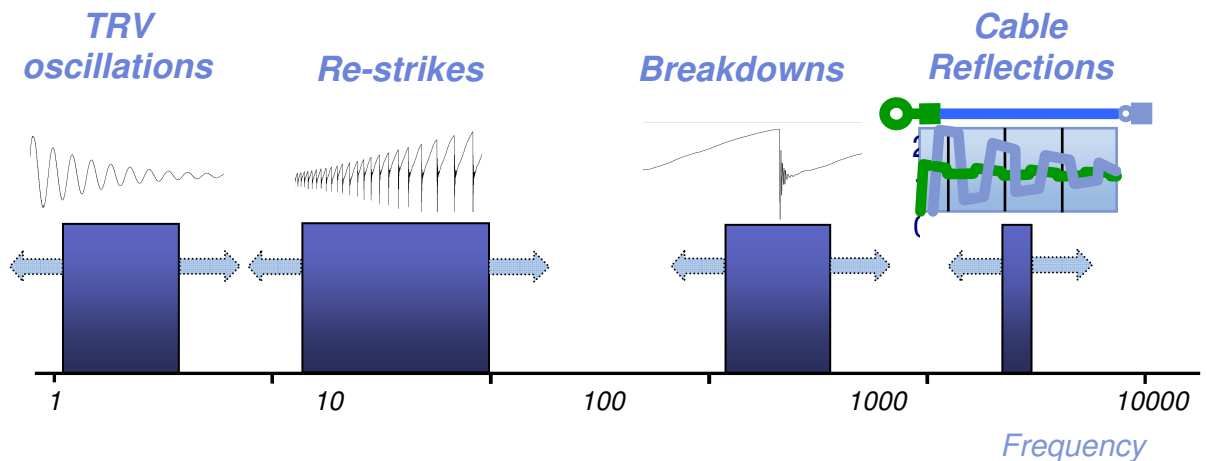


Fig 1: Organizational diagram of the report

For this purpose, accurate modelling of the cables in a system and the vacuum circuit breakers will be required. These two models, once complete, will be used to simulate an existing industrial system from where there exists a substantial amount of experimental data for comparison. Finally, a wind farm will also be simulated and due to the similarities between industrial systems and wind farms, conclusions will be drawn. Fig 2 below shows the organization and affiliations used in this report. The wind farm will be discussed in a fair amount of detail, but all the other 3 major components of the report (Cables, Vacuum CB, and Industrial System) are necessary stepping stones to produce valid and accurate results.

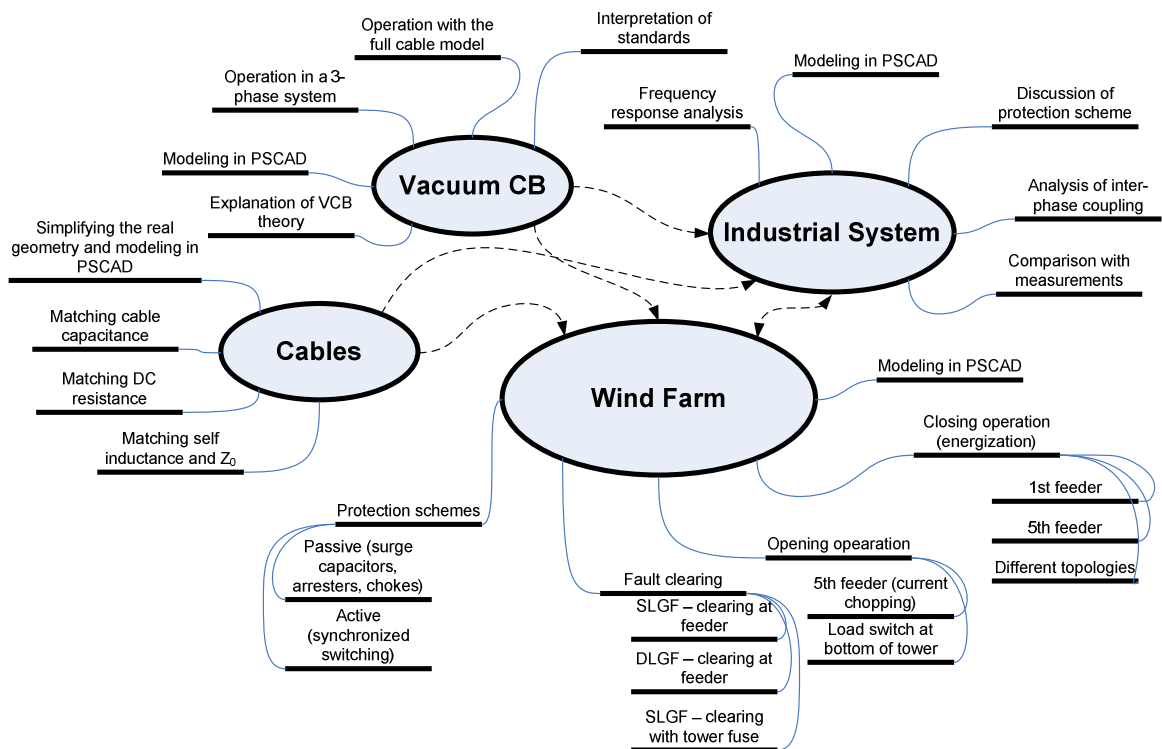


Fig 2: Organizational diagram of the report

1.1 Purpose

The final purpose of this work is to analyze and describe high frequency effects in offshore wind farms. However, all the other components in this work are requirements for the accurate modelling of the wind farm as explained above. Among others, the goal is to justify the models by comparison to measurements where available or to other papers on this topic. This report is to be submitted as both a thesis work and an internal report for ABB Corporate Research in Västerås, Sweden.

1.2 Definitions

| | |
|-------------|--|
| PSCAD/EMTDC | Power Systems CAD based on EMTDC from Manitoba Research Center |
| CB | Circuit Breaker |
| VCB | Vacuum Circuit Breaker |
| SF6 | Sulfur Hexafluoride |
| BIL | Basic Insulation Level |
| TRV | Transient Recovery Voltage |
| TOV | Transient OverVoltage |
| pu | per unit quantity |



2 CABLE MODELLING IN PSCAD/EMTDC

2.1 Introduction

The purpose of this section is to accurately model an actual cable in PSCAD. For this, data given both in cable guides and in system descriptions are used to create a model that closely resembles a cable in a real system. The idea is to be able to simulate both the low frequency effects and the high frequency effects, and to choose an approach for cable modelling that is able to accurately reflect the real conditions throughout a large frequency spectrum.

Due to the sheath that is present in an actual cable, the high frequency coupling phenomena will also be discussed. The purpose of this is to determine how the physical cable will respond to different frequencies and how the transients will propagate. Little work has been done on high frequency effects of power cables, but it is the purpose of this section to simply study the modelling of it, specifically in PSCAD. Some examples on the propagation on high frequency transients in a cable are given in [1] and [2] which, along with their respective references, give a good overview of how transients travel in cables.

2.2 Selecting the cable parameters for steady state

PSCAD v4.x has an interesting new feature which allows, after entry of the cable geometry, to output an equivalent π -section that can be substituted into a circuit for simulating the cable without taking into account reflections. The problem is of course deciding which geometric parameters to pick. One method will be discussed under the context of a specific example.

Specifically it is interesting if the system to be simulated describes the cable parameters in terms of R_{DC} , L , and C per unit length, which is usually the case for large systems. If it is important that the specific cable geometry follows these parameters, then that translates into a requirement of specifying the geometry of the cable to get the right low frequency behaviour of the cable. Clearly then, the cable should be able to simulate steady state conditions equivalent to the simplest representation of the π -section shown below in Fig 3.

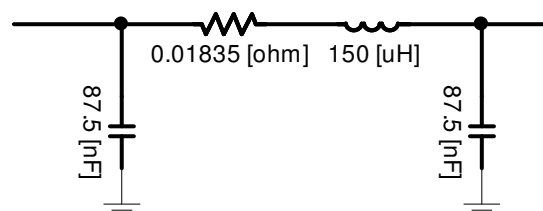


Fig 3: Simple π -section circuit

A simple π -section does not simulate reflections in cables at all, and it is thus usually only used for steady state studies and to see low frequency harmonics. For this, a more complicated cable model is required such as the one provided in PSCAD. As an example, take an equivalent 30kV 800mm² XLPE cable such as the one from ABB. The geometric data of the cable is shown below in Table 1.



Table 1: Sample cable data for 30kV 800mm² ABB XLPE cable [3]

| Cross-section of conductor | Diameter of conductor | Insulation thickness | Diameter over insulation | Cross-section of screen | Outer diameter of cable | Capacitance | Inductance | | Surge impedance |
|----------------------------|-----------------------|----------------------|--------------------------|-------------------------|-------------------------|-------------|---|---|-----------------|
| | | | | | | |  |  | |
| mm ² | mm | mm | mm | mm ² | mm | μF/km | mH/km | mH/km | Ω |
| 800 | 33.7 | 8 | 51.9 | 35 | 63.0 | 0.38 | 0.31 | 0.51 | 13.6 |

Since the simple π -model that makes use of the electrical information above cannot be used at high frequencies, it is thus imperative that the correct geometric data is entered into the simulation program. It will be shown in the following sections how the geometry affects the electrical parameters (capacitance, inductance, and resistance) and how it is possible to match the specified electrical information of the system at low frequencies while also treating high-frequency effects with good accuracy.

Assume then that one wishes to simulate a three-phase system with 3 single-core cables. PSCAD/EMTDC requires the geometric parameters for the conductors, sheaths, and insulators as shown below in Fig 4. The names of the geometric parameters will be referenced to Fig 4 throughout this section.

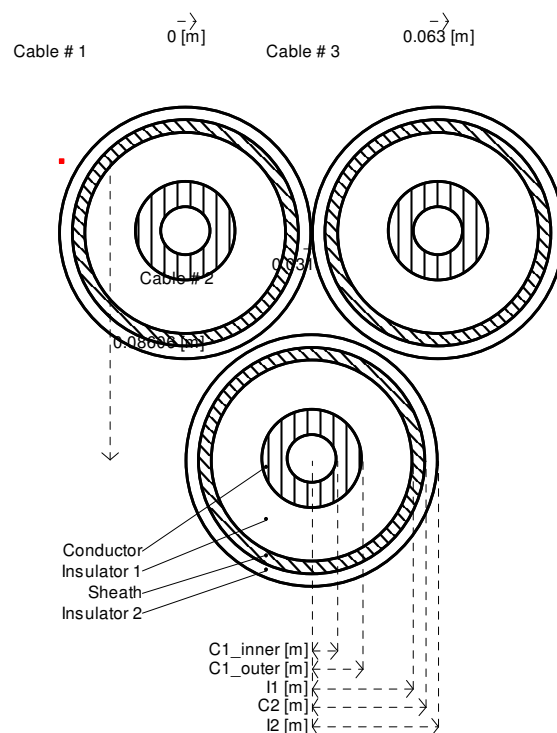


Fig 4: Geometry of the cable model required in PSCAD



The real cable geometry however is far more complex than what is described in PSCAD. One example of a three-core cable may among others, include a conductor screen (semi-conducting), insulation screen, water seal, inner sheath, fillers, bedding, and outer cover. This is in addition to the basic geometry in PSCAD composing of just a series of concentric conductor and insulator sections. The inner sheath is used as shield for the conductor by providing a path for high-frequency currents and equivalently providing electromagnetic protection. The task is to produce the best possible results for steady-state while also being aware of the high frequency effects.

For reference purposes, verbose variables as defined in the following equations (i.e. *DiameterOverConductor*) refer to values given by the ABB XLPE cable guide, while all other geometric variables are referred to Fig 4.

2.2.1 Matching the cable capacitance

This method begins with matching the capacitance, which is defined between the two concentric conductive elements in the cable (namely the conductor and the shield). The conductor is made up of a series of smaller copper wires and compressed into a cylindrical shape, after which a semi-conducting screen is wrapped around the conductor bundle to smooth it out. Because this screen is a semiconductor, it is almost as if the conductor is effectively thicker for high frequencies, and usually a good approximation is to add the semi-conducting screen to the *DiameterOfConductor* specified in Table 1 such as to get $2 \cdot C_{1_outer}$, the outer diameter of the conductor to be used in PSCAD. As will be discussed later, picking the right outer diameter of the conductor is very important for the resistance and inductance of the cable especially at higher frequencies.

$$C_{1_outer} = \frac{DiameterOverConductor}{2} + SemiconScreen \quad (1)$$

Knowing exactly what the thickness of the semi-conducting screen is can be difficult, but the ABB XLPE cable guide gives a hint. One can look at the table for the desired cable and determine it as described in (2). Knowing this value comes from experience, but it can be seen clearly how the thickness of the screen increases with increasing cross-section area of the conductor.

$$SemiconScreen = \frac{DiameterOverInsulation - 2 \times InsulationThickness}{2} \quad (2)$$

The capacitance under such a well-defined geometry can now be calculated as below,

$$C = \frac{\epsilon_r}{18 \cdot \ln\left(\frac{I_1}{C_{1_outer}}\right)}, \quad (3)$$

where I_1 = diameter over insulation, C_{1_outer} = outside diameter of conductor including the screen, and ϵ_r is the relative permittivity of the insulating medium (i.e. XLPE, $\epsilon_r=2.3$). Having already defined C_{1_outer} in (1), one can then easily determine I_1 based on the given capacitance as

$$I_1 = C_{1_outer} \cdot \exp\left(\frac{\epsilon_r}{18 \cdot C}\right). \quad (4)$$



2.2.2 Skin effect

Picking the correct diameter for the conductor in (1) is actually very important for high frequencies because of the skin effect. This will be proven below. At low frequencies or at DC, the whole conductor cross-section is responsible for carrying the current through the cable. The resistance of the conductor is then simply defined as

$$R_{DC} = \frac{\rho}{A}, \quad (5)$$

where ρ = resistivity of the conductor and A = area of the conductor. At higher frequencies however, most of the current travels along the skin of the conductor. For any type of conductor and specifically for a cylindrical conductor, the current density decreases exponentially with increasing distance from the surface of the conductor bundle. The *skin depth* δ is defined as the distance where the current density decreases to 37% of the surface current density [4],

$$\delta = \sqrt{\frac{2\rho}{\omega\mu}}, \quad (6)$$

where ω = frequency [rad/s], and μ = permeability of the conductor. This skin effect causes an additional AC resistance to be added on top of the DC resistance in (5) above, defined as

$$R_{ac} = \frac{2\pi\rho \int_0^a (J^2 r) dr}{I^2}, \quad (7)$$

where a = conductor radius, I = current, J = current density as a function of r and the skin depth. The DC resistance depends only on the total area of the conductor (discussed below), while the AC resistance requires that the current density be well defined starting from the skin of the conductor. Having the exact dimension for the conductor is thus extremely crucial for defining the parameters in PSCAD, because the current density profile will change based on the radius of the conductor [4].

2.2.3 Matching the DC resistance of the cable

Having now determined that the AC resistance is only dependent on the outside radius of the conductor C_{1_outer} , the radius of the inner conductor C_{1_inner} can be determined based on the desired DC resistance only. Consider a copper conductor where the resistivity is equal to $\rho = 1.68$ [nΩ/m]. The area of the conductor A in (5) is the only value that can be adjusted to set the correct R_{DC} , and for a cylindrical conductor with a hole in the center, it is equal to

$$A = \pi(C_{1_outer}^2 - C_{1_inner}^2). \quad (8)$$

Accordingly, using (1) and (8), the inner conductor radius can be determined as

$$C_{1_inner} = \sqrt{C_{1_outer}^2 - \frac{\rho}{\pi \cdot R_{DC}}}. \quad (9)$$

To summarize then, all the geometric values for the main conductor have been determined as well as the radius of the insulator, I_1 .



2.2.4 Matching the inductance of the cable

Another problem that requires solving is that of matching the inductance. This is slightly more complicated since the inductance is dependent on both the self coupling and the mutual coupling of the magnetic field. The latter is dependent on the physical layout of the cable and is harder to determine, but the self inductance can be defined as

$$L = \frac{1}{2\pi} \mu_r \mu_0 \ln \left(\frac{I_1}{C_{1_outer}} \right) + \frac{1}{8\pi} \mu_r \mu_0 . \quad (10)$$

At higher frequencies it has been shown that the second term disappears from the equation [4]. It is this inductance at higher frequencies and the capacitance that determines the surge impedance of the cable as

$$Z_0 = \sqrt{\frac{L}{C}} . \quad (11)$$

The physical explanation for this is that a low frequency wave will travel through the main conductor of one of the phases and return through the other two, at least in a balanced system. In contrast, a high frequency wave will travel on the skin of the conductor and back through the shield of the same cable. This is due to the skin effect which effectively eliminates the last term in (10) [4]. This is further examined in section 0.

As for matching the geometry of the cable to get a desired L , it is the opinion of the author that using the data above for C_{1_inner} , C_{1_outer} , and I_1 will produce fairly good results for the self inductance. This is because both the self inductance and the capacitance are solely based ratio of I_1 and C_{1_outer} . The mutual impedance can be matched by using the proper cable layout geometry as specified in Table 1 (flat or trefoil). For simulation of a cable with a common outer layer (i.e. a three-core submarine cable), the best layout is the trefoil formation. PSCAD does not yet allow simulation with a common shield or armour, but this feature is expected to appear in newer versions.

This simple trick of matching the capacitance and inductance also helps to match the surge impedance, since this is also dependent solely on the C_{1_outer} and I_1 ratio. To sum up, the goal of matching the electrical parameters has been achieved.

2.2.5 Determining the remaining parameters

Two parameters are still required for the purpose of simulation in PSCAD: C_2 (the radius over the shield), and I_2 (the radius over the last layer of insulation on the cable). The armour will not be used in this report. In Table 1, the cross-section of the copper screen is given. A screen can be either made up of a thin sheet of copper tape or equally spaced strands of copper wire around the screen. It is usually such that if strands are used for the screen, these will be embedded in the insulation. When the *DiameterOverInsulation* is given in the table, this diameter includes the screen as well since it is effectively embedded inside the insulation. The PSCAD shield is however only a simple copper tape screen, so an equivalent sheet of equal screen area must be placed around the insulation for simulation purposes. For a given screen area A_{screen} , and having already figured out the insulation radius I_1 , the radius over the screen, C_2 , can also be determined.



$$A_{screen} = \pi(C_2^2 - I_1^2) \tag{12}$$

$$C_2 = \sqrt{\frac{A_{screen}}{\pi} + I_1^2} \tag{13}$$

The last parameter to be determined is the radius over the last layer of insulation I_2 . Since there is no armour however, the thickness of this layer may only have an effect on the mutual inductance in a three-phase system. A good approximation is just to use the outer diameter divided by two as your radius over the last layer of insulation. The material can be any type of insulator, but commonly XLPE is used with an ϵ_r of 2.3. The effect of this last layer is minimal if no armour is used. Accordingly,

$$I_2 = \frac{OuterDiameterofCable}{2} \tag{14}$$

2.3 Comparison of results

In this section, the validity of the previous sections is verified through comparison of three different cable models described in Fig 5.

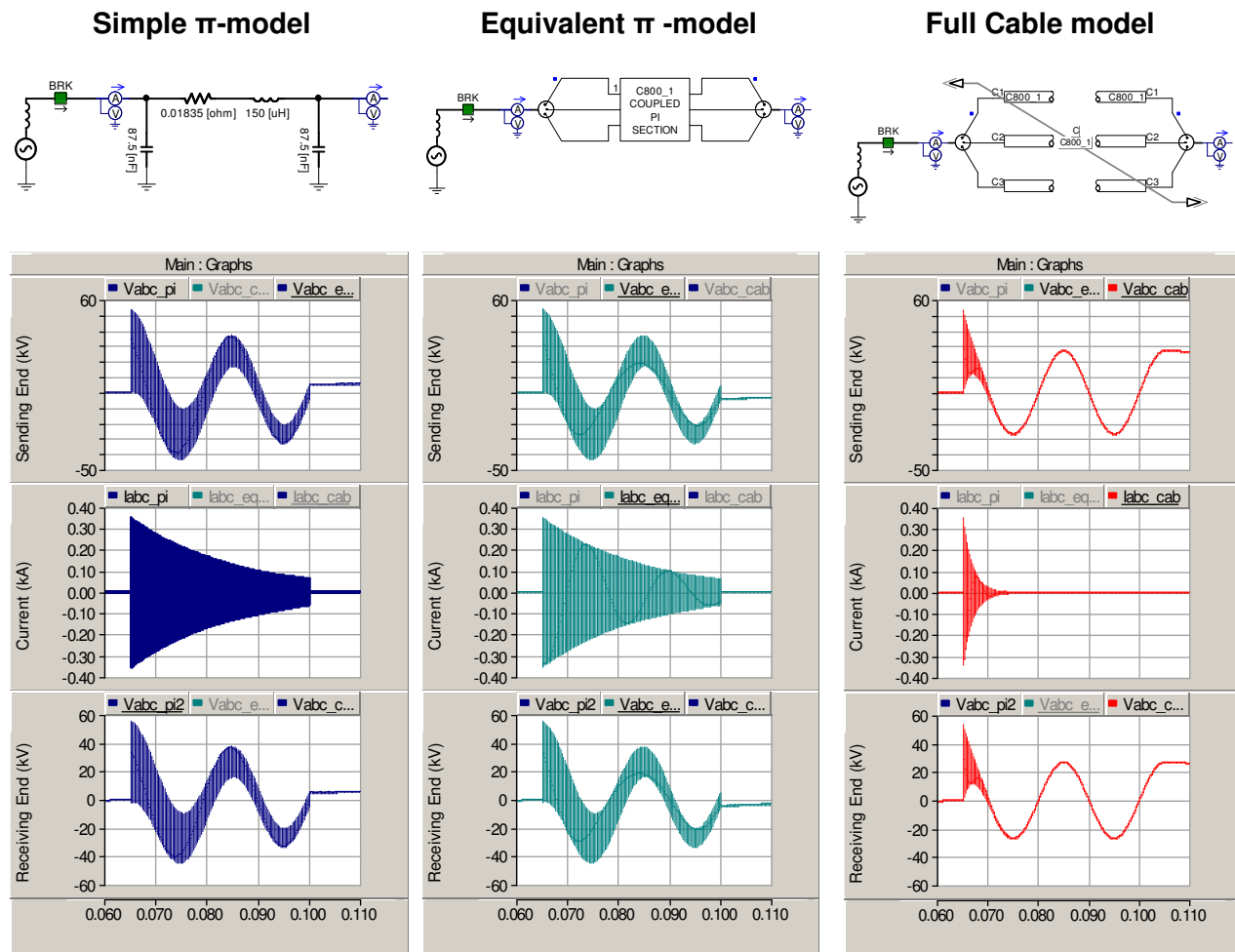


Fig 5: Results for one phase during cable switching



The “equivalent π -model” refers to the component that is outputted by PSCAD during compilation, and is based on the theory in [5]. The “simple π -model” is just made up of only 4 passive components as shown in the diagram, and the “full cable model” is able to simulate reflections along the line.

At first glance, it appears that the results for the first two models are almost the same. The equivalent π -model however does take into account the coupling between the lines while the simple π -model does not. Due to this, a small phase shift is introduced in the waveform, and it is for this reason that at 0.10s, when the breaker is opened, the instantaneous values of the voltages are different. However, upon closer inspection, the high frequency components are exactly the same in both phases, with exactly the same damping. This shows that the PSCAD model, with the correct geometry, can give the right results equivalent to a simple π -section. The model of PSCAD is henceforth accurate at least for the lower frequency components.

The result for the full cable model is fairly different. For one, the high frequency part of the current dies down a lot quicker but starts at the same value when the cable is energized at 0.065s. The reason for this quicker decay is simply that the cable model takes into account the AC resistance of the cable as well as the DC, and thus high frequency components will decay faster than in the simpler models where the decay is less frequency dependent. The result is therefore expected.

For completeness, a zoom in of the high frequency oscillations is shown below. Note also that the reflections are not present in the full cable model because the rate of rise in the system is not quick enough to create propagation. This behaviour is also expected.

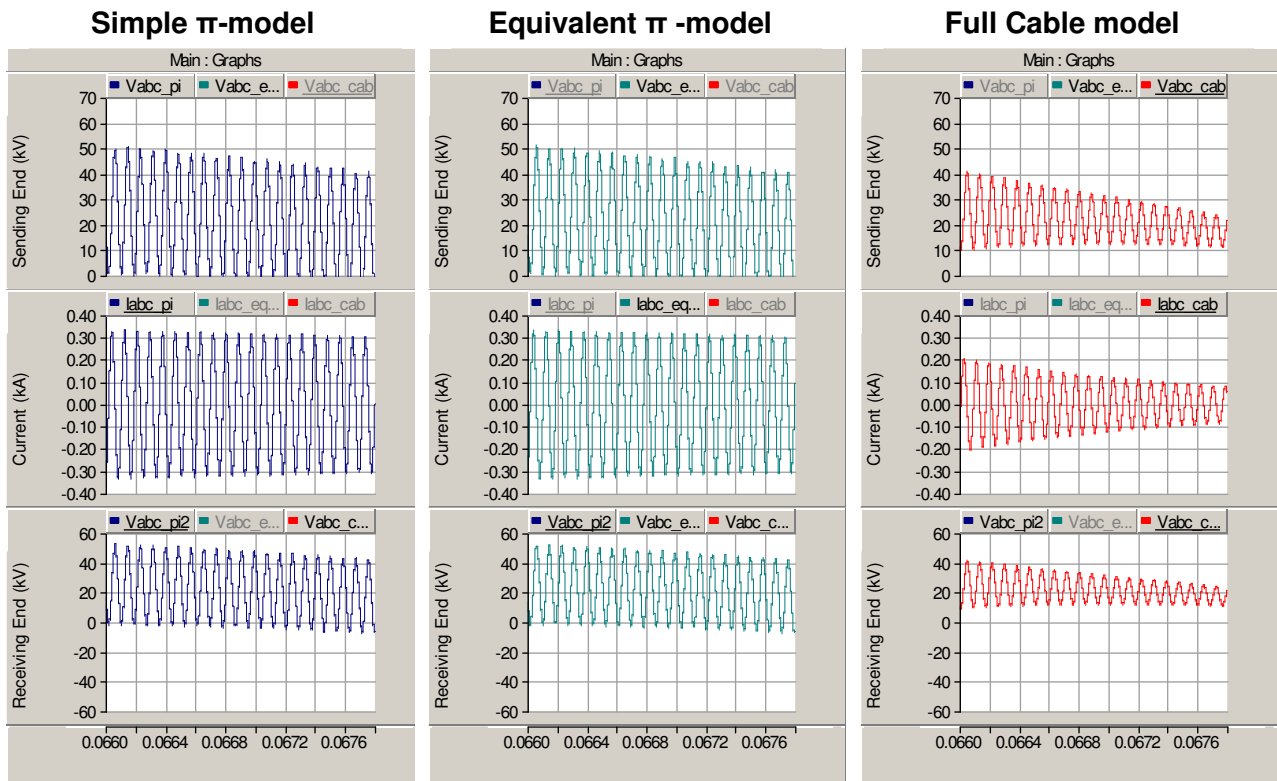


Fig 6: Zoomed in view of oscillations



2.4 High frequency effects

In this section it is desired to characterize the high frequency effects of a cable system. For simulation purposes two parallel single phase cables will be used. One of the cables will have a voltage inserted at a certain time while the other cable is earthed at both ends. All the shields are also earthed at each end, while a load of 20Ω is used to roughly simulate the surge-impedance loading for the system.

2.4.1 Description of the test circuit

While it appears that there are 4 cables in Fig 7 below, it is only so because this is the only method to measure the line current and the shield current in the middle of the line using PSCAD. For all intents and purposes, this is as close as possible to an actual cable system with two cables (top and bottom) of a total length of 2km. Physically, the cables are laid out right next to each other, 1m under ground with a ground resistance of $100 [\Omega\text{m}]$ in PSCAD.

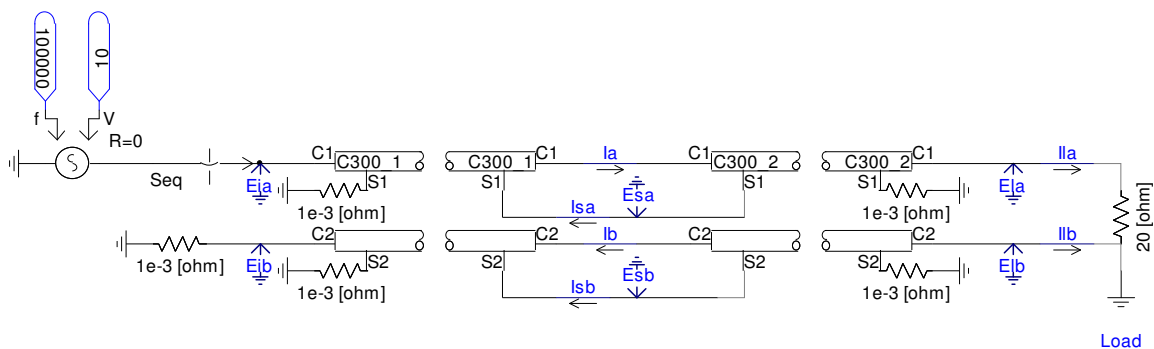


Fig 7: Test circuit for determining coupling between lines

2.4.2 Coupling coefficients

The simulation is performed by injecting a voltage, and hence a current, at the left side of the top cable through the main conductor. The current through line A (top line), through both shields, and through line B (bottom) is measured. Line A and B refer to the conductor of the cable and not the shield. The results are plotted below as a function of the frequency of the injected current, with Fig 8 displaying the magnitude of the current with respect to line A current and Fig 9 displaying the current phase angle with respect to the phase angle of line A current. Fig 9 can be interpreted as follows:

- *Positive angle*: leading with respect to line A current
- *Negative angle*: lagging with respect to line A current

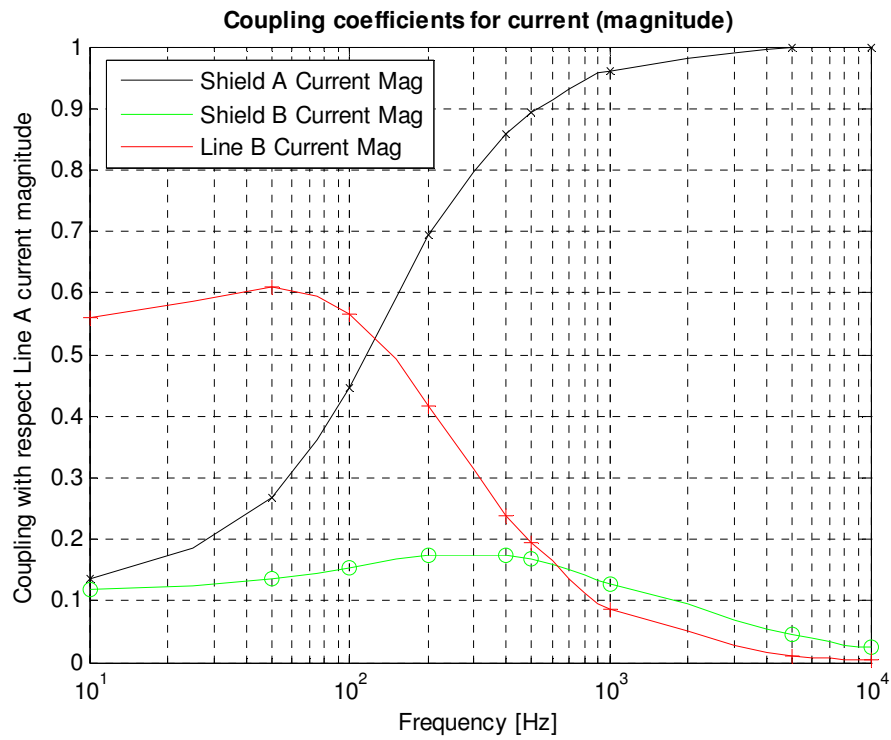


Fig 8: Coupling coefficients for current

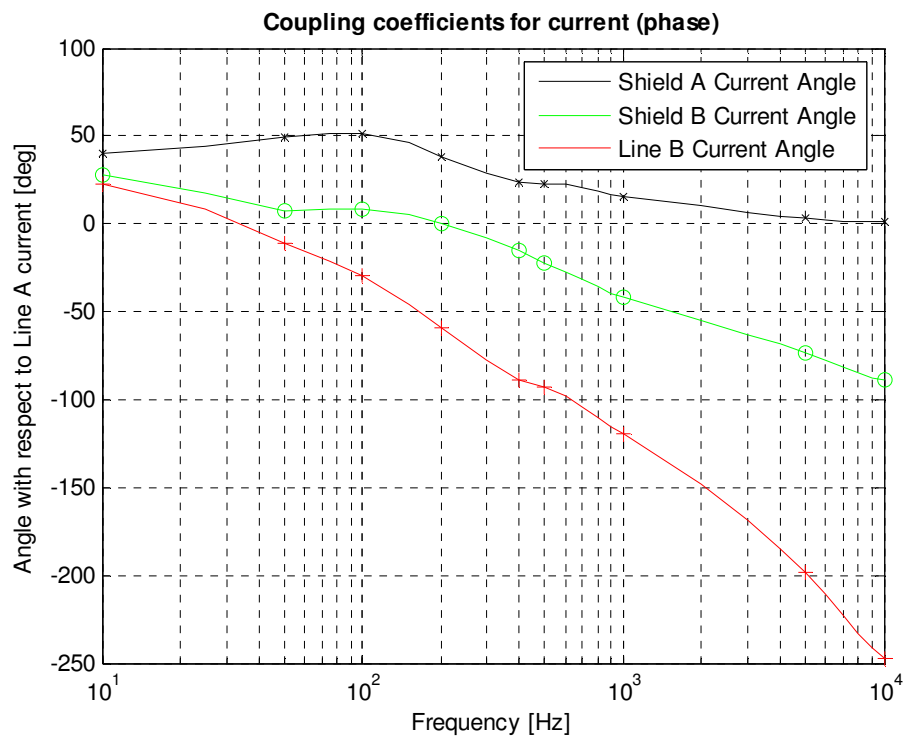


Fig 9: Coupling coefficients for current



The conclusion that can be drawn here is that at high frequencies, most of the current in line A will get coupled into its own shield, while at low frequencies, most of the current will be coupled into line B. The graphs of Fig 8 and Fig 9 describe a series of complex numbers (since there exists both a magnitude and a phase). The sum of these complex numbers should according to Kirchoff's Law add up to unity. In simulation, they add up close to unity (within roughly 10%) because not all the currents are accounted for in the sum. For example, there also exists currents in the ground path on either side of the cables, but one in this case is only interested in values in the middle of the cable.

The result can be explained by thinking of the cable as an infinite section of pi-links. At each point on the circuit, some of the current can go through the line inductance or get directed to the shield via the capacitance between the line and the shield. At low frequencies, the impedance of this capacitance is very high, so very little current is coupled back into the shield. As the frequency increases, the impedance of the capacitance decreases, and thus almost all of the current that passes through the line will couple in back through the shield via this capacitance. The current coupled to line B becomes less and less because the inductance of the cable becomes higher and higher as the frequency increases.

Note that this is just an example, and the curves may change for different loading conditions. However, it can be said that the pattern is fairly similar for most cable systems. At frequencies as low as even 1kHz the current will couple directly back into its own shield rather than the other phases in the system. This implies then that the high frequencies, such as those caused by re-ignitions, will have a hard time coupling in to other phases such as to give way to virtual current chopping. This will be discussed in more detail in 4.2.5 in the context of a specific example.

2.5 Conclusion

This section discussed cable modelling in PSCAD/EMTDC. Due to the complex geometry of an actual cable, several assumptions were made and justified for the purpose of providing the geometric information necessary in PSCAD/EMTDC. A detailed analysis of the coupling effects in cables was also performed, showing that at high frequencies, the wave travels almost exclusively back into its own shield. For verification, the cables were simulated along with two simplified models (a coupled π -model and an un-coupled π -model) to determine the validity of the assumptions made. This information is crucial to the proper modelling of the cables used in the industrial system and the wind farm that will be discussed later in the report. The method described here is not unique, but according to the author it is the best method for this purpose to closely simulate the cables through a large frequency range.



3 THE VCB AND MODELLING IN PSCAD/EMTDC

3.1 Introduction

The correct modelling of CBs is crucial to the proper analysis of high speed transients. There are two main types of CBs currently under development today: SF6 breakers and VCBs. SF6 breakers account for large transmission systems, while VCBs are common in medium voltage designs such as in industrial systems and wind farms. References [6] and [7] give a good overview of the different types of CBs installed today and how each deals with phenomena such as re-ignitions and pre-strikes.

The proper and complete modelling of a VCB in EMTDC is dealt with in [8] and [9]. Both these models are extremely complex and rely also on empirical data due to the fact that breakdown phenomena in vacuum cannot be well described by formulas. Furthermore, the actual occurrence of the re-ignitions is dependent on the following 4 criteria described in [10], which are important to take into account when modelling a VCB in PSCAD/EMTDC.

- Contact separation of the first pole starts before current zero crossing
- High recovery voltage is present to cause the first re-ignition
- Re-ignition causes high frequency current with zero crossings super imposed
- Breaker is able to interrupt the high frequency current (which the VCB can do)

The final purpose of modelling a CB in PSCAD/EMTDC is for the simulation of high speed transients in cable systems. This issue is dealt with in [11], where a simple model of the CB similar to what will be developed here is simulated in PSCAD/EMTDC.

3.2 The Physically Complete Model

3.2.1 The main phenomena

The complete model is as described in [8] and [9], and models the following phenomena in detail:

- *Current chopping*

While the contacts are opening at the start of the opening operation, an arc is formed since the current has not yet necessarily reached a natural zero. At low currents the arc can become unstable, lose its inertia, and hence extinguish unnaturally. This usually occurs at 5A or less and can cause high voltage spikes depending on the system.

- *Cold gap breakdown*

Contact separation physically takes a finite amount of time, and during that time, the breakdown strength of the vacuum gap increases almost linearly. If the voltage applied across this gap does however exceed the breakdown strength, then the arc can itself reignite and cause the circuit to close once again through the arc. The cold gap breakdown is dependent on the rate of rise of voltage, and this is further explored and explained in the sections below.



- *Voltage escalation and re-ignitions*

Voltage escalation is a function of the external circuit and depends on the resonating paths created externally across the CB. By definition, a re-ignition is a temporary voltage breakdown that occurs during the first $\frac{1}{4}$ cycle after the first current interruption. A re-strike however occurs after a $\frac{1}{4}$ cycle, and is usually due to capacitive circuit switching [10],[11],[13]. An example is shown in Fig 10.

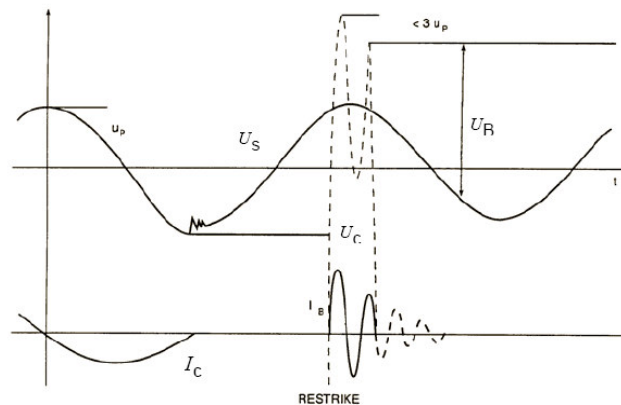


Fig 10: Re-ignitions/re-strikes and voltage escalation

The re-ignition due to the voltage breakdown across the CB causes an oscillating current while the arc is conducting. The oscillation frequency is due to the external circuit and the stray capacitances and inductances of the VCB itself if any. This high frequency current can be interrupted by the VCB [13], which will cause the voltage at the load side to be clamped at a high value. In this case, U_R represents the voltage across the breaker, and it can be seen how a situation can arise where the voltage will keep increasing across the gap and cause a further breakdown. This is known as voltage escalation because every subsequent breakdown can clamp the voltage at a higher and higher value.

- *Quenching capability of the high frequency current.*

The arc itself has a certain inertia, and while it is passing through a high frequency current zero, this inertia may not allow it to interrupt. Hence, it is important that in an accurate model, some high frequency zeros are allowed to pass before the interruption of the arc. This quenching capability is determined by measuring the derivative of the current against a threshold, and if that threshold is passed then the high frequency current can continue. Otherwise, the current is extinguished. Therefore it may be such that several current zeros pass before the vacuum gap is able to extinguish the arc.

- *Pre-strikes*

While re-ignitions and re-strikes occur during the opening operation of a CB, the pre-strikes will occur during the closing operation. The high frequency phenomena are similar even though voltage escalation will not occur since the gap is becoming smaller with time.



- *Finite arc resistance*

Right after a cold gap breakdown the arc conducts the high frequency current. However, the arc has a finite resistance which imposes a certain finite arc voltage (of several tens of Volts) across the gap. This re-ignition voltage, as it is known, will also depend on the rate of rise of the current, which is further dependent on the external circuit.

- *Virtual current chopping*

In a three phase system, certain stray capacitances exist between each of the phases. A CB interruption in one phase can produce transient currents in the other two phases through the cable capacitances or other strays in the system. If this coupled current creates unnatural zero crossings, the vacuum gap can extinguish the arc and start voltage escalation in this other phase. A situation can also arise whereby one pole cannot interrupt the current for whatever reason, and another pole will be in a situation to open the CB before the first pole to operate has a chance to do so.

- *Statistical and empirical nature of model*

As it was mentioned above, the breakdown phenomena are statistical in nature and sometimes based on empirical values. A proper and complete model would include these effects.

- *Residual charge carrier breakdown (hot gap breakdown)*

This is another type of voltage breakdown that can occur at lower voltage levels right after an arc has extinguished. Residual charge carriers can exist at the cathode surface, which effectively reduce the breakdown gap length and causes a breakdown at a lower voltage than expected. This is also dealt with in the next section.

3.2.2 Feasibility of accurate simulation

The complete model is however infeasible to implement for large systems (such as industrial systems or wind farms). One reason is that the empirical data would have to be experimentally determined for the specific CB used in the simulations. This adds extra complexity and the amount of extra knowledge gained from such an implementation is minimal unless the purpose is to study the CB itself. Secondly, the system is fairly large, and statistical data for individual CBs tends to play a smaller role in the aggregate. Finally, when the effects of re-ignitions are to be studied, only the basics of the VCB characteristics are important (main phenomena). Whether three or four re-ignitions are observed is irrelevant since each individual CB will behave differently in a real system anyways, and the complete behavior is dependent on many different parameters. The purpose for modelling is hence to have a good approximation that can be used as a source of transients and nothing more.

3.3 Description of the main phenomena

3.3.1 Vacuum gap breakdown

The phenomenon of cold gap breakdown requires further explanation. In its basic form, it occurs when the voltage across a gap (in this case a vacuum gap) exceeds that of the breakdown strength of the gap itself at a certain time. This breakdown strength is time varying since the contacts take a finite amount of time to open, usually around 10ms.



IEEE C37.04 [7] describes in detail the breakdown characteristics of a breaker, and how a CB is to be chosen based on the TRV response of the system. The IEC standards also have a similar requirement [14]. Specifically, a system TRV is the transient response that a system would produce upon the opening of an infinitely fast CB controlled by external resonating branches. The CB is given the task of ensuring that the gap opens faster and is able to handle more voltage than the system can produce. This idea is shown in Fig 11.

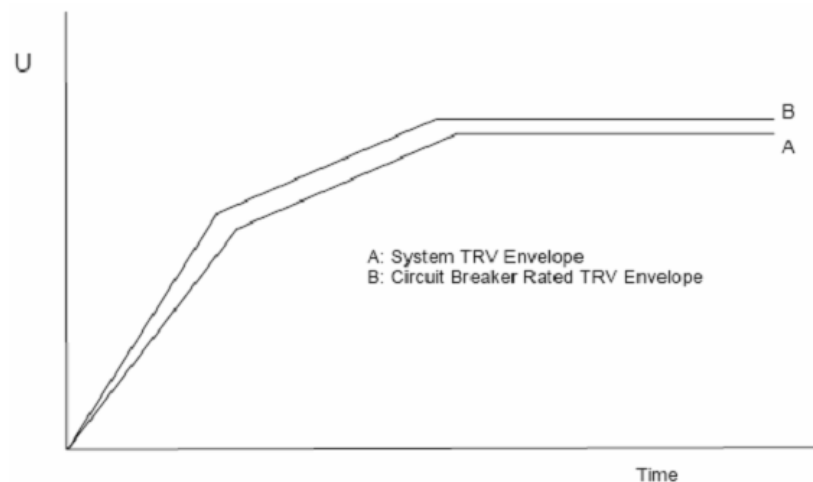


Fig 11: The CB characteristics vs. System TRV characteristics (reproduced from [7])

One source of contention that is not very well explained in the standards is that there are in fact two methods of voltage breakdown that can occur in a vacuum gap. This will be explained by looking at the theory of voltage breakdown in vacuum gaps.

When the contacts begin to separate, the gap is cold in the sense that it is at room temperature. When the voltage across the contacts, and hence the electric field in the gap, becomes too great, a breakdown will occur. In air, the initial breakdown occurs because energy carriers present in the background radiation (free-floating electrons and ions) gain enough energy to cause an avalanching process which eventually leads to full arc breakdown between the contacts [15].

In vacuum however, no such background radiation exists because by definition, a vacuum should be free of any such particles. The breakdown actually occurs due to metallic particles being produced from the electrodes themselves from thermionic emissions and field emissions. Under field emission, the field between the contacts is so great that several metallic particles on the surface of the electrodes become dislodged from the electrode surface. This is common in electrodes such as those made from copper, silver, and other similar metals [16]. Breakdown caused by this phenomenon is called “cold gap breakdown” because the gap is cold and a relatively long time has passed after a previous re-ignition, if any. As an example, Roguski describes in [16] a cold gap breakdown curve for a VCB in Fig 12.

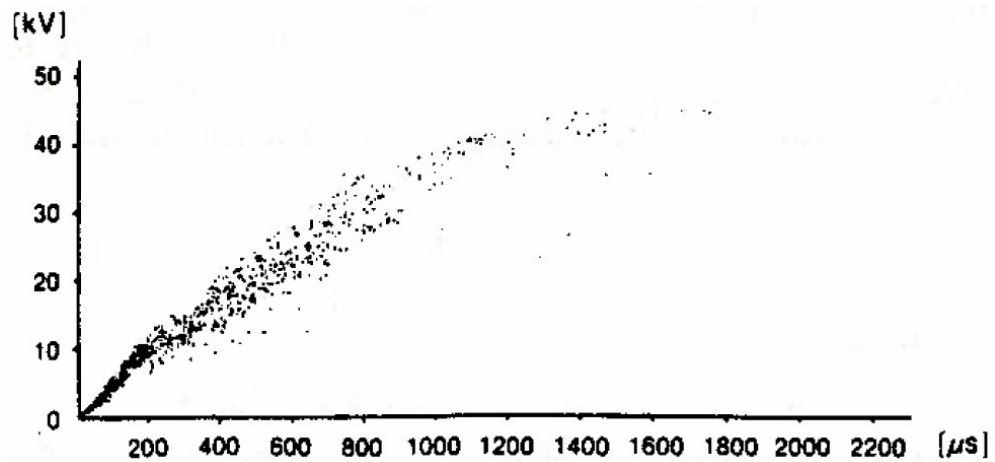


Fig 12: Cold gap breakdown curve (reproduced from [13])

A re-ignition refers to the creation of an arc between the two contacts in a vacuum gap. When the arc is present in the vacuum gap, heat is produced and consequently the pressure and temperature in the vacuum increases. When the arc is extinguished, due to a zero crossing in the current, the gap is still fairly hot, and it may be so that metal vapors and ions are still present in the gap. These residual carriers have a certain time decay and subsequently cause a certain time delay in the recovery of the dielectric strength in the gap from the time the vacuum arc is extinguished. An example of this hot gap breakdown curve is shown below in Fig 13. Time zero is when the arc has extinguished whereby 40kV is the full withstand voltage of the gap assuming contacts are almost completely open.

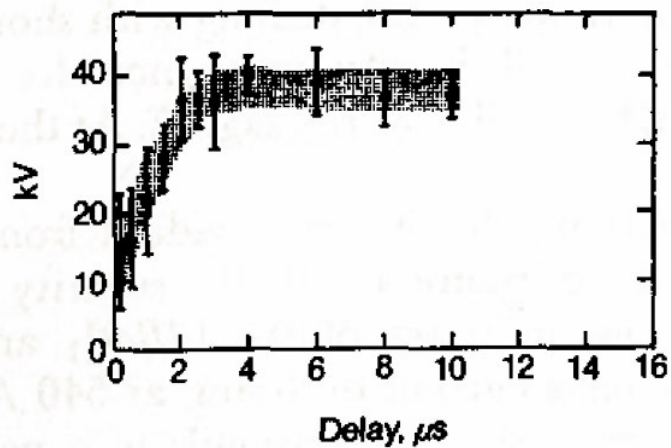


Fig 13: Hot gap breakdown curve (reproduced from [13])



The slope of the cold gap breakdown is mainly dependent on how fast the contacts open in the gap, while the hot gap breakdown slope is mainly dependent on the material used for the electrodes. Electrode materials that can readily give out metallic particles under field or thermionic stress are usually not good as the gap takes a longer time to recover after a vacuum arc has been extinguished. In IEC standards [14] and IEEE standards [6],[7], it is the slope of the hot gap breakdown, usually several orders times higher than the cold gap breakdown slope, which is specified as the requirement for the CB to handle. However, it is the cold gap breakdown curve which, according to Roguski, determines the time varying re-ignition behavior of the VCB [16].

Theoretically, if the slope of the TRV across the vacuum gap exceeds the slope of the hot breakdown curve, then it would be so that a re-ignition will occur almost every time that the arc is extinguished between the contacts, because the hot breakdown curve is always present no matter if the vacuum contacts are fully or partially separated. Practically, such high rates of rise after arc extinction (around $1\text{kV}/\mu\text{s}$) are not usually seen in systems. Rather, it is a safe guideline for CB manufacturers to follow. From the point of view of simulating re-ignitions this information is not necessary, and more informative is the cold gap breakdown curve, which is not necessarily provided in IEC standards.

3.3.2 High frequency arc interruption

By the nature of vacuum gaps, VCBs are very good at interrupting high frequency zeros. During a re-ignition, a high frequency current will be superimposed on the system frequency current while the arc is conducting. This total current will have several high frequency zero crossings, and these zero crossings can cause the arc to extinguish, due to the nature of the vacuum gap, until the next gap breakdown occurs or successful interruption has occurred. There are in fact three possible outcomes when a trip signal has been delivered to the CB [9]:

1. After a series of re-ignitions and high frequency current interruptions, the gap can finally withstand the system TRV and thus interrupt the current completely.
2. If the voltage escalation is too high, a point will come about when the high frequency zeros will no longer occur. Hence, the power frequency current will keep conducting and successful interruption will occur at the next power frequency zero.
3. The chain of re-ignitions and high frequency current interruptions can cause damage to the equipment itself, and a successful interruption will not occur. It will then be up to the fuses to break the current.



3.3.3 Current chopping and importance of it

The question is whether the extra complexity of trying to chop the current at the first current zero is worth the effort. Three arguments can be made against current chopping. For one, the only effect that the current chopping causes is a finite voltage spike at the beginning of the opening operation. This extra injected energy contributes to the spike magnitudes later on and starts the voltage escalation slightly earlier, but this extra spike can hardly be justified because the effects are minimal, at least for this simple system. Secondly, after the initial voltage spike due to the current chopping is created, the breaker begins to open. Due to the magnitude of this spike and the low withstand capability of the breaker at the very beginning, the gap will immediately break down causing an oscillating current. As will be seen later in Fig 25(a) with a finite chopping current, these oscillations will have no zero crossings, and the power frequency current will have to wait until a natural zero to extinguish the arc. It is in this case that the current chopping will appear as if it has not even occurred.

Finally, there is also something to be said about the computation complexity of the circuit when trying to simulate current chopping. The problem lies in the fact that current chopping is dependent on the frequency of the current, and hence the mechanisms, at least for the simulation purpose, are different. This adds complexity to the system for a result which much information cannot be gained from. Hence, it is the opinion of the author that for the purpose of simulating high speed transients in a cable system, such current chopping would not have any appreciable effect. The matter would be different if the simulation was purely for simulating the VCB properties, but this is beyond the scope of this work.

3.4 The test circuit

References [8] and [9] provide a simple test circuit that produces 4 different frequency components used for analysis of the performance of the VCB. The goal of the model that was developed in this report was to at best emulate their results. The circuit is shown below in Fig 14 as described by Helmer in [8] with some simplifications. The diagram simulates a 3.46kV single-phase system in a very general form, in the sense that another system could be readily simplified to an equivalent circuit with the following impedances. One exception perhaps is when the line or cable (composed of R_k and L_k) is modeled as a π -section, which would require an additional capacitance to ground where “ E_{load} ” is situated (π -section theory).

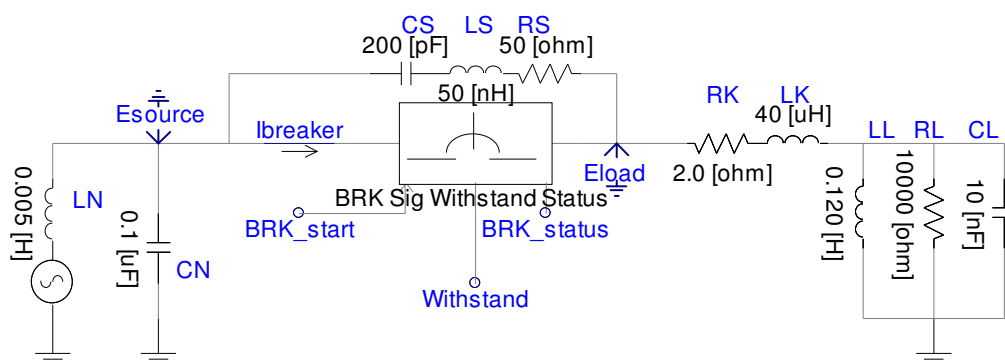


Fig 14: The test circuit



What is important here is to determine the resonating branches in the circuit. Obviously a 50Hz component will be present, but the interest is in the high frequency components and what is to be expected across the breaker.

The first frequency component that will be present is due to the natural frequency of the load. These oscillations are due to the energy exchange between the load capacitance and the load inductance, and it is at a frequency of

$$f_{load} = \frac{1}{2\pi\sqrt{L_L C_L}} \cong 4.6 \text{ kHz} . \quad (15)$$

To determine another frequency component, imagine that the breaker closes instantaneously, shorting out C_s , L_s , and R_s . This creates a step input change in the voltage across the load (see diagram), which produces an oscillation. The frequency of this oscillation is dependent on L_k and L_l in parallel, but since L_l is larger, L_k will dominate in a parallel connection. The only capacitance available here is C_l , and hence another resonant frequency of oscillation for the breaker current occurs at

$$f_1 = \frac{1}{2\pi\sqrt{L_k C_L}} \cong 250 \text{ kHz} . \quad (16)$$

Finally, if the breaker contacts are opened instantaneously, then a step input change in voltage is applied across the breaker. The resonant branch is made of L_s and L_k in parallel with L_l , meaning that L_k dominates. Furthermore, Capacitances C_s and C_l are now in series, and no approximation can be made here because they are both of similar magnitude. The voltage will then have an oscillating component at a frequency of

$$f_2 = \frac{1}{2\pi\sqrt{L_k \frac{C_s \times C_l}{C_s + C_l}}} \cong 1.8 \text{ MHz} . \quad (17)$$

As a final note, the circuit also predicts another resonant frequency across the breaker contacts due to the series resonant tank (C_s and L_s). The frequency is around 50MHz and is excluded here because to capture such high frequencies, an extremely small time step is required. The magnitude of this component is very small however and is damped quite quickly (in the order of μs), and hence plays little part in the understanding of the problem.

To test that in fact the frequency content is present, an impedance sweep is performed across the circuit using PSCAD. Under the open breaker condition in Fig 15, the oscillation frequencies that appear in the voltage will be present.

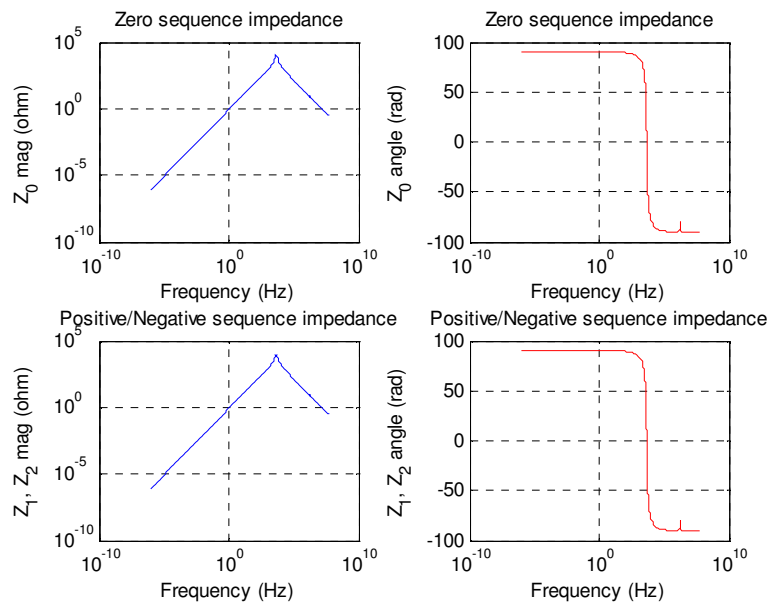


Fig 15: Bode diagram with breaker as an open circuit

What is apparent in Fig 15 is the one large peak at about 4.6kHz, but there is however a much smaller peak at 1.7MHz which is fairly invisible here. Under simulation, this latter component dies down very quickly and explains why it is very faint on the bode diagram.

The second case is when the breaker is simply a closed circuit, which helps to determine the current harmonics, shown in Fig 16. Since one is trying to determine the excitation frequency of the current, the negative peak as opposed to the positive peak in the bode diagram is of interest. Here, the negative peak is at around 250kHz, confirming the theoretical calculations shown above. The 50MHz component is so faint that it cannot even be seen as a blip on the bode diagram.

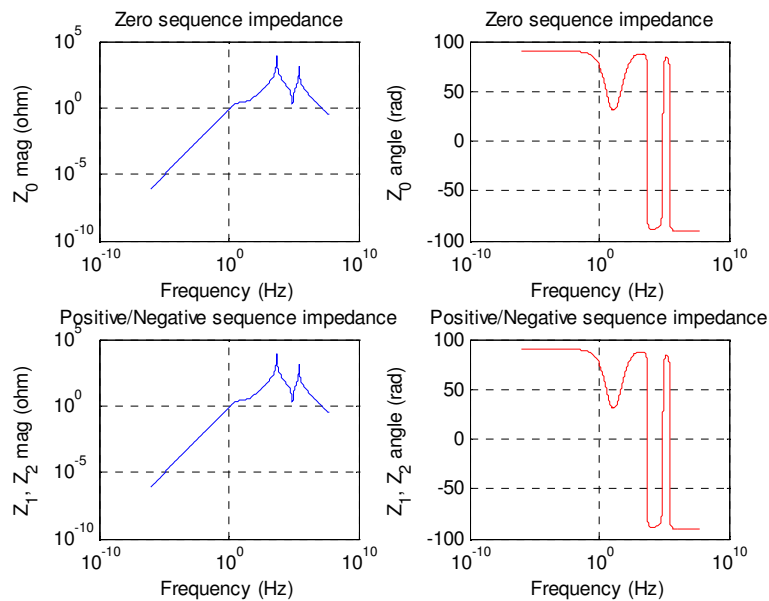


Fig 16: Bode diagram with breaker as a closed circuit



3.5 The PSCAD/EMTDC model

3.5.1 Introduction

The basic model introduced in this section simulates the following phenomena:

1. Cold gap breakdown
2. Re-ignitions and pre-strikes
3. Finite number of high frequency zeros before arc interruption

The justification for only modelling the above phenomena lies in the complexity of the problem to be studied later on. For larger systems, small random deviations in parameters such as gap breakdown voltage will even out. Further to this it is more important to study the effects of these re-ignitions rather than to create an exceptionally accurate model of the CB. The CB in this section can only handle one opening operation and one closing operation in this sequence at the moment which is good enough to study the main effects.

3.5.2 Results of simulation

In Fig 17 the whole span of the opening and closing operations is shown, while in Fig 18 the beginning of the opening operation is seen whereby the voltage across the CB is plotted along with the breakdown withstand of the gap. At first, an almost instantaneous jump in breakdown withstand is seen, which helps to account for the first criteria required for multiple re-ignitions as specified in [10], mainly the fact that contact separation must begin before current zero interruption.

The second requirement occurs shortly after the contact separation, and begins the process of voltage escalation by causing the first breakdown across the gap. The third requirement is satisfied by the external circuit which provides a high frequency oscillating current, while the fourth requirement is satisfied by waiting for several high frequency zero crossings before the arc is interrupted. In this case however, it is broken on the first current zero, providing the worst-case scenario for voltage escalation.

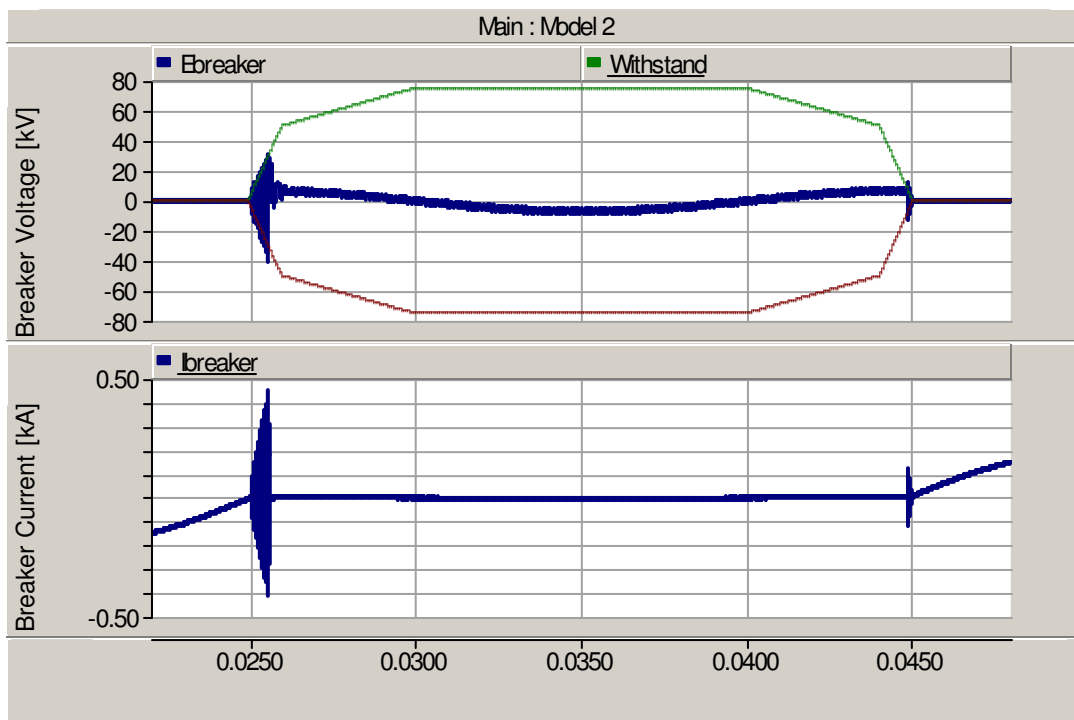


Fig 17: Opening and closing operation

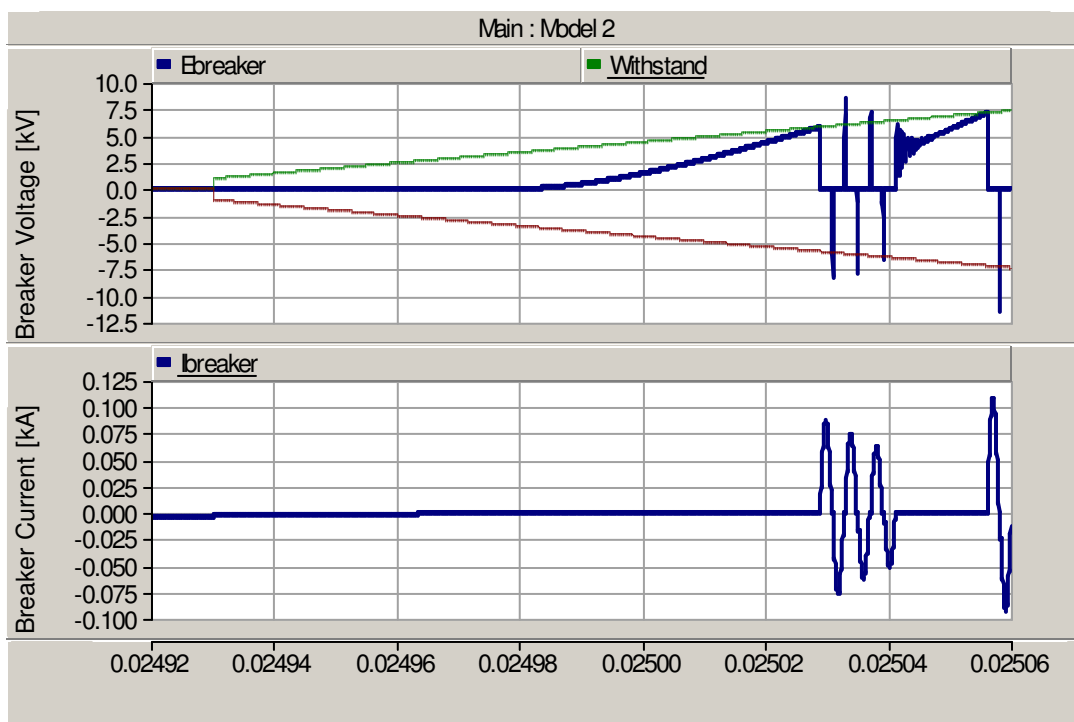


Fig 18: Start of opening operation



Fig 18 also reveals the frequency components that were described in section 3.4 of this report. The 50Hz component is hardly visible because of the small time step used in the channel display. This simulation was run at a solution time step of $0.05\mu\text{s}$, which is required to accurately capture the 1.8MHz frequency component. Verification of this model is done by comparing it to the results obtained in [8] and [9]. The outcomes are fairly similar, considering that the other papers simulate a multitude of other factors and also include empirical data in their analyses.

One more point that needs further explanation is the narrow voltage spikes that occur in Fig 18 (further zoomed in Fig 19). When a set amount of high frequency zeros have passed the arc is extinguished and the voltage across the breaker begins to increase. The 1.8MHz component is the first to appear, and hence the initial rate of rise is very high for the voltage. In fact it is so high that before the 1.8MHz component has a chance to die down, the voltage across the vacuum gap has already passed its breakdown strength and causes a cold gap breakdown. This is why they appear as spikes on the graphs, which are of course also predicted and present in [8] and [9].

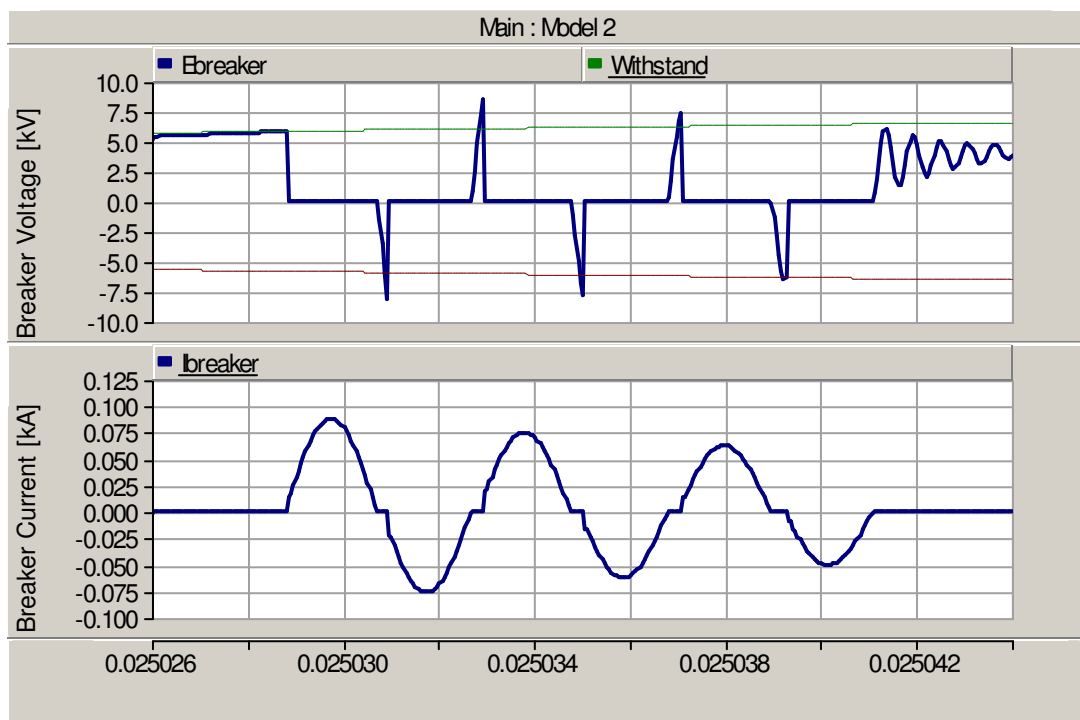


Fig 19: Voltage spike due to current chopping

The objective of the CB is to break the current, and this is precisely what is shown in Fig 20. The time scale is different than in the previous picture, but it demonstrates that successful interruption can occur when the TRV does not exceed that of the CB.

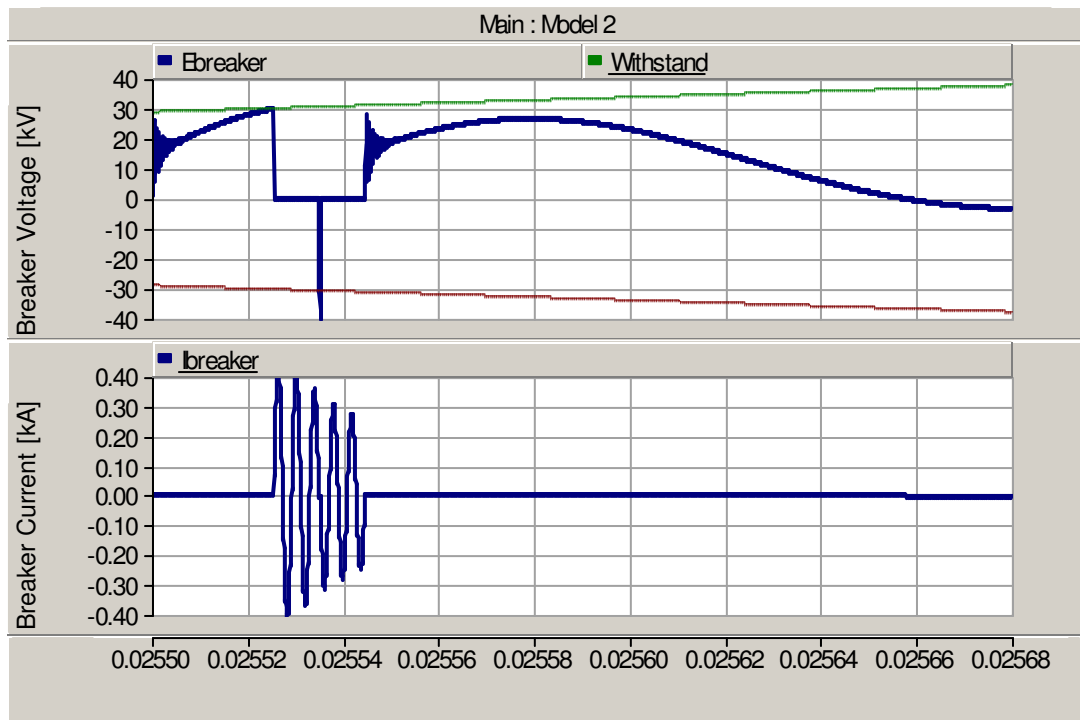


Fig 20: Successful interruption of current

The previous diagrams have shown the process of opening, while Fig 21 shows the closing operation. The problem of pre-strikes is shown to occur in such a case, and the number of pre-strikes is dependent on the speed of closing (or more specifically, on the profile of the cold gap withstand of the gap). In some closing operations, again depending on the speed of operation, it can be such that the arc starts conducting the power frequency current before the contacts come into galvanic contact. This is not a problem as such, and rather it is just a comment that there is a distinct possibility for this to occur.

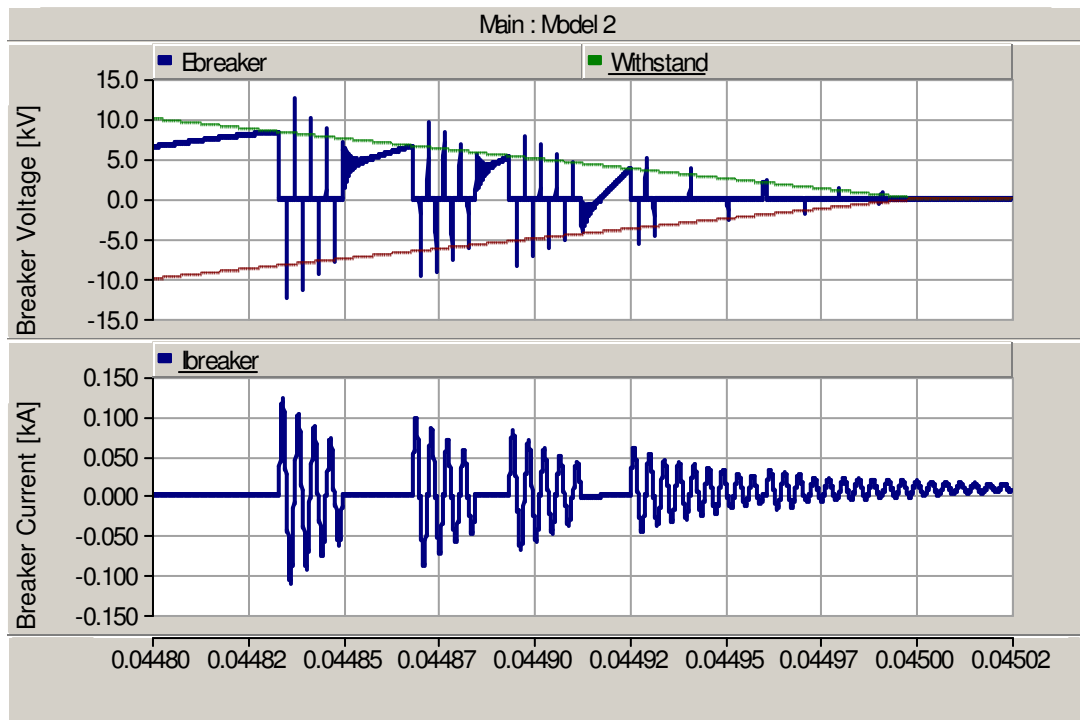


Fig 21: Pre-strikes during a closing operation

An unsuccessful interruption refers to when the CB is not able to break the current at the first natural zero. Fig 22 shows this scenario, with Fig 23 displaying a zoomed-in view. Because of the arc inertia, the high frequency current after several re-ignitions may not be easily broken, and hence a time will come when there will be no more zero crossings. The circuit will then have to wait for the next natural current zero to interrupt the arc, and this next natural current zero will usually be free of the high frequency zeros present before. This effect is usually important in 3-phase systems, whereby unsuccessful interruptions as seen here can cause another pole to operate before the first pole to open has a chance to interrupt the current. The advantage is that even though the arc is required to conduct for an extra half cycle, the voltage withstand of the breaker will be so high that it should be able to prevent further breakdowns when the arc is finally extinguished.

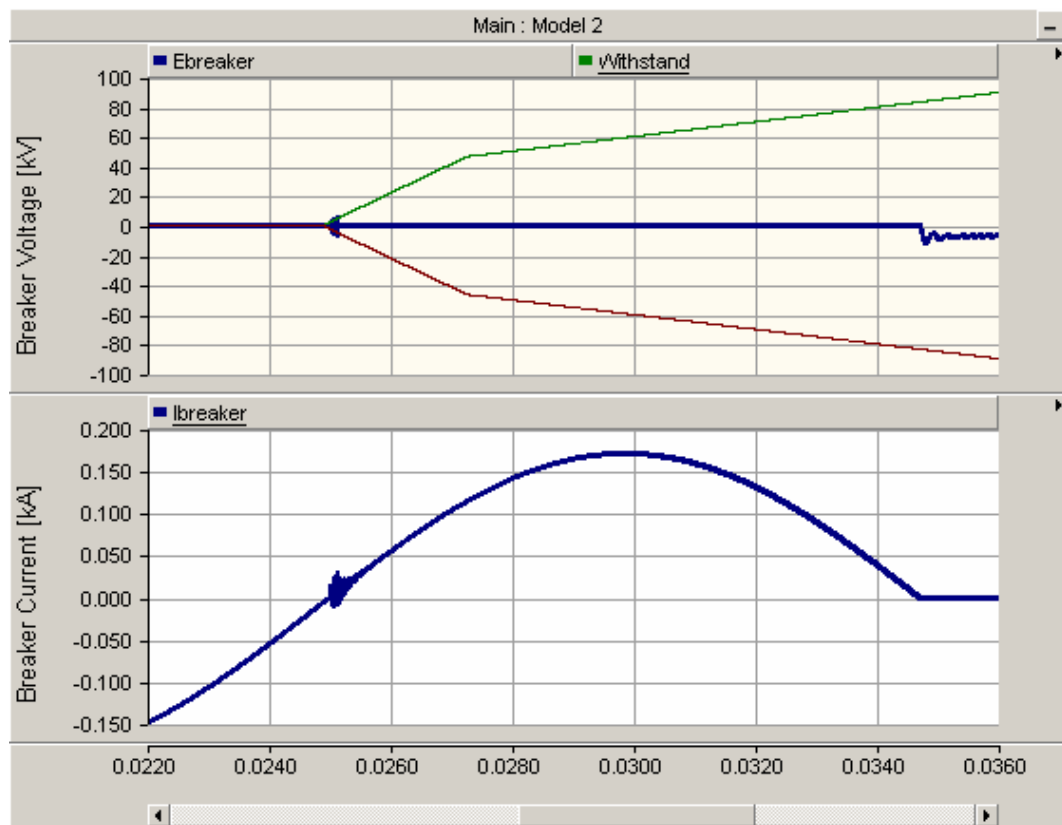


Fig 22: Unsuccessful interruption of the high frequency current

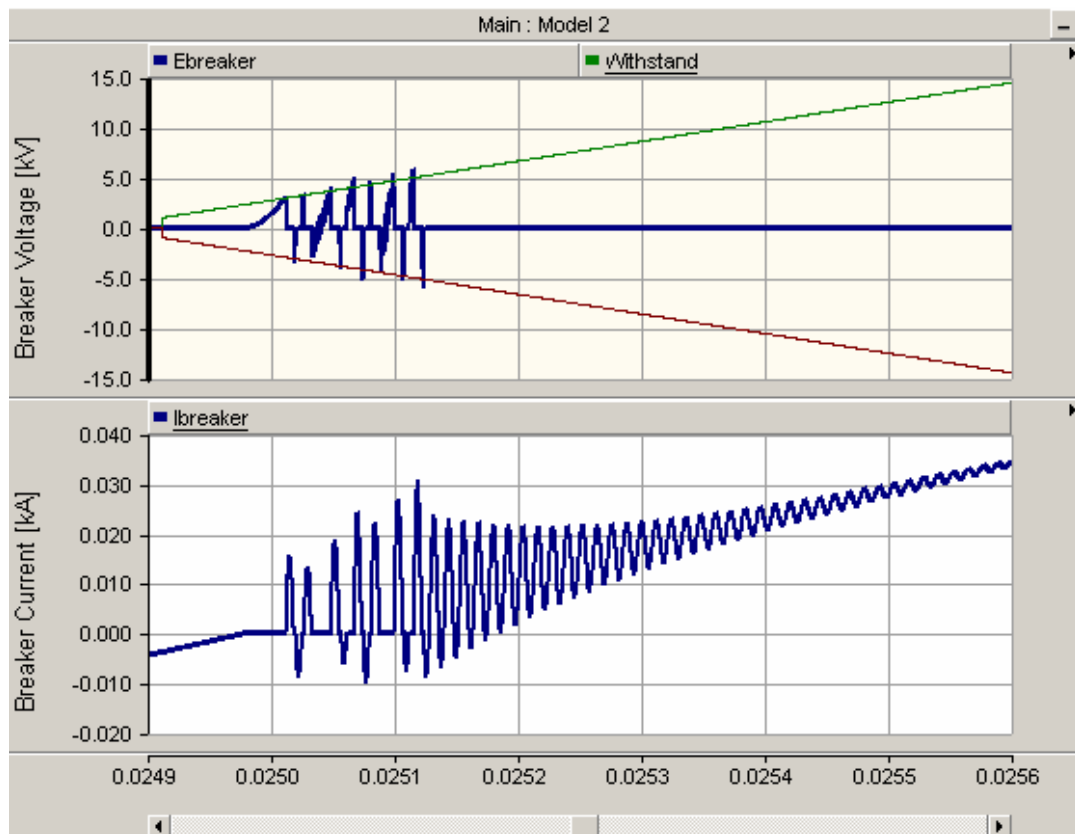


Fig 23: Zoomed in view of the above diagram



3.5.3 Problems with the model

One fundamental issue with this model is in the choice of time step. Since the highest frequency component that is to be expected is 1.8MHz, by using the Nyquist criterion a solution time step of smaller than $0.27\mu\text{s}$ is required. This increases the computation time, but can also lead to undesired effects. Fig 24 describes such an effect. The graph with the larger time step almost completely misses the high frequency component in its solution, which leads to inaccuracies. It would appear that the high frequency current is less severe than in the actual system (200A vs 380A) which may lead to under dimensioning of the vacuum gap and/or fuses.

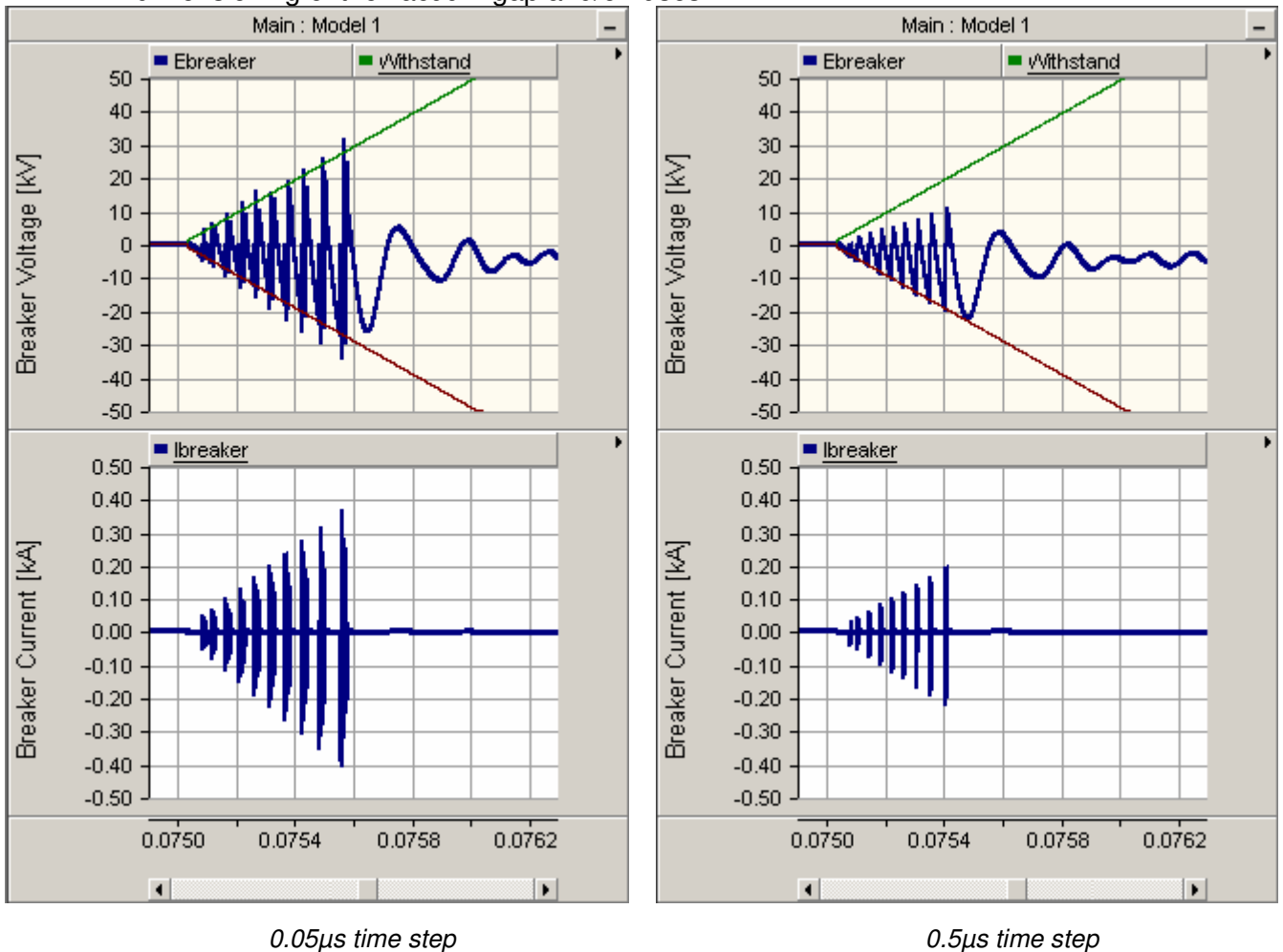


Fig 24: Comparison of the same model with different time steps

If and when the finite current chopping at the first current zero is taken into account, a situation may arise whereby the incorrect choice of time step causes the incorrect representation of the current. Consider Fig 25 where the wrong time step selection of $0.5\mu\text{s}$ causes the current to have enough zero crossings that allows the model to extinguish the arc (on the right). The situation on the left is the correct situation which appropriately models the 1.8MHz component present in the current. The result on the right will then incorrectly show that re-ignitions can occur.

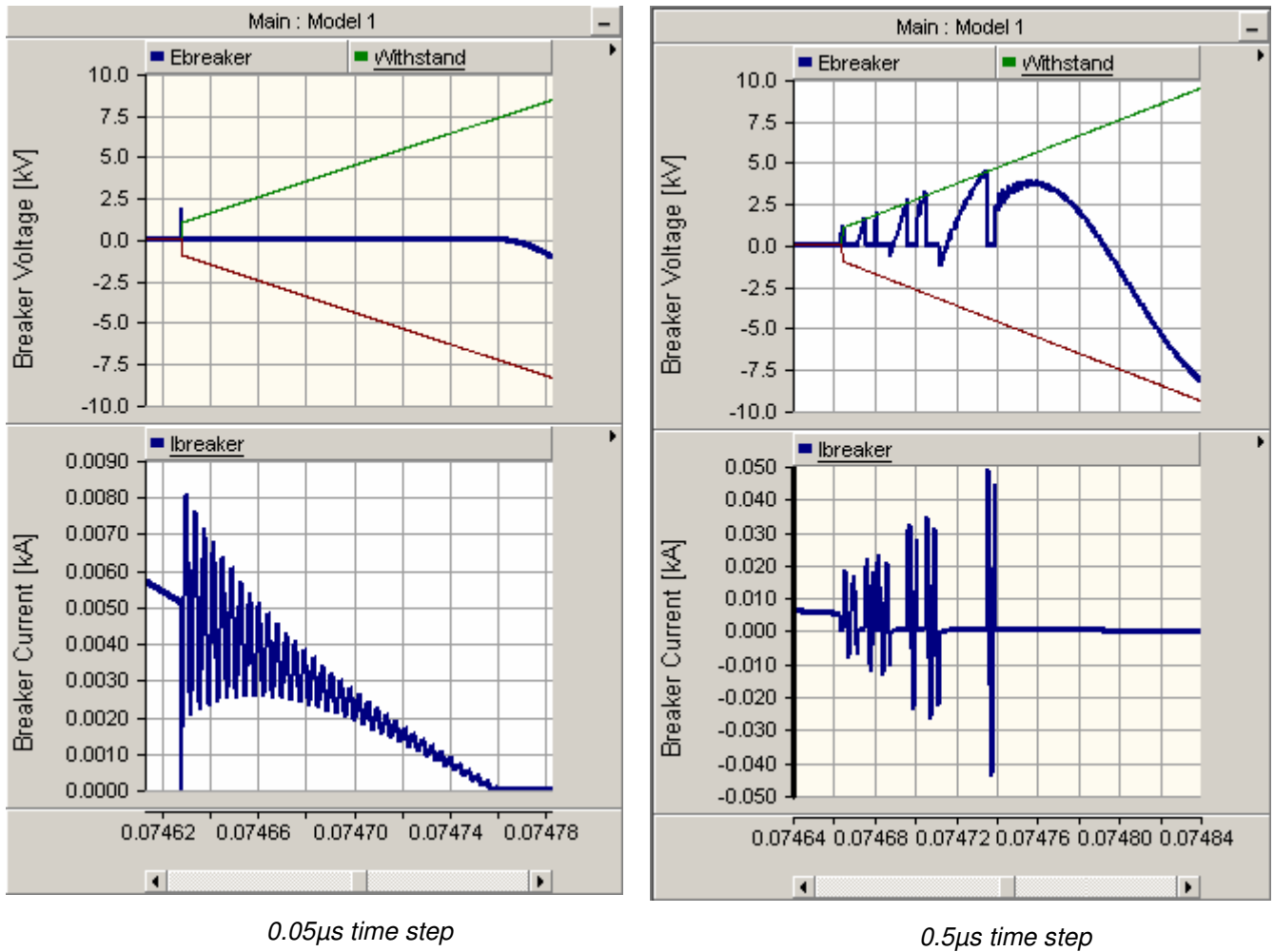
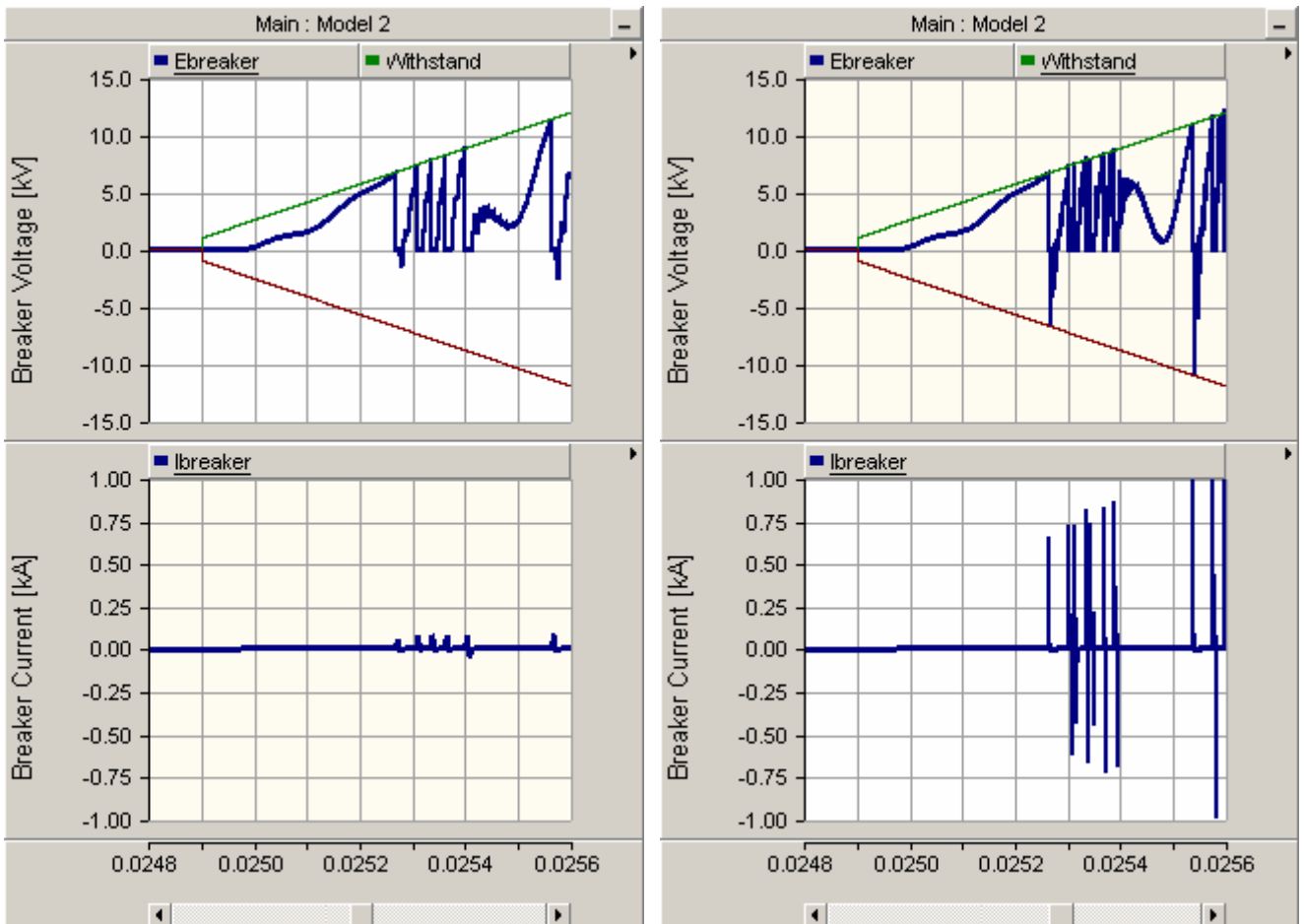


Fig 25: Comparison of the same model with different time steps with a finite chopping current

3.6 Operation of VCB with full cable model (reflections)

The systems under investigation are connected with cables, and hence it is important to be able to study the reflections accurately. For comparison purposes, the VCB is used on two models: one with an equivalent π -section installed, and one with a reflective cable model installed. The equivalent π -section is not calculated, but rather solved by PSCAD v4.2, as this gives more accurate results and includes the effects of the shielding which are not as easily predicted with a simple π -model. The results are now shown in Fig 26 for both models. It is clear that the reflections in the line cause additional oscillations in the system, and the effects of these extra oscillations are now examined in detail.



Equivalent pi section

Complete cable model

Fig 26: Equivalent pi section vs. the complete cable model

The cable dimensions used in PSCAD are taken from [1] for a 10kV 800mm² cable. The reason for this is that the system under investigation is a 3.46kV single phase system as specified in [8] and [9]. The circuit as specified with the cable is shown in Fig 27 below.

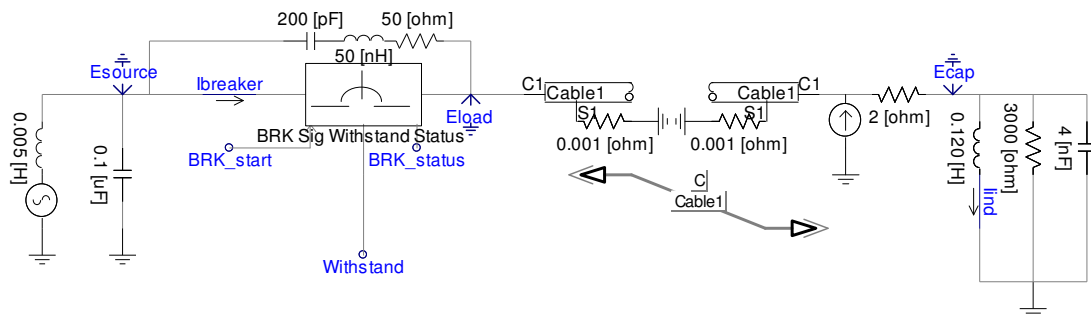


Fig 27: Test circuit used for the VCB with the cable model

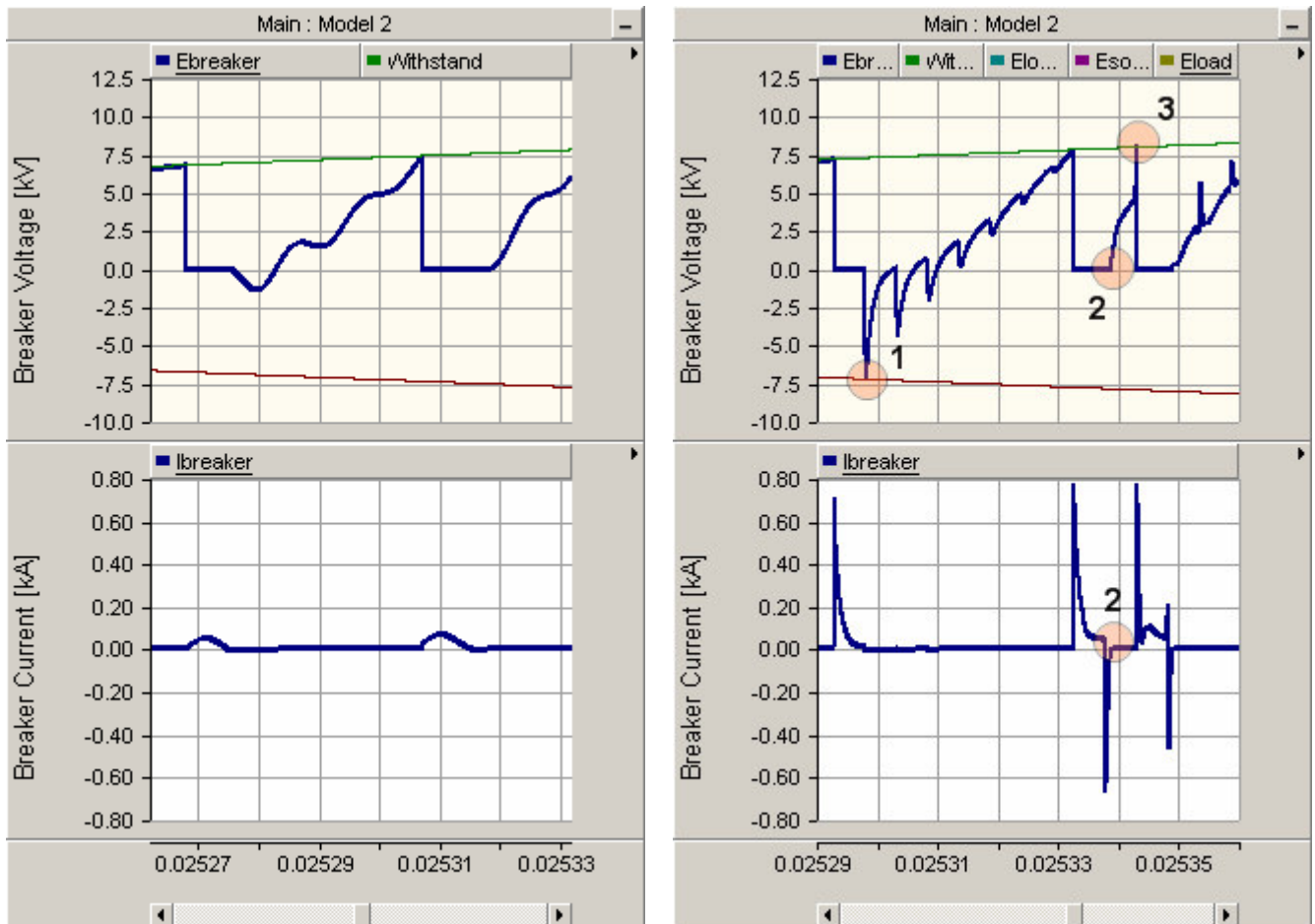


Referring to this circuit diagram, the voltage at the starting of the cable (E_{load}) and the end of the cable (E_{load2}) is shown below in Fig 28. The difference between the spikes denotes the travelling time of the wave which is $2.62\mu s \pm 0.05$ from the simulation. Using the equivalent circuit parameters however, a theoretical travelling wave speed of $210m/\mu s$ is obtained. For a 500m long cable the travelling time should then be roughly $2.38\mu s$. The discrepancy is due to the fact that the theoretical calculations are very simplistic approximations and do not take into account many of the effects that the cable model in PSCAD does, such as shielding.



Fig 28: Reflections on the cable

Furthermore, the current appears as a spike as opposed to a smooth current wave as expected in the equivalent π -model. This is explained by the fact that the voltage spike that enters the cable will initially see the surge impedance of the cable, and the current imitates the shape of the voltage wave at least at the very beginning. The important question however is to determine the effect of the cable on the VCB. Fig 29 shows a zoomed in version of Fig 28 for both models. The first voltage drop is experienced at different times in both models because of the time-varying effects of the cable model.



Equivalent pi section

Complete cable model

Fig 29: Zoomed in version of both models

There are two important points to discuss here. Point 1 shows the voltage spike that occurs because of the first breakdown (shown shortly after the beginning of the diagram). The first drop in voltage creates a travelling wave along the line, which reflects back after several μs . Subsequent reflections also cause further voltage spikes with decreasing magnitude, but it is apparent that after the travelling waves have settled, the voltage profile becomes similar to that of the π -section model.

Following the picture from left to right, a second breakdown now occurs in both diagrams, but what is interesting here is that because of the extra reflections introduced by the cable, the high frequency extinction occurs sooner than in the π -section model (at Point 2). Since the arc is now extinguished, the voltage across the breaker can now begin to increase. However, several reflections are still present in the system, and it so happens that a reflection from the second breakdown in the diagram causes the voltage at Point 3 to increase beyond the withstand limit. By looking at the two diagrams, it is clear that the equivalent π -model does not predict this extra re-ignition at Point 3, and hence the models differ in that regard.



Fig 30 now shows the pre-strike phenomenon during a closing operation. Obviously the reflections may cause extra pre-strikes to occur similar to what happens during the opening operation, but one important point to note is that even after galvanic contact, the breaker current can still see the effects of the pre-strikes because of the finite reflection time of the cable. That is one important difference that is noted here when using the cable model with reflections.

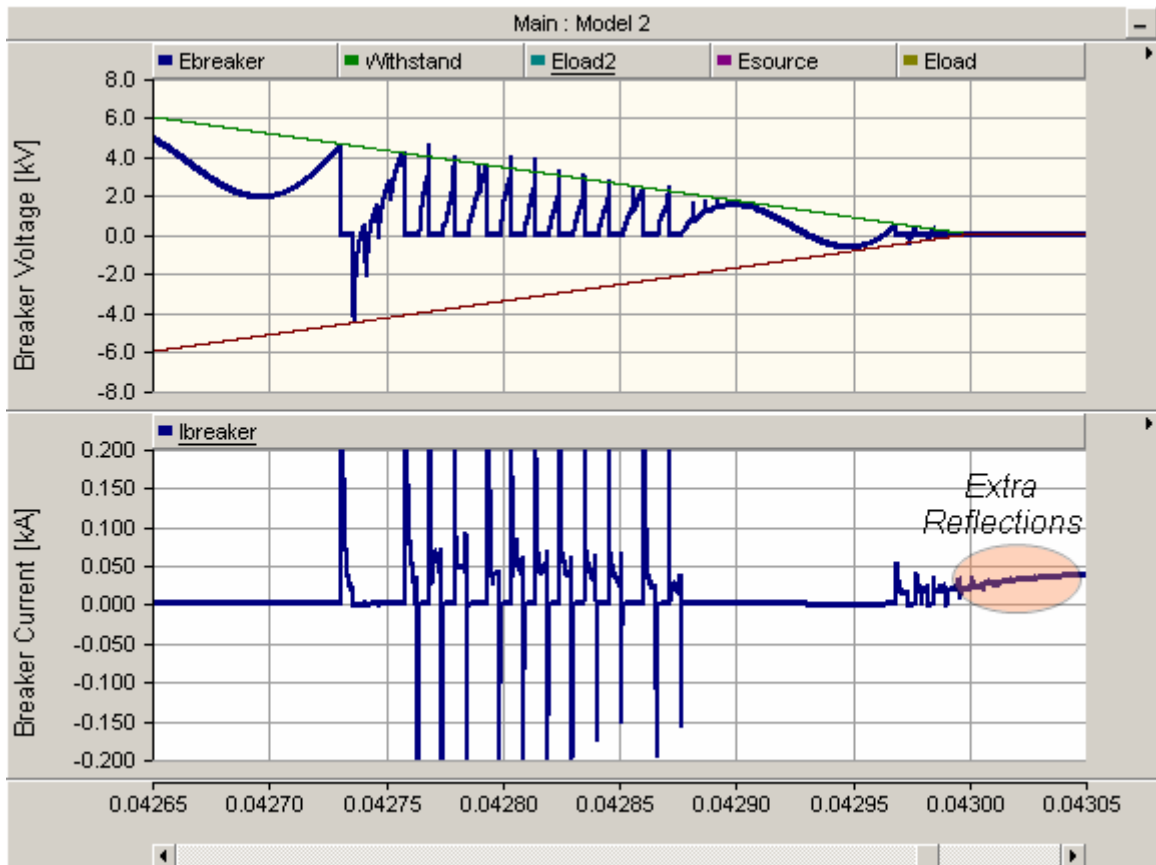


Fig 30: Pre-strikes using the cable model

3.7 Operation of VCB in a 3-phase system

For the purpose of performing a complete analysis, the VCB model is used in a 3-phase system because this model allows the user to see the effects of selecting a different opening time for each phase. Fig 31 below shows the test circuit for this purpose, with the components being exactly the same as those used in the single phase system.

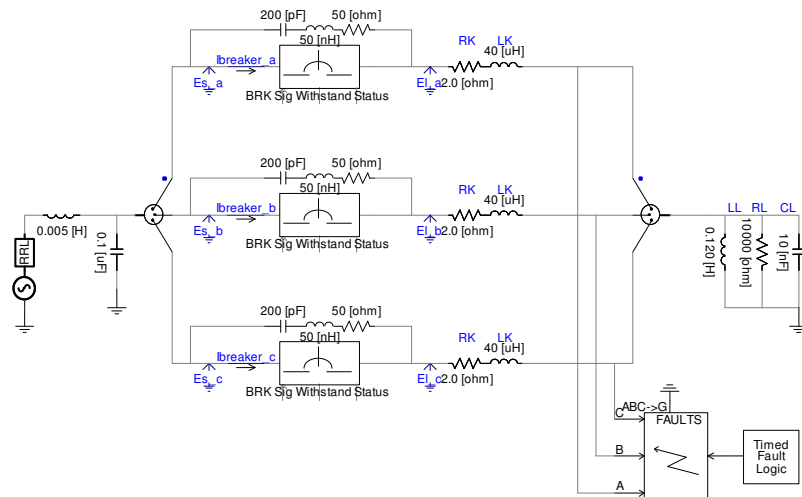


Fig 31: 3-phase circuit for testing the VCB

The results, at least on a small time scale, should be similar to those achieved using a single phase system. However, the goal of this simulation will be to determine what happens during a 3-phase fault (i.e. in the worst case scenario), and especially during a 3-phase ungrounded fault. The fault will be located as shown in the diagram, and the tripping instants will be chosen accordingly such that re-ignitions are observed.

Several interesting scenarios can be observed when discussing 3-phase systems. The simplest and best-case scenario (i.e. no re-ignitions) will be left out because the result is intuitive. In a 3-phase ungrounded fault, using synchronized breakers, the first pole to operate will be the first that reaches zero current first. In Fig 32 below, the first pole to break is A causing the system to become unbalanced. The current in phase A also affects the current in the other phases because it is an ungrounded fault and coupling is present, and hence the high frequency current in A is also present in B and C. The second and third poles will operate at the same time, roughly $\frac{1}{4}$ of a cycle after the first pole opens, to simulate a special case. Single pole operation is possible in synchronous switching systems.

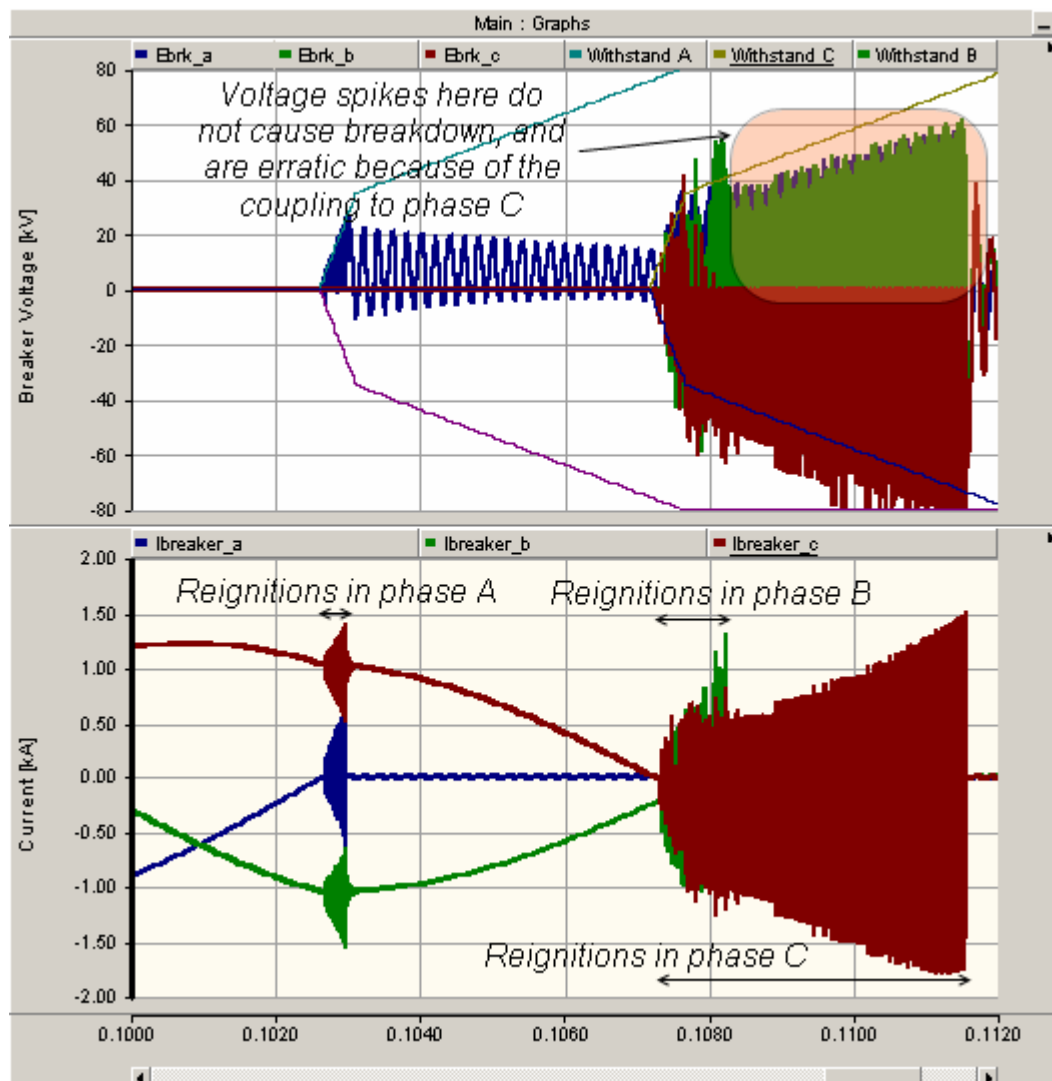


Fig 32: Breaking of a 3-phase ungrounded fault

After phase A successfully breaks the current following several re-ignitions, it is up to poles B and C to do the same. It would appear that phase C (in red) should break first because it reaches the zero crossing before phase B (in green). The recovery voltage in phase C can lead to re-ignitions in that phase which further cause an oscillating current to be coupled into phase B. This oscillating current in phase B begins to have zero crossings as well which causes phase B to break at an unnatural high frequency zero, thus beginning the voltage escalation in this phase as well. Depending on the frequency of the oscillations and other factors, it could occur that phase B breaks before phase C. As mentioned before, in a best-case scenario with no re-ignitions, it would be phase C that breaks before phase B.

Virtual current chopping is a phenomenon whereby the TRV and the currents can be coupled to other phases, thus starting unnatural zero crossings where they should not occur. These zero crossings could then cause another phase to break before the first pole to clear has a chance to do so. Fig 32 to some extent exhibits this property, but really this virtual current chopping is most severe when it occurs while the first pole to open is exhibiting re-ignitions.



3.8 Conclusion

This section described in detail the main phenomena present in VCBs and how modelling has been performed in other papers. A justified and simplified model, useful for studying transients further on in the report, was created, analyzed, and compared to actual results obtained in papers. For completion and validation, the operation was performed under different conditions such as with the use of a fully-reflective cable model and in a 3-phase system.



4 INDUSTRIAL SYSTEM

4.1 Introduction

At a certain steel mill, problems with the equipment were recognized and a team was sent to determine and fix the problem. Several technical reports on the solution were created at the time explaining the solution and the results in detail. The purpose of this section is to first simulate the industrial system as closely as possible to the actual system in question. Verification is performed by matching the measured results with the simulated results while attempting to explain any discrepancies.

An attempt will also be made to explain the purpose of this section with context to the wind farm section, which is the final scope of this document. It will be shown that a certain part of the industrial system matches a wind turbine configuration, and this information will be used to draw conclusions further on. A verification of the validity of the protection scheme used at the steel mill will also be performed.

4.2 Description and analysis of the industrial system circuit

4.2.1 Introduction

The industrial system has several distinct sections. The figure below, Fig 33, shows the industrial system to be simulated in its entirety. The section between busses *MottagnStnM1* and *StvU4* is the input power branch of the circuit. It consists of a 90MVA transformer along with several filters to remove the low-frequency harmonic disturbances. A TCR is also installed off of *StvU5* to compensate for the power factor required by the loads, but under heavy loading the inductive load will make it such that the TCR is not required.

Following *StvU4* there are two branches. The left branch is the high power branch which connects an arc furnace through a reactor and a transformer. An arc furnace is a fairly complex load because its power demand is always fluctuating based on the steel structure coming into the furnace. The right branch however is a lot simpler since the load is fairly stable (a ladle furnace which simply needs to hold the temperature steady) and because it demands less power. The transformer connecting the load on this side is coupled through a 75m cable to a CB which connects this cable to the bus. The CB is of the vacuum gap type, which is described in detail in section 3 of this report. This branch is good for studying transients due to re-ignitions since the short cable length approximates the type of system installed in a wind turbine, and several conclusions may be drawn.

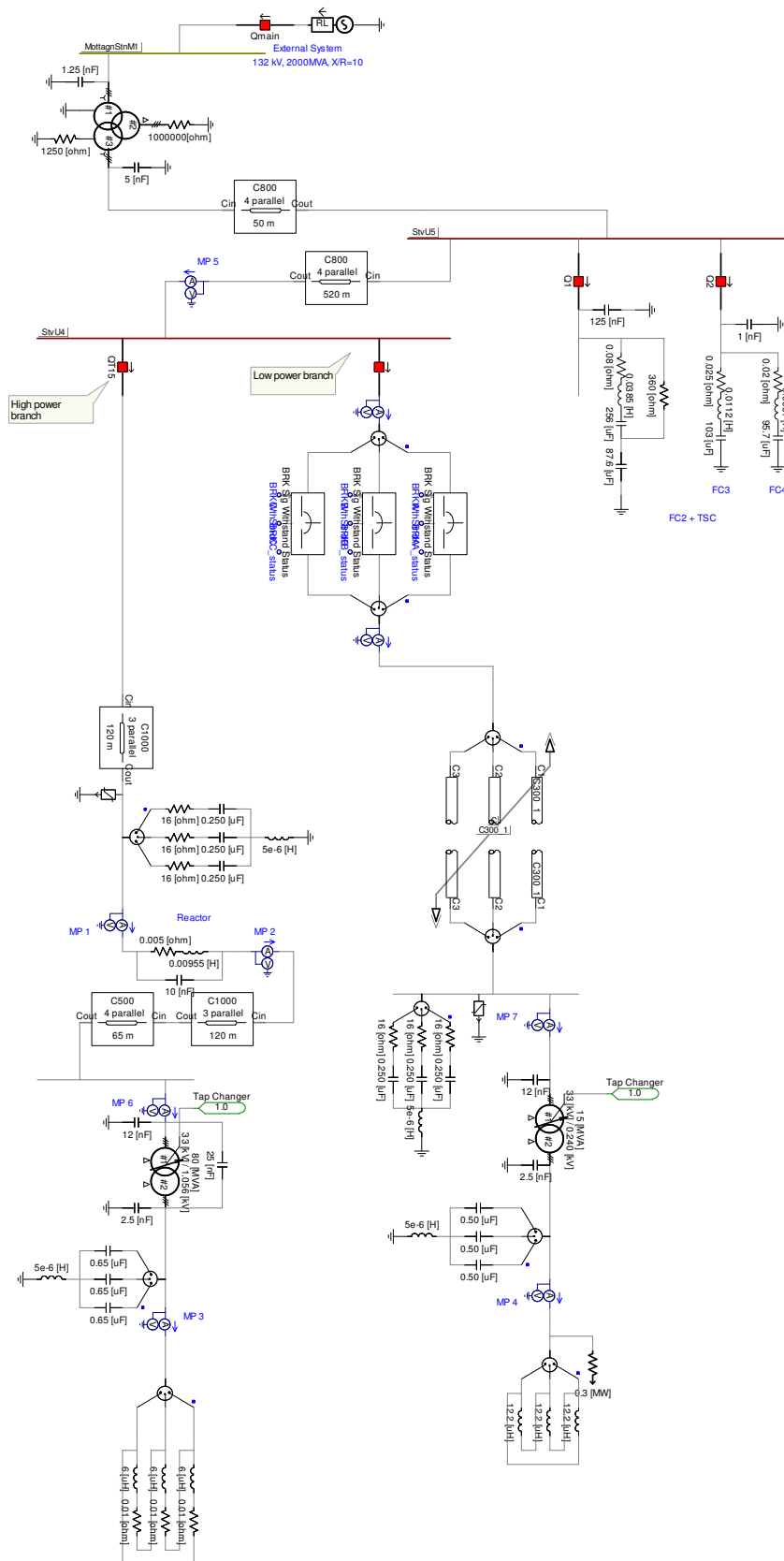


Fig 33: Industrial system circuit



4.2.2 Modelling the system

Using the given technical data in conjunction with [1] and section 2 of this report to get the dimensions for the cables in the system, an equivalent π -section model of the cables was also created for the purpose of speeding up simulations and tuning the final circuit.

For the sake of minimizing the computational complexity of the problem, several components were simplified. The TCR was replaced by simply an inductor and resistor in a star-connected fashion, and the surge arrestors connected in delta fashion were also removed from the model. Under loading however the TCR was removed completely because the load was already drawing too much inductive current. Most importantly however is the simplification of the arc furnace (EAF) and the ladle furnace as ideal resistive/inductive loads. According to the measured results, the current zero can be determined to be close to a voltage peak, implying that the arc furnace is mainly inductive.

The equivalent π -section model for the cables was created using a new function available in PSCAD v4.2 that automatically outputs the equivalent model when using actual cable data from [1] while matching the DC resistance and the capacitance described in the technical data. For information on how this model is created, see [5]. Of course, using π -sections implies that the effects of the reflections on the line will not be present.

Finally, because re-ignitions occur at high frequencies, it is important that all the possible capacitances and inductances are included in the model. For example, the capacitances across the transformer windings are shown, as well as the stray admittances at the busses. It will be shown however that some strays can be ignored in special cases, while others are vital for simulation.

4.2.3 The purpose of RC protection

During the initial analysis of the industrial system, it was discovered that re-ignitions during the opening operation of the breaker caused high frequency transients. As mentioned before, such oscillations can lead to voltage escalation and produce a multitude of re-ignitions.

One solution is to limit the rate of rise of the voltage across the VCB through the use of surge capacitors. Another solution is to use RC protection, which also limits the rate of rise, but most importantly removes the high frequency current zero crossings that occur after the first re-ignition. This allows the arc to conduct long enough (for an extra half-cycle) for the CB to produce enough withstand across the breaker such that no further breakdowns occur once the arc is broken at a natural zero.

The RC protection solution is used here. A capacitor of $0.250\mu\text{F}$ is used in series with a resistance for each phase. The resistor is chosen such that the current's high frequency components do not cross the zero point, and thus not giving the arc a chance to extinguish. Fig 34 shows a graph of the currents with different values of resistances used and the case with no RC protection. The 38Ω resistor does the best job of preventing high frequency zero crossings. For comparison, the case with no RC protection shows that many high frequency zero crossings can occur thus creating more re-ignitions across the gap than with protection installed.

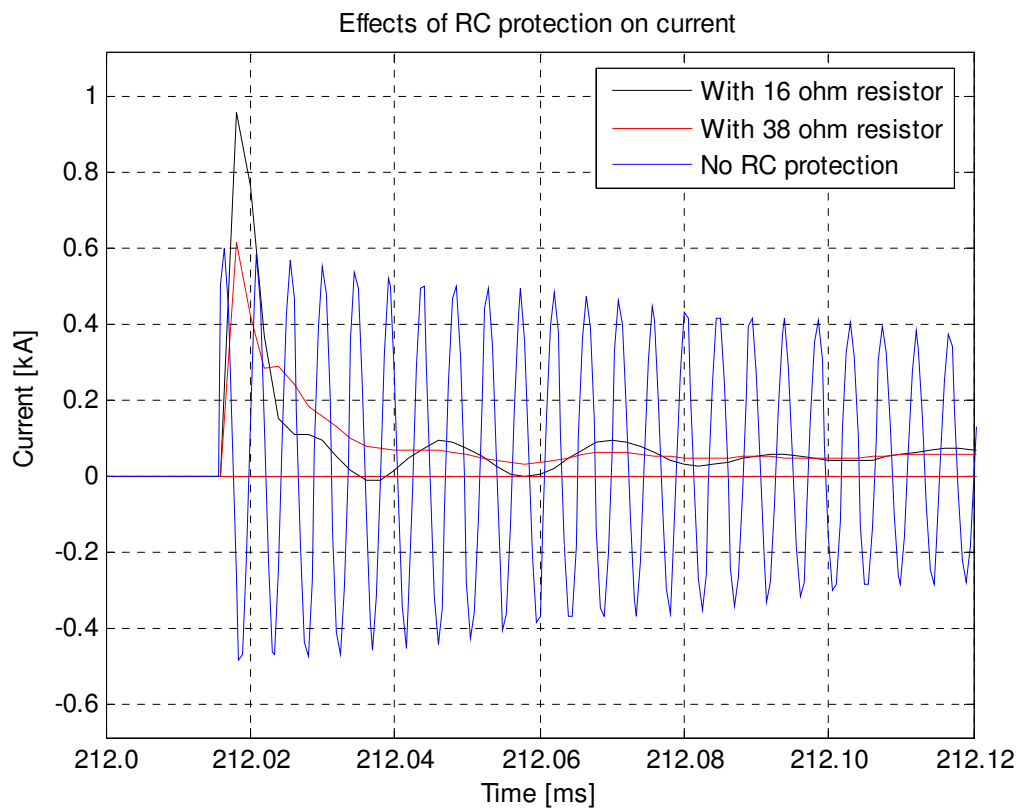


Fig 34: Effects of RC protection on current (low power branch)

In Fig 35, the voltage and the current for the CB without RC protection is shown. Note the multitude of re-ignitions present during the opening operation. The measurements are performed on the low power branch, but the principle remains the same for both loads.

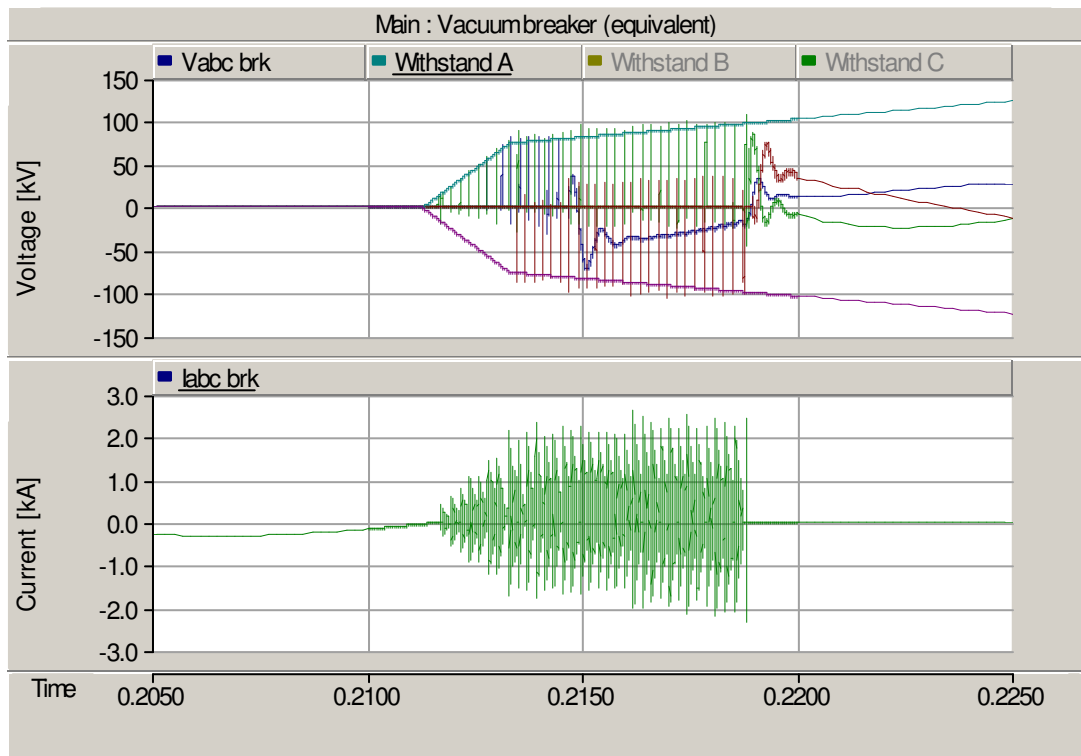


Fig 35: Voltage and current at the breaker without RC protection

Note now what happens in Fig 36 when RC protection is installed with $R = 38\Omega$ and $C = 0.25\mu\text{F}$. In this case, the RC protection works successfully by allowing only one re-ignition to occur by preventing zero crossings. The current through the arc is allowed to continue until the next natural current zero occurs when the voltage across the breaker can be withstood.

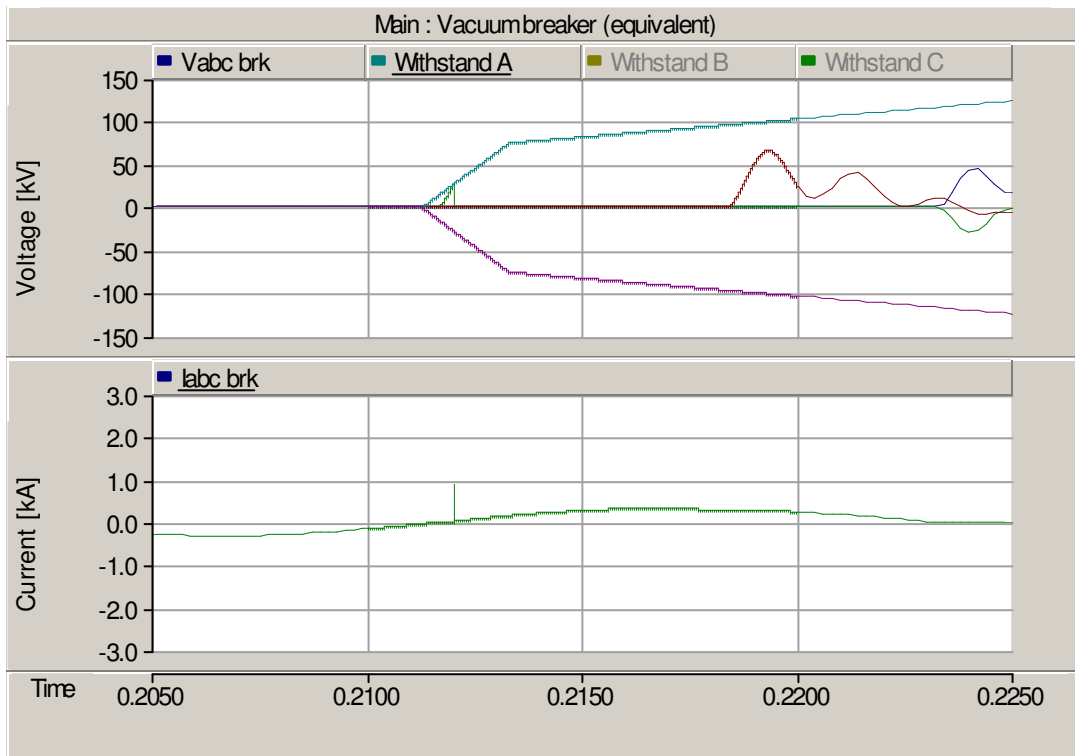


Fig 36: Voltage and current at the breaker with RC protection

The above diagrams actually dealt with the ideal system where no coupling exists between the phases. In reality, the mutual coupling between the phases will cause more re-ignitions than expected because the current in one phase will cause another phase to interrupt before it reaches its first natural current zero (virtual current chopping). This is a problem and depends on factors such as how close the two phases are to each other. One example of a strongly coupled system is shown below in Fig 37 with the proper RC protection installed. The RC protection does a good job of removing the high frequency zeros, but it is the virtual current chopping that causes more re-ignitions than expected. This cannot be helped, but it demonstrates that the analysis done on the uncoupled system is still valid.

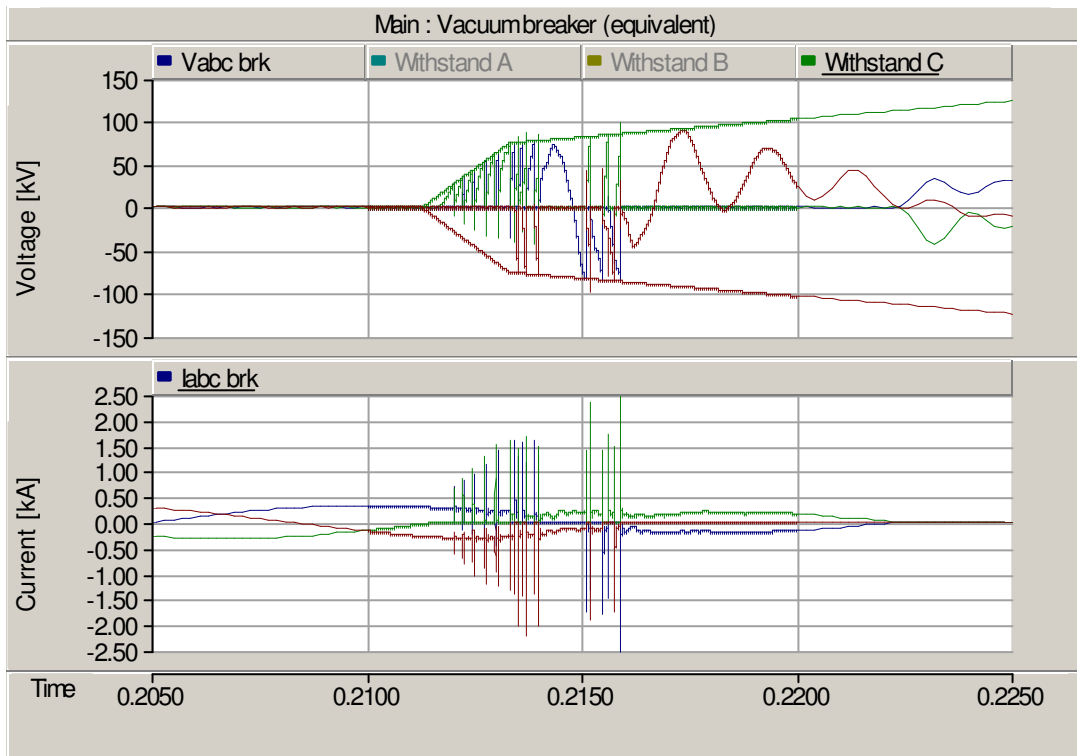


Fig 37: Voltage and current at the breaker with RC protection (coupled system)

For completeness, the analysis is also performed on the system with the reflection model of the cable installed, shown in Fig 38. It shows that the reflections do not have an impact and that it is not as strongly coupled as expected. This was dealt with in section 0.

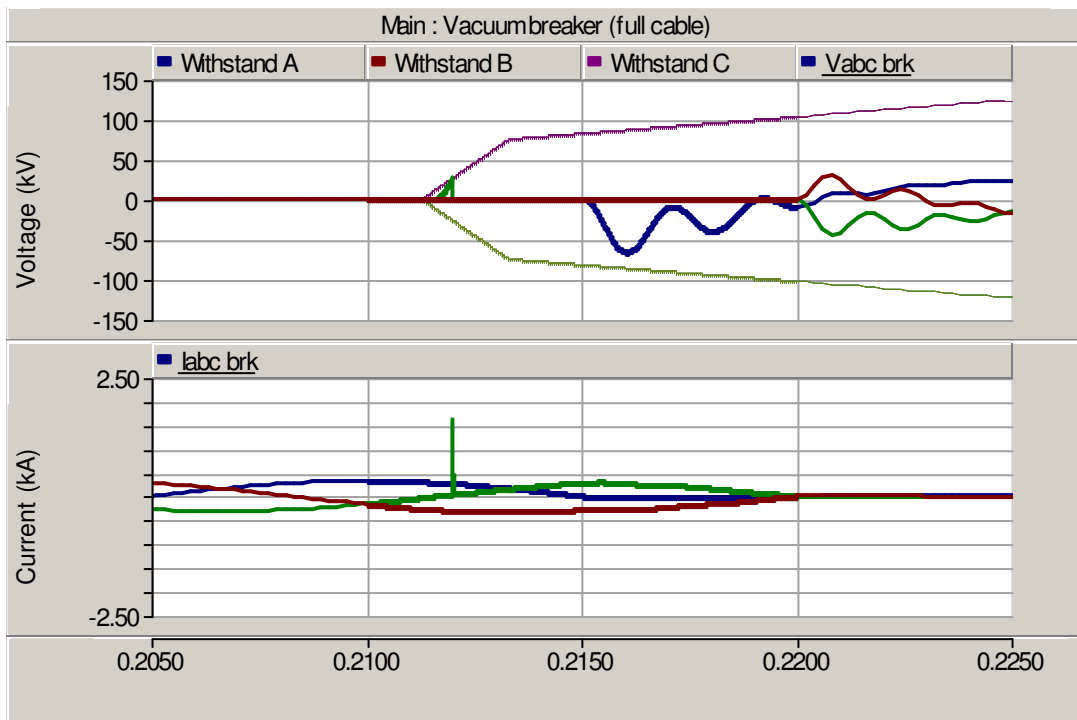


Fig 38: Voltage and current at the breaker with RC protection (full cable model)



4.2.4 Frequency response

4.2.4.1 High power branch

The high power branch is fairly complex, but it can still be simplified to a few components and thus analyzed using a frequency sweep. The frequency spectrum below in Fig 39 is for the case with π -sections installed instead of the cables.

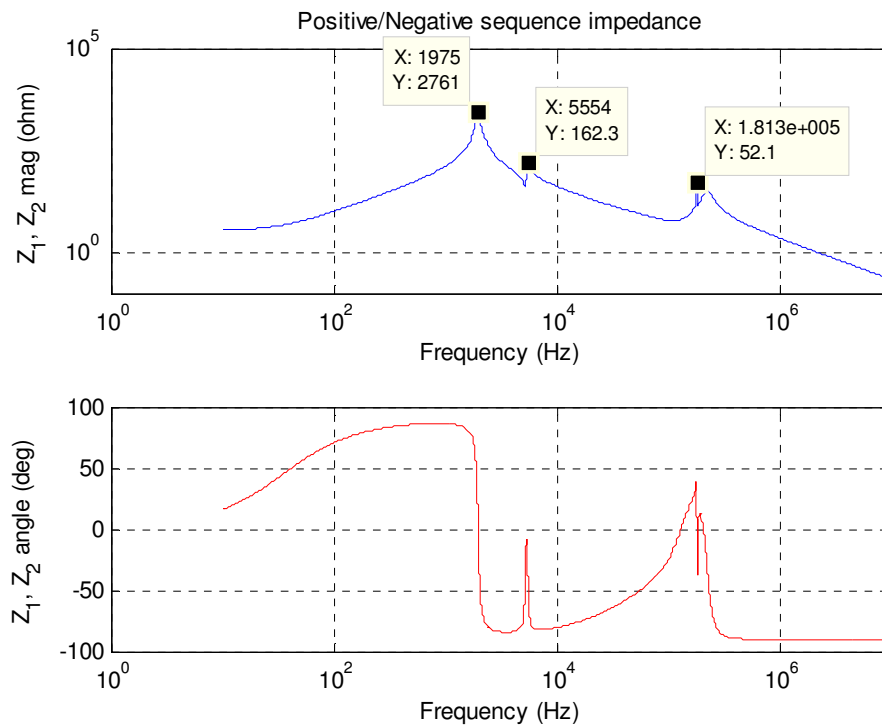


Fig 39: Frequency response - π -section model (high power branch)

The interesting frequencies in this case are roughly 2kHz, 5.5kHz, and 181kHz, but it is such that the 2kHz frequency is fairly dominant in the waveform.

The spectrum becomes far more complicated when considering the cable reflections since there are several cables on the same branch, making it harder to at least analytically determine the resonating frequencies. The figure below, Fig 40, shows the frequency spectrum with the cables installed. The low frequency peaks still lie around 2kHz and 5.5kHz, but the high frequency peak has been shifted quite a bit.

At high frequencies approaching 1MHz, resonating branches that cause frequency spectrum spikes are caused by the reflections in the cable. The high peak in the π -equivalent frequency plot (Fig 39) is caused by energy interchange between the equivalent capacitances and inductances used to create the π -sections. However, these π -equivalent sections are only valid for lower frequencies since they are only used to simulate steady-states and not high frequencies. Hence, Fig 40 is the actual response and the resonating peaks after 1MHz are to be expected, while Fig 39 is only good for approximating relatively low frequencies.

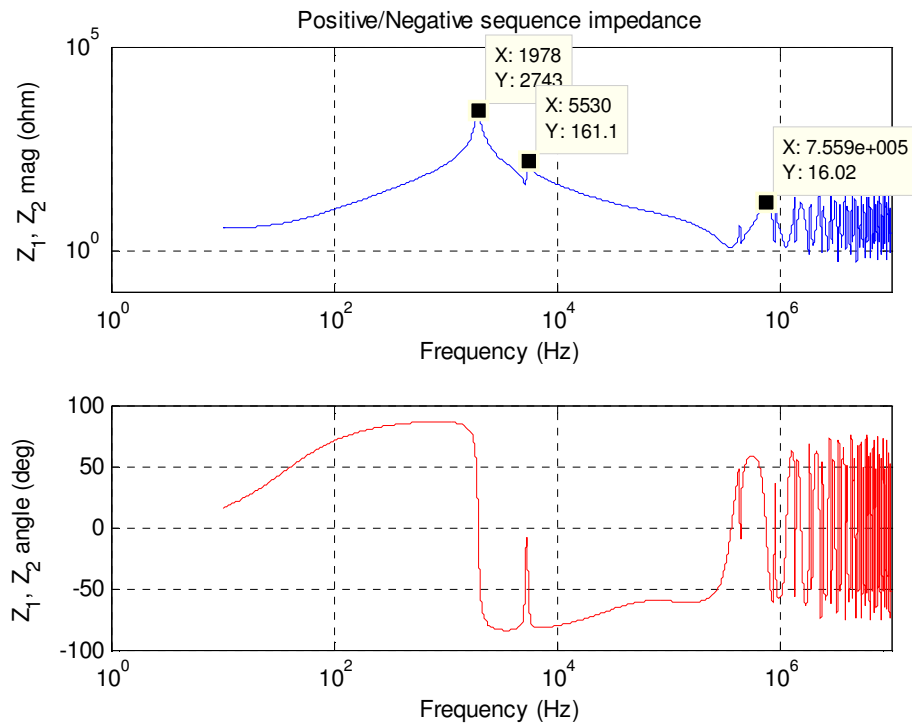


Fig 40: Frequency response – full cable model (high power branch)

Under normal circumstances, these are the frequencies that are to be seen during transient events, such as during the opening of a CB. However, the above frequency response diagrams deal almost exclusively with the single phase or uncoupled case. When coupling between multiple phases is apparent, such as through the cable coupling, the frequencies will change. So, while these results are accurate for uncoupled systems, it only provides a good approximation for coupled system. Examples will be shown to further clarify this claim.

4.2.4.2 Low power branch

The low power branch is now examined. The positive sequence impedance is plotted as a function of frequency in Fig 41.

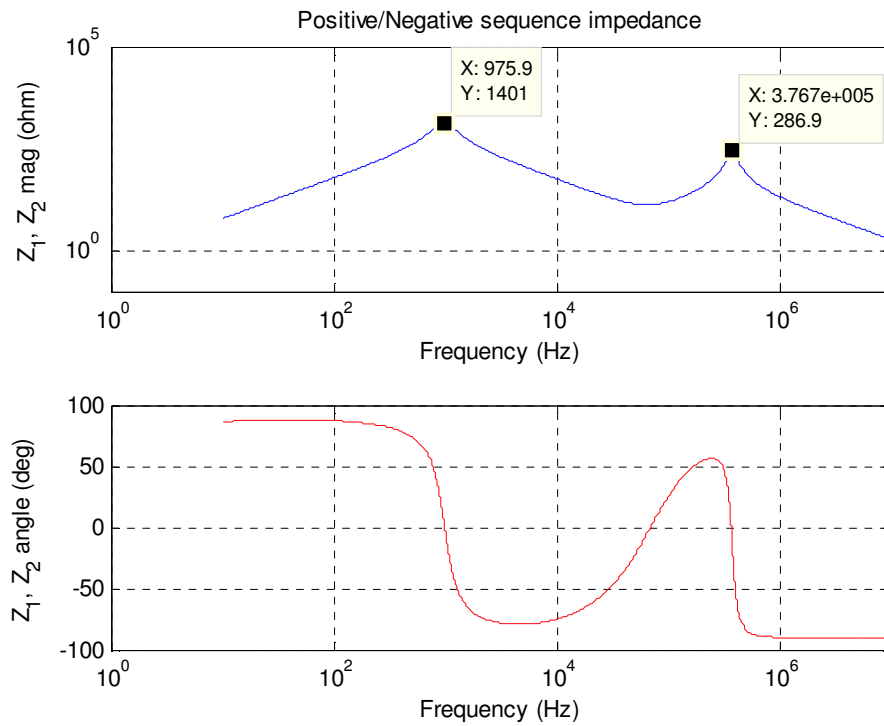


Fig 41: Frequency response - TT-section model (low power branch)

Here it can be seen that the interesting frequencies are roughly 1kHz and 380kHz. Similar to the analysis above, the frequency response with the full cable models installed is shown in Fig 42.

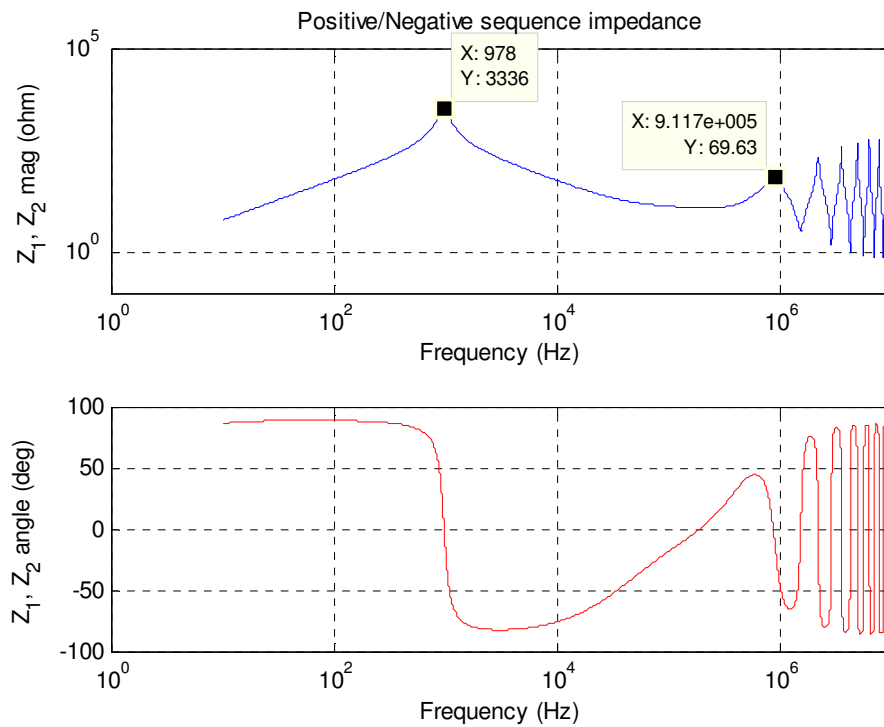


Fig 42: Frequency response – full cable model (low power branch)



The first frequency still remains at around 1kHz but the second frequency shifts quite a lot. The reasoning is the same as on the high power branch, but what is more obvious here is the periodicity of the high frequency zeros and poles in Fig 42 after 1MHz. There is in fact periodicity in Fig 40, but it is not as obvious there since this low power branch has only one cable while the high power branch has several. The peaks in the frequency plots come at very distinct frequency intervals depending on the length of the line.

4.2.5 Coupling between phases

In section 2 it was discussed that high frequency components on one cable will readily couple into its own shield rather than into the other two phases in the system. This further implies that when high frequency events occur, it will be very hard for virtual current chopping to occur, since the high frequency current cannot induce enough change in the other two line currents to cause an early interruption in those phases.

The discrepancy however is that although the simulated model does not predict virtual current chopping, it does exist experimentally as verified in the actual measurements. For the frequency of interest which lies around 800Hz, it is apparent that most of the current gets coupled back into its own shield as predicted by Fig 8, which is consistent with the simulated results.

The question is now, how does virtual current chopping occur. Somehow the high frequency current in phase A must have a path into the other phases somewhere outside the cable (since it's apparent that the cable cannot provide the necessary coupling). One way to achieve this is to look at the non-idealities in the system. Cables that connect, among others, capacitors to the bus will have stray inductances. Similarly, the grounding plane with respect to the perfect earth will also have some inductance. Only a small value is required to show the effect of strays on the current.

Below, in Fig 43, two different simulations are performed; one without stray inductors (left side), and one with a stray inductance of 5 μ H at the RC protection and C protection grounding terminals (right side).

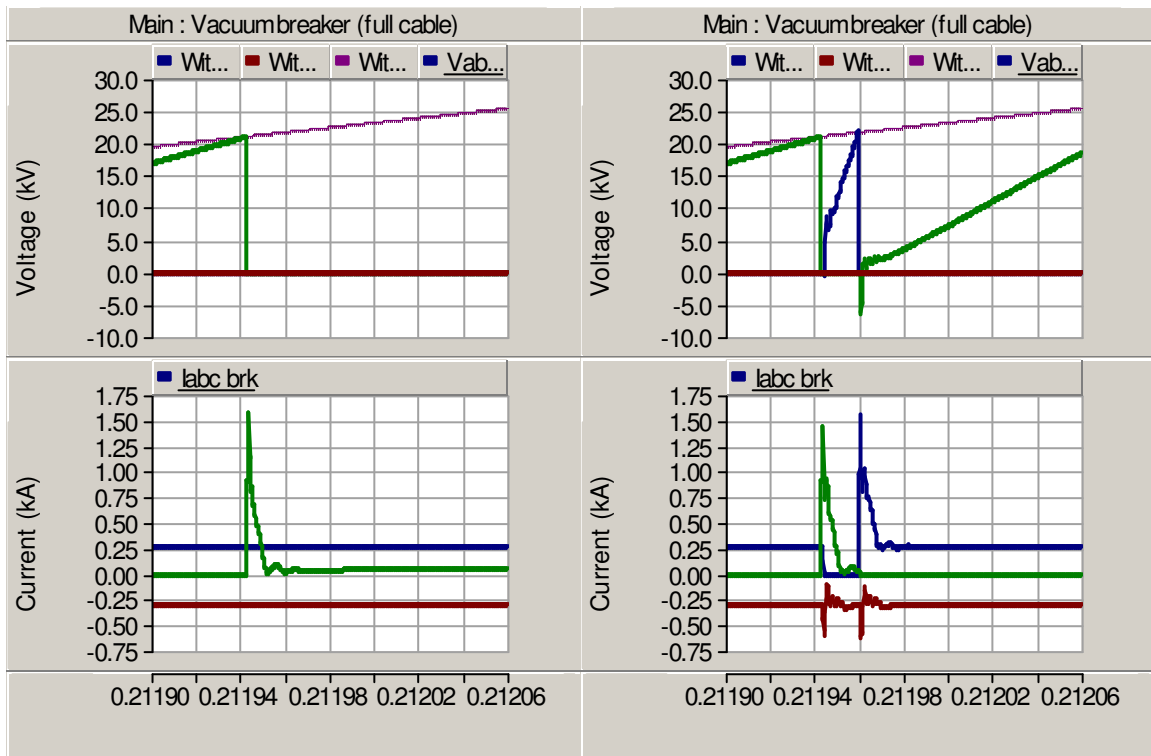


Fig 43: Currents across breaker without and with stray inductances

On both systems, the voltage drops at 0.21194s because the cold gap breakdown strength has been reached, which gives way to an oscillating current in phase A (green). On the left side of Fig 43 (without stray inductance), the current spike produces no currents in the other two line currents (red and blue) because there is no possibility for the high frequency currents to couple into the other phases.

Now that a small stray inductance has been added, right side of Fig 43, the current in phase A couples into phase B (blue) causing a change in line B current. This change is so drastic that it causes the current in line B to go to zero and hence extinguish. This extinguishing of the arc allows phase B to increase the voltage across the vacuum gap, thus eventually leading to more breakdowns in this phase as well as phase A.

In the case with no stray inductances, the spike in phase A current did not have a chance to extinguish, but that is not the case with stray inductances installed. It is therefore crucial to put in the stray inductances so as to simulate the actual system. Observe now in Fig 44, in an expanded time scale, the difference between the two cases. The left side (with no stray inductances) only has one re-ignition, and the RC protection successfully protects the system by allowing the arc across the vacuum gap to conduct until the next natural current zero. The right side (with stray inductances) has several re-ignitions due to the virtual current chopping phenomenon.

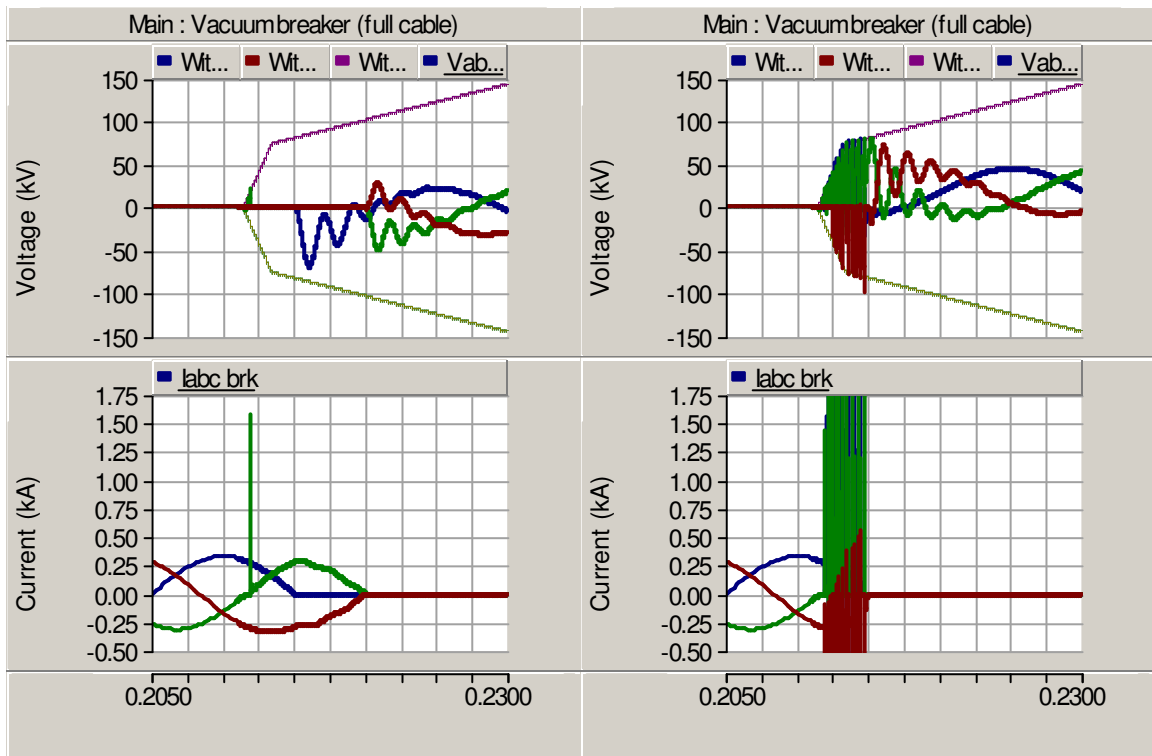


Fig 44: Currents across breaker without and with stray inductances (expanded)

The increasing magnitude of these re-ignitions causes a problem in the system, so big in fact that the arrester is called into action to keep the voltage level to a minimum. In Fig 45, at around 70kV, the impedance of the surge arrester decreases significantly thus effectively clamping the voltage. This simulation shows the necessity of using strays in the initial analysis of the system, since otherwise only one re-ignition will be observed even though there could be several.

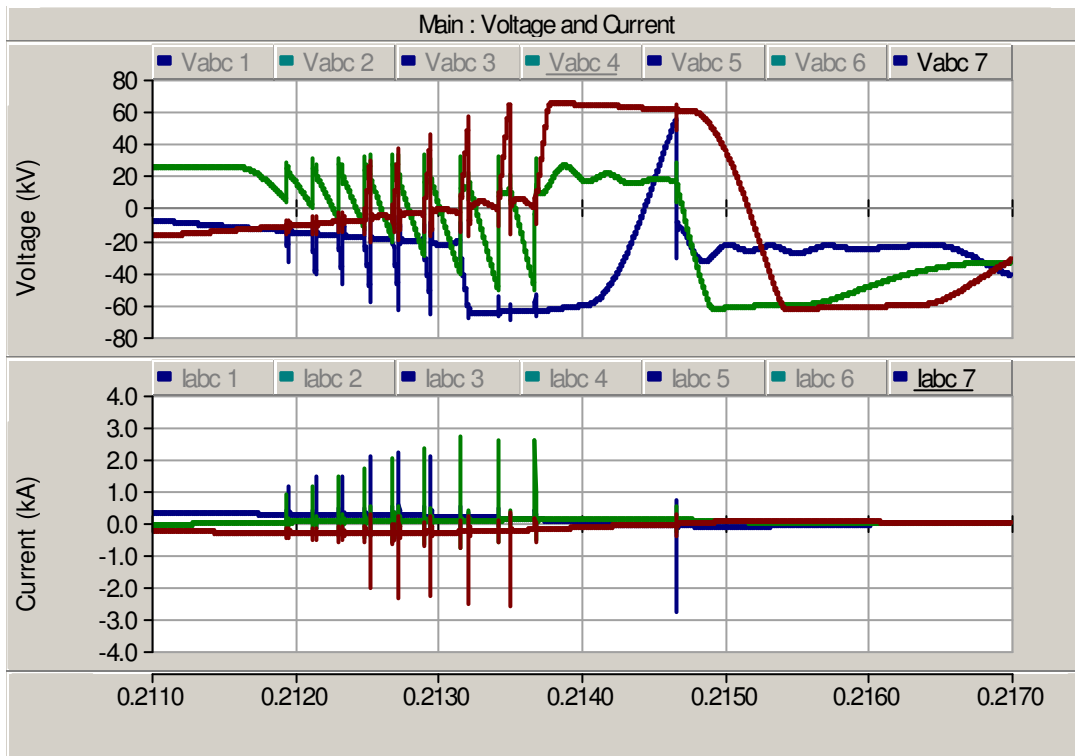


Fig 45: Voltage at MP7

4.3 Results and comparison

4.3.1 Purpose

The aim of this section is to compare the results from the simulated cases with those obtained from the actual physical system. Several examples will be given and discrepancies in the results will be explained as best as possible with regards to some of the features discussed in section 4.2.

One source of contention however, and thus held under scrutiny, is the value of the load. A value must be chosen such that it does not saturate the transformer and which at best matches the equivalent loading of the arc furnace at the time of CB operation. This was one of the main variables that had to be adjusted accordingly to produce the correct resonating frequencies.

4.3.2 Normal opening operation

4.3.2.1 High power branch

For the high power branch, a series resistor and inductor connected in a delta fashion is used to replace the arc furnace. The equivalent loading produces about 80kA on the furnace side, which is a fairly standard value for such a large arc furnace. The values were picked by trial and error, since the exact loading is unknown at the time of breaking, and thus a free variable in this simulation. In Fig 46 below, the measured results are reproduced, and in Fig 47 the simulated results are shown.

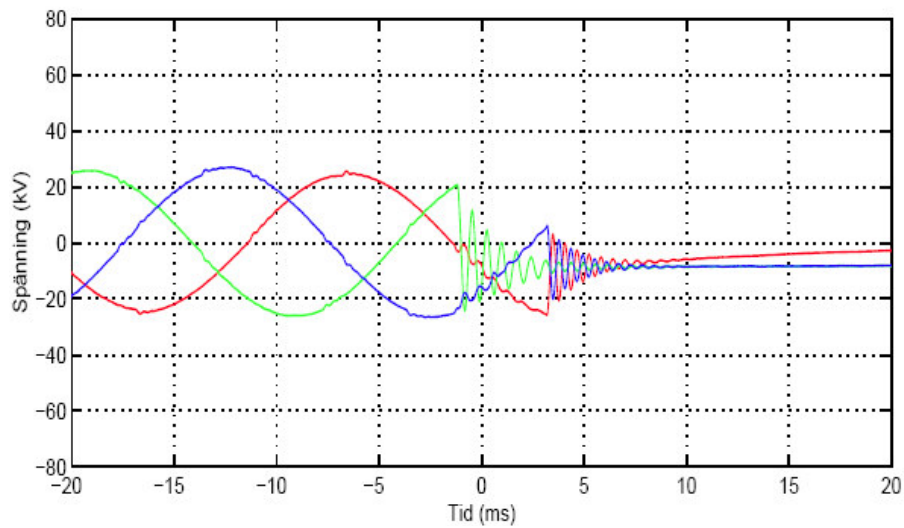


Fig 46: Voltage at MP1 with no re-ignitions - measured results

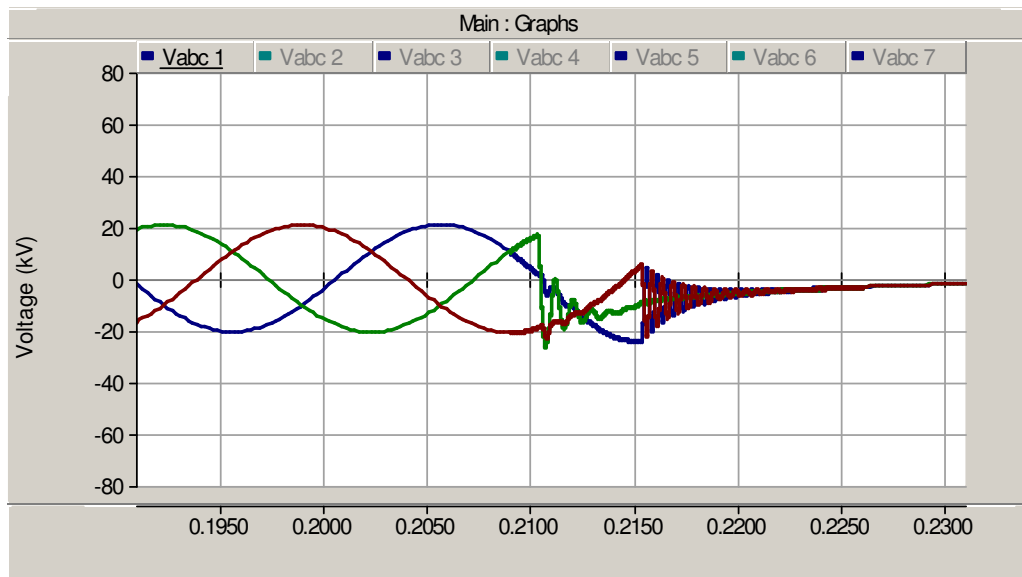


Fig 47: Voltage at MP1 with no re-ignitions - simulated results

According to Fig 40, the main resonant frequency sits at roughly 2kHz. However, this is the frequency that would be resonant after one phase has completely disconnected, since then two identical paths to ground exist for the current. When two phases are still conducting, the current in the first phase to break has an option to pass to the other two phases as well. This implies that the frequency plots determine earlier only predict the frequency after the first phase has interrupted, and only provide an order-of-magnitude estimation for the frequency of the first phase.



The measured results show two frequencies: one at 1.4kHz for the first phase to break, and 2kHz for the other two phases. The simulated results show a first frequency of 1.2kHz for the first phase and 2kHz for the other two phases. This is the best possible matching that can be achieved here. The discrepancy is due to the coupling between the phases, which in most cases is hard to predict exactly. For example, the physical layout of the cable has an impact on the impedance of the cable and the coupling between the phases and/or other parallel cables.

4.3.2.2 Low power branch

A similar opening operation was also performed on the low power branch. Fig 48 below shows the measured results and Fig 49 shows the simulated results. The frequency of interest for the measured case is roughly 800Hz which is verified for the simulated case, at least for the first frequency to interrupt. The second and third frequencies for the second and third phases to interrupt are quite different. The measured case still shows a frequency at around 800Hz, while the simulated case shows a frequency at around 1kHz. The discrepancy is somehow related to the coupling between the phases.

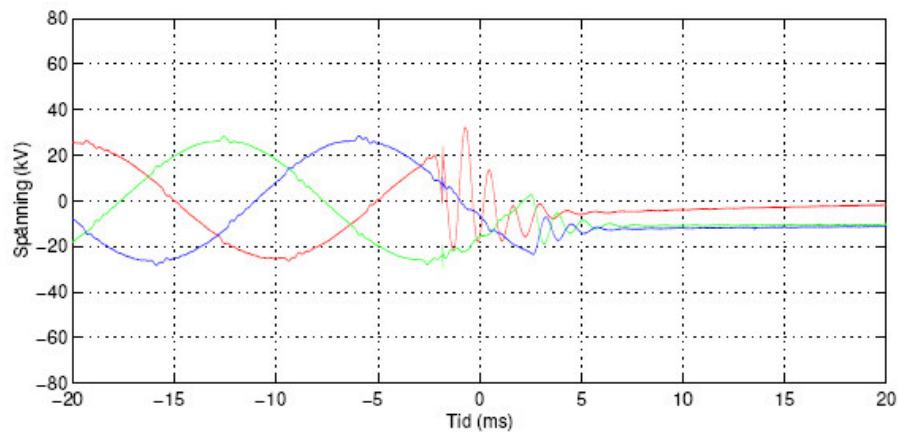


Fig 48: Voltage at MP1 with one re-ignition - measured results

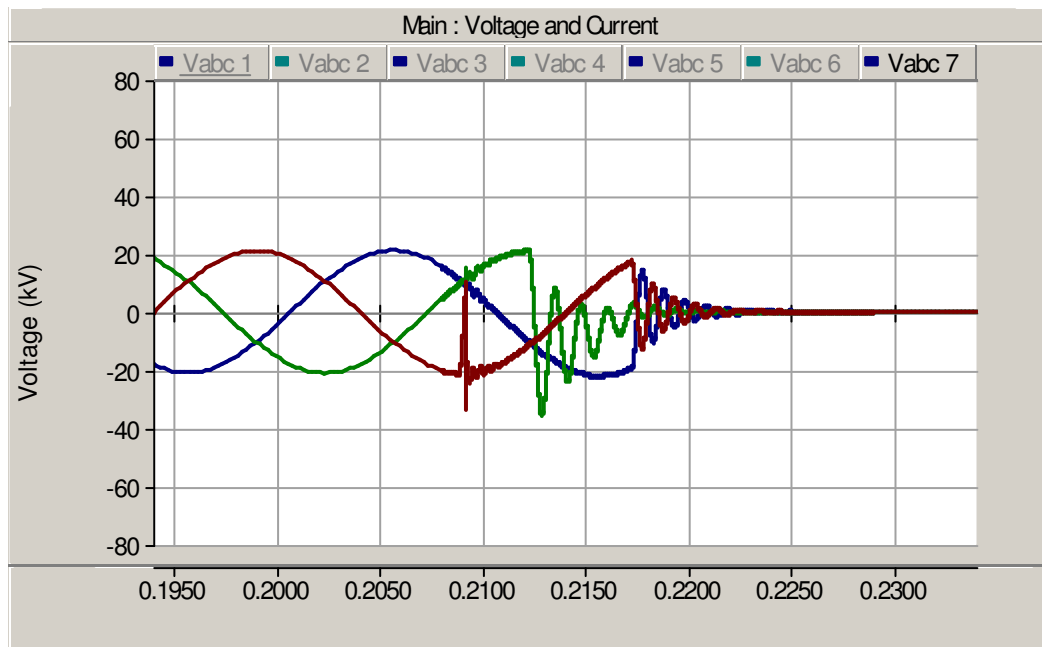


Fig 49: Voltage at MP1 with one re-ignition - simulated results

4.3.3 Opening operation with multiple re-ignitions

4.3.3.1 High power branch

Matching the graphs when it comes to re-ignitions is quite difficult especially on this branch where a lot of variables come in to play. The rate of rise for the voltage withstand across the vacuum gap can be estimated by looking at Fig 50, the measured results with multiple re-ignitions. This estimation is exactly that, an estimation, so some adjustments for the simulated case will have to be done. Fig 51 shows the simulated case where the load and the rate of rise for the voltage withstand have been adjusted to produce similar results.

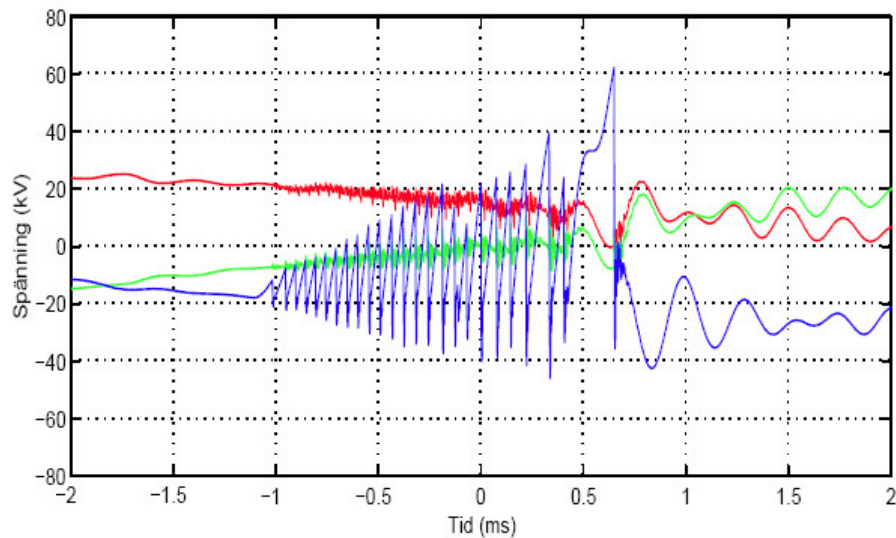


Fig 50: Voltage at MP1 with multiple re-ignitions – measured results

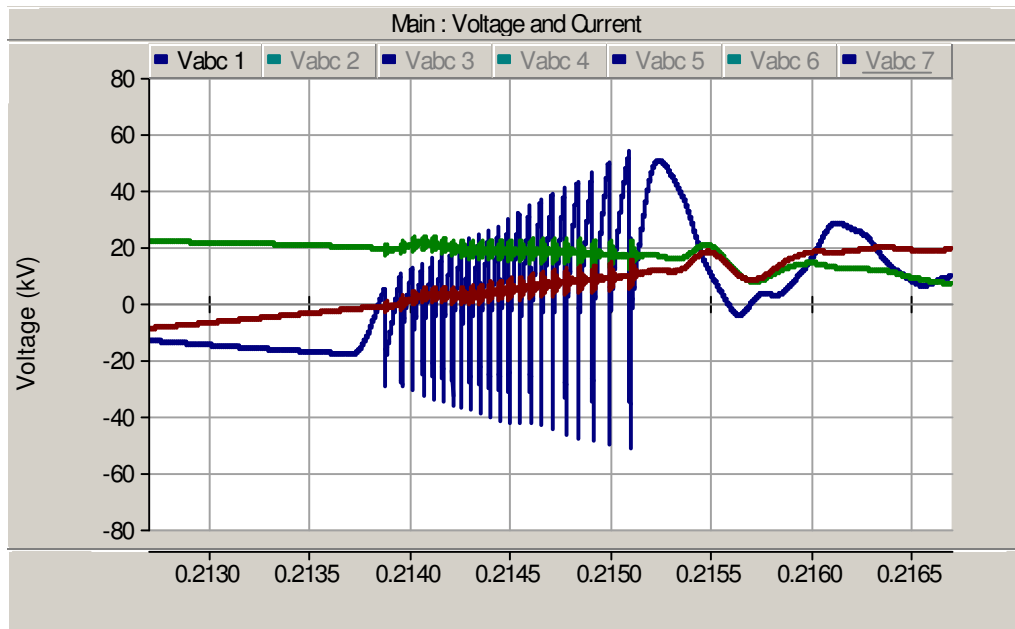


Fig 51: Voltage at MP1 with multiple re-ignitions – simulated results

It is obvious that the results do not match perfectly, but what is important to take from these simulations is that they are at best a verification of the phenomena observed in the measured case. A lot of work has been done to match the results exactly, but perfect matching is not possible because of the many variables that come into play.

4.3.3.2 Low power branch

A similar test is also performed on the low power branch with different results. One difference is that virtual current chopping is observed on this branch which creates a very interesting case since it calls the surge arrester into action to protect against the over-voltage. Much explanation is not required since virtual current chopping has been discussed previously, so only the results will be shown. Fig 52 shows the measured results while Fig 53 shows the simulated results.

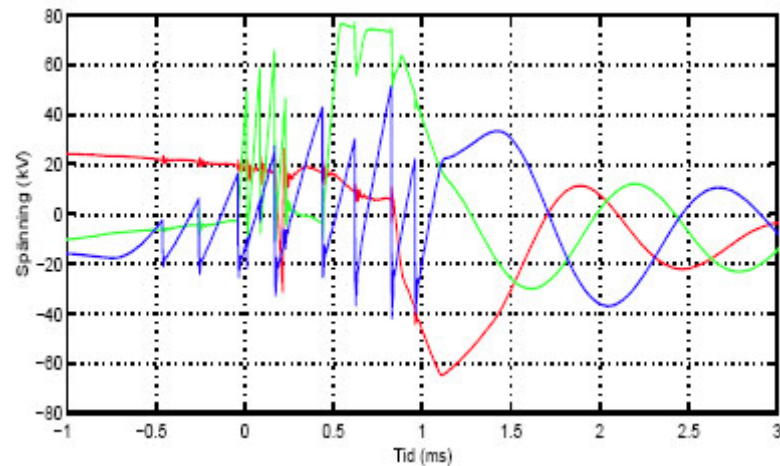


Fig 52: Voltage at MP7 with multiple virtual current chopping – simulated results

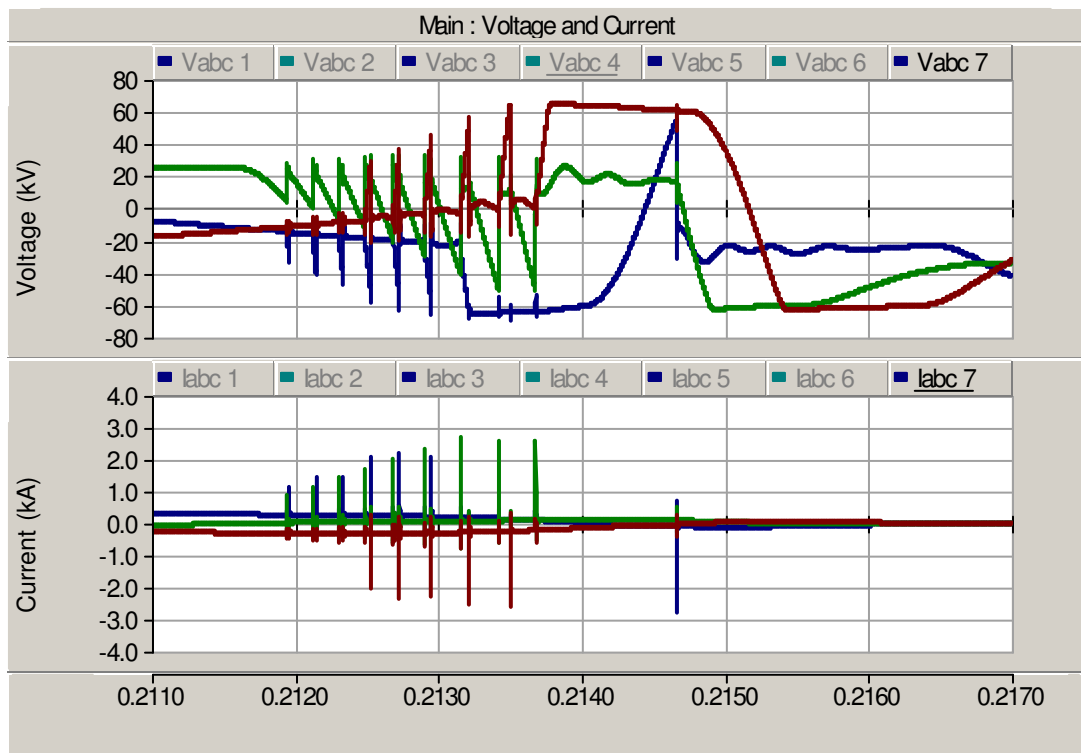


Fig 53: Voltage at MP7 with multiple re-ignitions – simulated results

4.4 Conclusion

The purpose of this section was to simulate the local power supply network of a steel mill plant for the purpose of studying transients along cable systems. The frequency response on the load-side of the vacuum breakers was performed to get an idea of how the system would perform in transient conditions. The high speed transients were studied and compared to measured results for accuracy and validation. Discrepancies and mismatches are explained as best as possible, and the protection schemes used in reality were analyzed for consistency.



5 WIND FARM

5.1 Introduction

In the following pages, the information obtained in the previous sections will be put to use to analyze an actual wind farm system. The general body of knowledge of transients in wind farms is fairly small but it is such that the similarities between industrial systems and wind farms can be used to an advantage to deduce the results and recommend protection schemes.

Transients in wind farms have been studied in [11] under the context of a specific wind farm. This paper deals with very similar topics that will be dealt with in this section while at the same time attempting to increase the body of knowledge on this topic. Several papers also exist on grid topologies for offshore wind farms ([17],[18],[19],[20]), but the results only deal with steady state conditions and are derived mainly based on economic and reliability considerations. In this report, the energization of the wind farm will be performed under different topologies while looking only at the propagation of the transient overvoltages in the system.

In some of the cases below, generators were added to the simulation to, as best as possible, simulate the real wind farm. For very short time scales, generators are not required since the transient events that will be dealt with occur very quickly, more so than the slow mechanical constants of the generators. This will be shown through the use of simulations with and without the generators attached, analyzing both the short time scale and the long time scale. One case however that cannot be performed with generators is energization, since for an actual wind farm this requires synchronization. This is beyond the scope of this report, so generators will only be used when it is seen fit.

Finally, a discussion on protection schemes for wind farms will also be carried out through the use of simulations and common sense.

5.2 The wind farm circuit

The wind farm under investigation is currently operational. ABB was provided with the technical data for the components in the system which were used to, as best as possible, simulate the topology in question. The original topology is shown below in Fig 54. Fig 55 also describes the layout without showing the cables, illustrating how there are 80 turbines connected through 5 feeders.

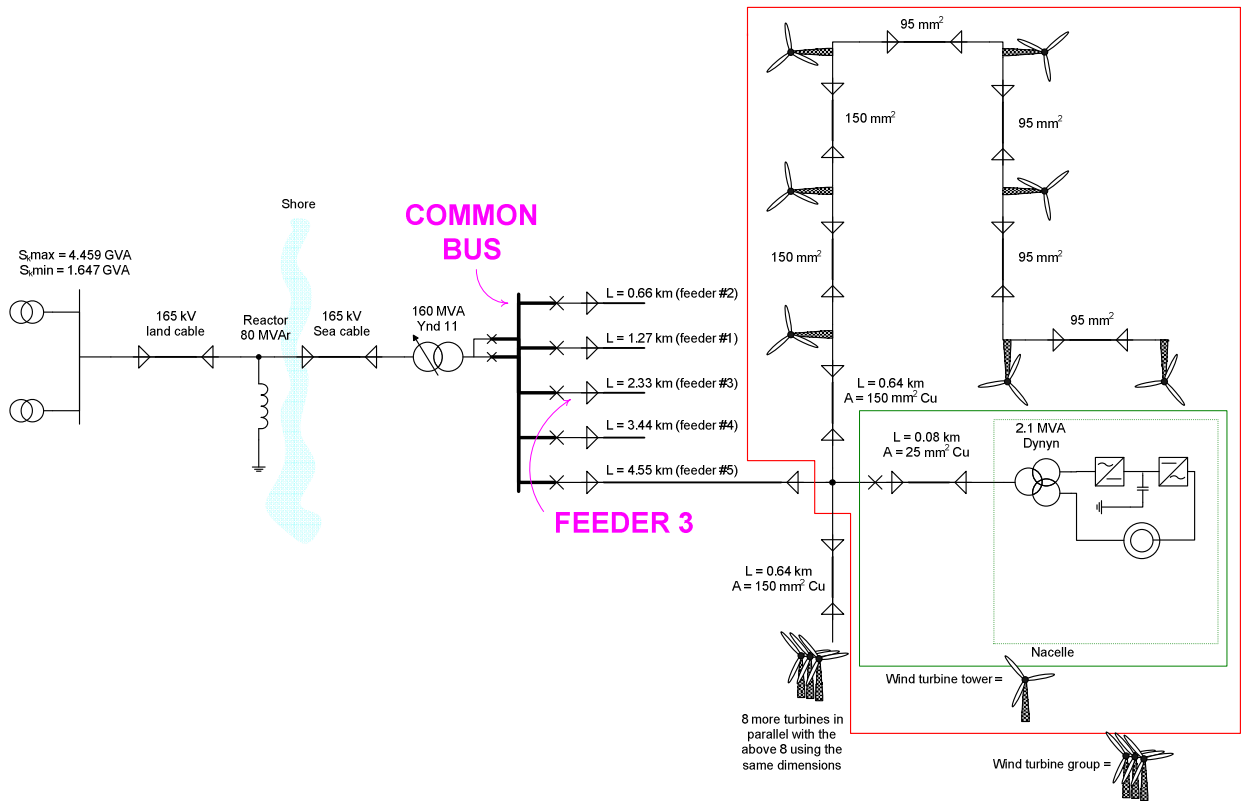


Fig 54: Wind farm diagram

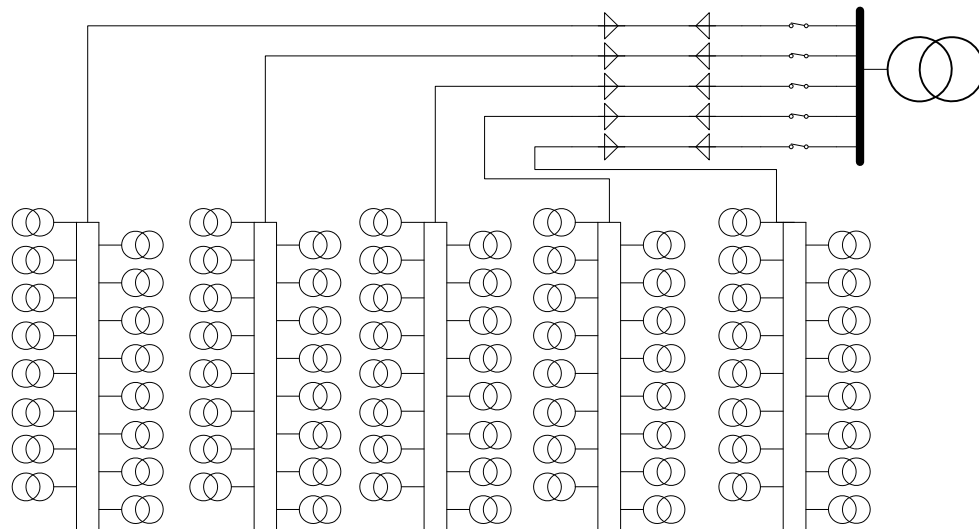


Fig 55: Wind farm diagram – simplified, all 80 turbines



The system can be described as consisting of 5 feeders of varying lengths, each connecting in parallel two groups of 8 turbines in series. The distance between, and hence the cable length, was 640m with varying cable dimensions along the line since the cables closer to the common bus will have to handle more current than the cables further away.

Each turbine consisted of an 80m long cable connected to a nacelle transformer. In the transient simulations, the generator at the nacelle was ignored since the desire is to simply study short time transient propagation along the cables in the system. Several simulations were performed and the results are discussed below. The violet text (“COMMON BUS” and “FEEDER 3”) relate to the measuring points used in the results section below.

5.3 Opening a feeder

5.3.1 Current chopping and necessity of simulation

In Section 3.3.3 a claim was made that the VCB models developed here did not need to take into account current chopping. This claim is justified when looking at normal switching operations in the farm. Under normal circumstances, the value of current chopping is less than 3A, and when chopping the current during an opening operation of the feeder, the maximum theoretical current chopping value is related to the surge impedance that the current wave sees, in this case that of the 400mm² cable.

This would set the theoretical maximum value of overvoltage produced by current chopping to

$$\hat{V} = \hat{I}_{chop} \times Z_{0,cable} = 3A \times 18.8\Omega = 0.056 kV . \tag{18}$$

This value is well justified and simulated for completeness below for an opening operation of the 2.33km long feeder. The small peaks shortly following the current chopping establish the validity of the current chopping equation and show that no harmful transients would be produced in this case as expected.

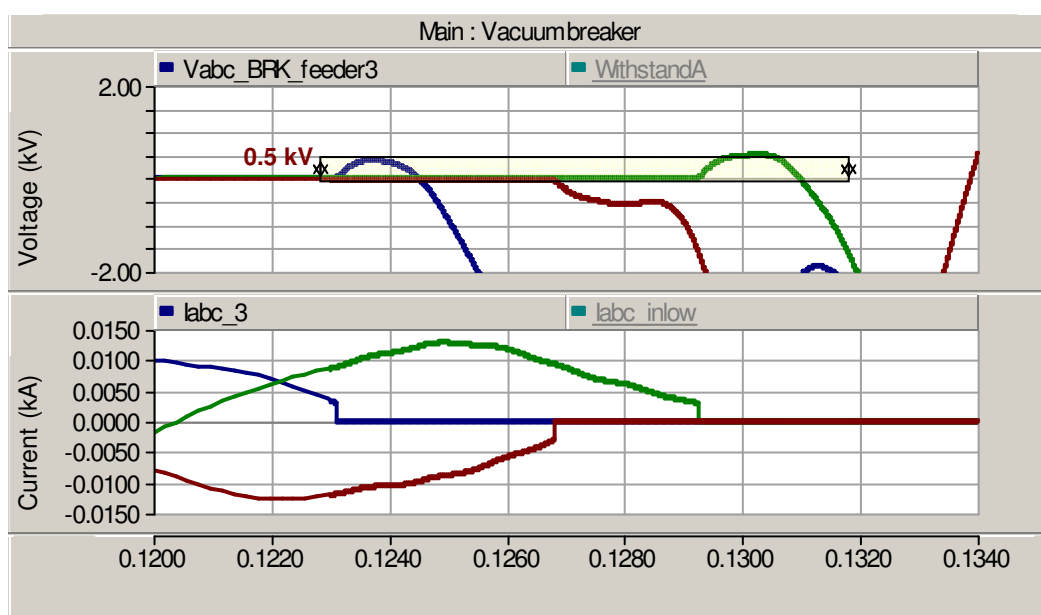


Fig 56: Voltage and current at feeder bus 3



The issue becomes more complicated when the CB is at the base of a transformer. A transformer's surge impedance is comprised of its magnetizing impedance (several Henrys to several hundred Henrys) and its stray winding capacitances (in the range of nanoFarads). This implies a very large surge impedance (possibly in the range of several kΩ), which further implies a large overvoltage purely dependent on the current being chopped.

$$\hat{V} = Z_0 \times \hat{I}_{chopped} \tag{19}$$

In reality, it is shown that at most only about 55% of this theoretical maximum can be achieved due to the hysteresis curve of an actual transformer which means that not all the energy trapped in the magnetizing core can be transferred to the winding capacitance to produce such high overvoltages. Reference [21] describes the phenomenon in more detail. For this section however, the opening of a breaker at the base of a turbine tower is simulated. The important thing to note is that the problem occurs when the current is chopped due to VCB operation at the base of the tower.

Consider then the worst-case scenario of opening the breaker at the transformer terminals on the high-voltage side, with the transformer being at the bottom of the tower. On the low-voltage side, an 80m cable leads up to an induction generator used to simulate, at least in a small time scale, the wind turbine generator. Fig 57 shows the diagram of the simulation set-up. The induction motor on the right represents the turbine generator, and BRK_36 represents the breaker opening at the base of the tower.

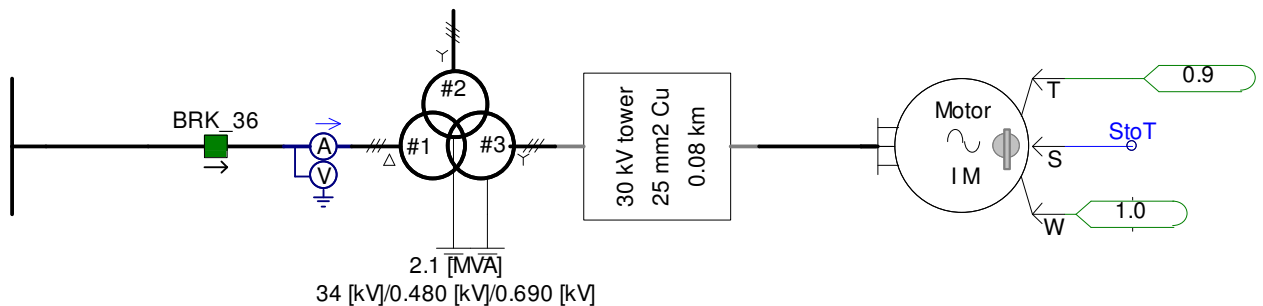


Fig 57: Diagram of the simulation set-up

Fig 58 now shows the voltage and the current in phase A when the arc is extinguished due to current chopping at a value of 3A, right after the opening command is given. This imposes a very large overvoltage in the system when the current is chopped, easily surpassing the BIL. If this breaker were to be a VCB, then this current chopping would almost inevitably lead to re-ignitions. The reference cold gap breakdown is not shown here simply because the VCB model cannot model current chopping well over a large frequency range as the EMTDC model in [8] can.

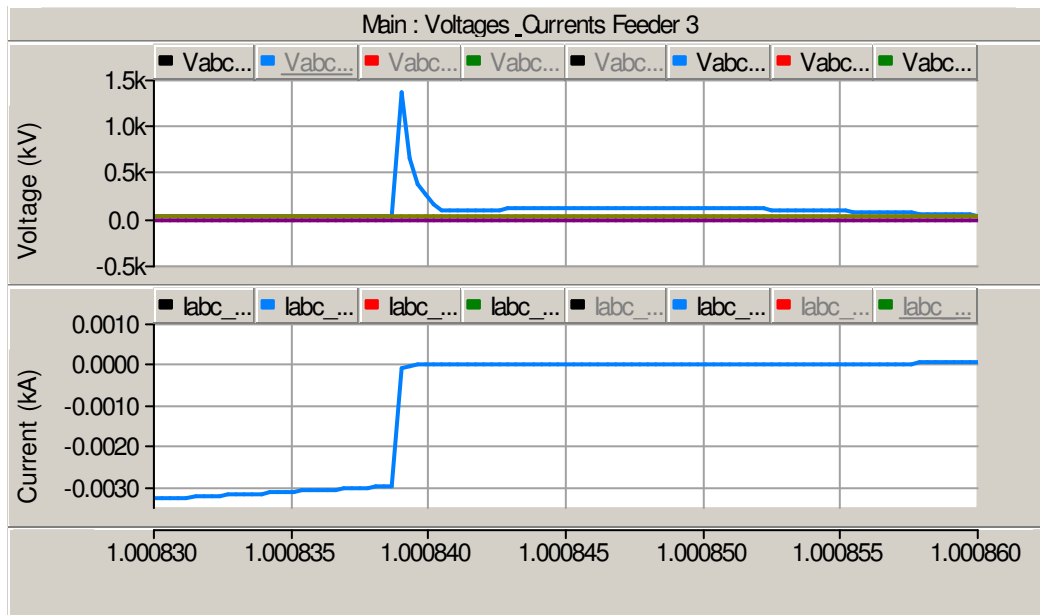


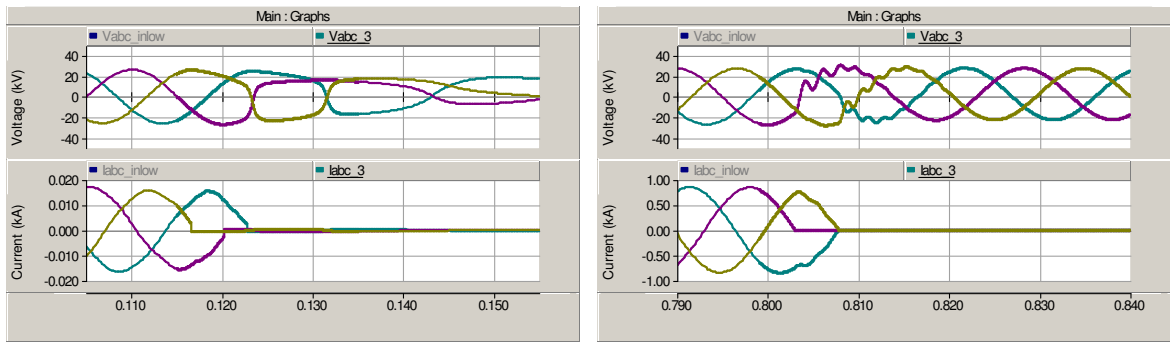
Fig 58: Current chopping effect upon opening of BRK_36

This is however an over-exaggeration of the problem since the winding capacitances have not been well defined, and because the system in question had an extra cable connecting the circuit breaker to the transformer, somewhat damping the maximum overvoltage by providing a larger and more defined capacitance at the transformer terminals. What this simulation does show however is the importance of taking into account the effect of current chopping when designing the system. This phenomenon was not simulated in the VCB model simply because such problems only occur in special niche cases. Experience can dictate when it is and when it is not important to take into account current chopping as illustrated here.

5.3.2 Opening one of the feeders

It has been shown then that current chopping during an opening operation is not dangerous when switching out a feeder. Henceforth, an opening operation is performed on the feeder to determine the system response. Note that this is simply an opening of the feeder under load (i.e. no fault applied anywhere). A comparison will also be made between opening the feeder with and without generators attached to the nacelle transformers, since this case does not require synchronization and assumes that the power electronics will not affect the results (although erroneous, this is simply for the purpose of illustration).

Observe now what happens to the bus 3 voltage when the feeder is opened in Fig 59. The left side (without generators) shows that when the breaker is opened, the transformers begin to saturate slightly as seen by the non-sinusoidal waveform of the voltage. On the right side, the transformers do not go into saturation because even after the feeder is isolated from the common bus, the generators will still be spinning. In fact, because the load is lost, they will actually speed up, eventually causing a mechanical or electrical brake to completely lock up the turbine.

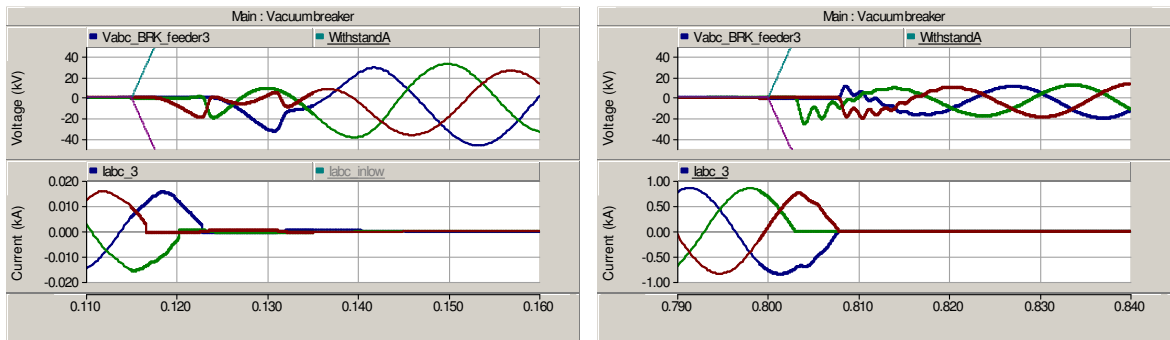


Without generators

With generators

Fig 59: Opening of one feeder – voltage at feeder 3 bus

The transients for the period following the opening operation are quite different. It shows the importance in the fact that switching out a loaded feeder is different than switching out an unloaded feeder. The transient with generators installed is simply a harmonic disturbance, while in the other case it is a saturation of the nacelle transformers. Notice then what happens across the VCB during the opening operation, illustrated in Fig 60. Notice that the case without generators produces an overvoltage which is almost 3 times higher than in the case with generators, but that is because the voltage on the feeder 3 bus is dependent on the transformer saturation curves.



Without generators

With generators

Fig 60: Opening of one feeder – voltage across the VCB

There are, depending on the system parameters, possibilities for re-ignitions as well in the system. These re-ignitions have been shown to occur in [11] for the case of opening a feeder with no generators connected. This specific case was caused by high transformer saturation as shown in Fig 60(a), but the effect in reality depends quite a lot on system parameters. To be sure however, according the above analysis, it is best to open the feeder first for roughly one cycle, after which a brake is to be applied to the generator to prevent the generator from speeding up. This ensures that the initial system transient during the opening operation is not too volatile due to the transformers not having the ability to saturate, since it is the saturation that causes high rates of rise and high overvoltages required for the VCB to produce re-ignitions.



5.4 Energization of the wind farm

A non-ideal VCB will cause pre-strikes as discussed in Section 3 because of the finite closing time of the feeder breaker. A step in voltage can henceforth occur since the pre-strike can occur quite close to the peak of the grid-side voltage, providing the worst-case scenario for such a wind farm. Energization is not performed with the generators because this operation requires careful synchronization, which as mentioned before is beyond the scope of this report. What will be studied however is the period right after energization which will be fairly short.

5.4.1 Energization of the 1st feeder

This scenario relates to when the feeder is first energized with no voltage present on the wind farm side (right side in Fig 54). Feeder 3, of length 2.33km, is energized by closing the VCB at the offshore busbar (i.e. before the cable) with no other feeders connected to this common busbar. The results are determined to be accurate from experience and from comparison to results obtained in [11].

When the cable is first energized, no voltage is present on the common bus, and hence the voltage on the grid side drops from the maximum voltage to zero for the first instant. This voltage is shown in Fig 61, expanded further in Fig 62.

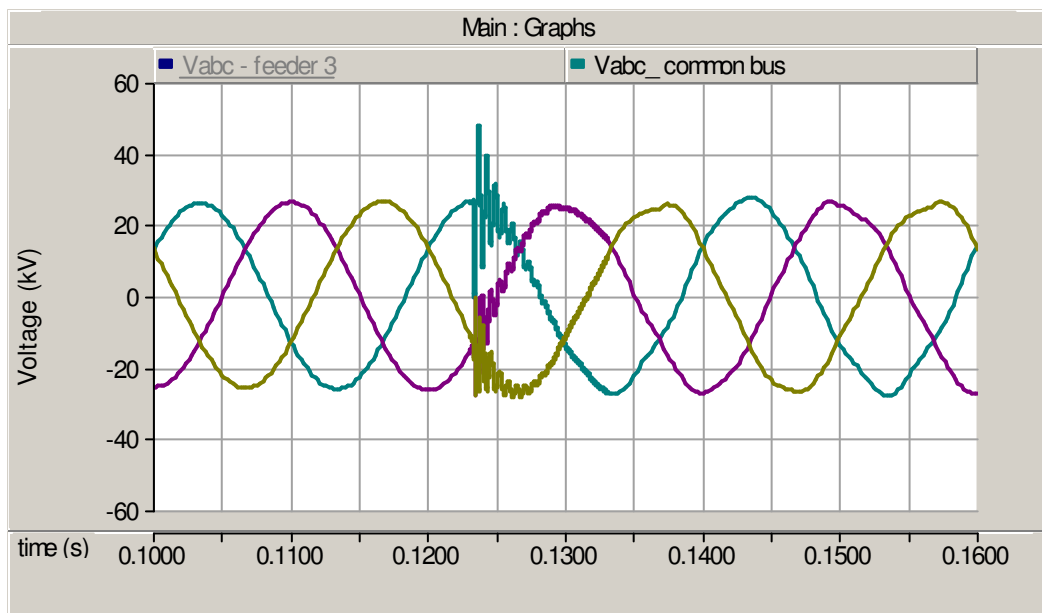


Fig 61: Energization of first feeder – voltage at the common bus

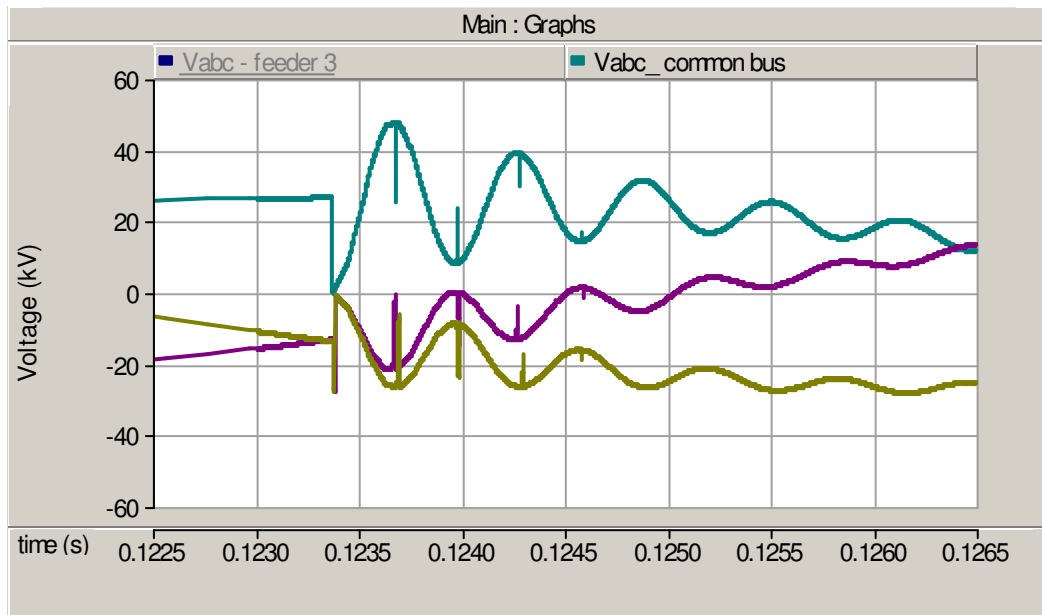


Fig 62: Energization of first feeder - voltage at common bus

Fig 63 shows the voltage across the breaker. As the gap is closing, a certain possibility exists that the voltage across the gap gets violated, causing a pre-strike. Once the current due to this pre-strike is extinguished, the voltage can once again rise across the gap. However, all that is connected at the common bus is the 160 MVA transformer's impedance and its stray capacitance, hence leading to high frequency spikes according to:

$$f = \frac{1}{2\pi\sqrt{L_{trafo} C_{stray}}} \quad (20)$$

For small stray capacitances (in the range of nF), this would correspond to very fast rising peaks, causing henceforth quick breakdowns and sharp spikes in the voltage.

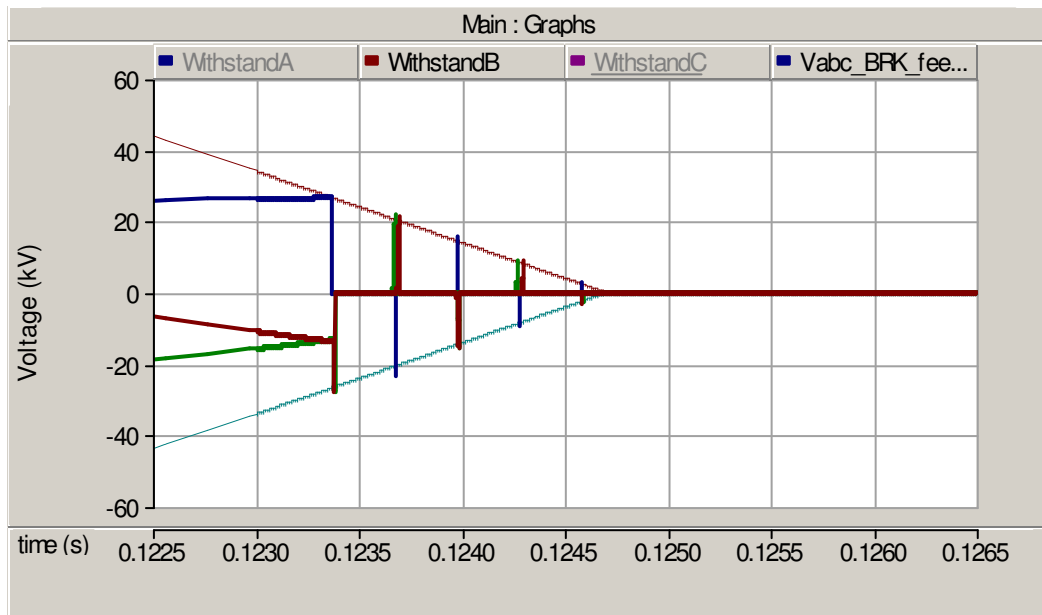


Fig 63: Energization of first feeder - voltage across the CB

Fig 64 shows the current through the breaker at the instant of energization. For the first 5ms the oscillating current is due to the energization of the cables in the feeder, after which the transformer inrush current becomes apparent. The transformers saturate and produce high amplitude currents which sum up at the common bus.

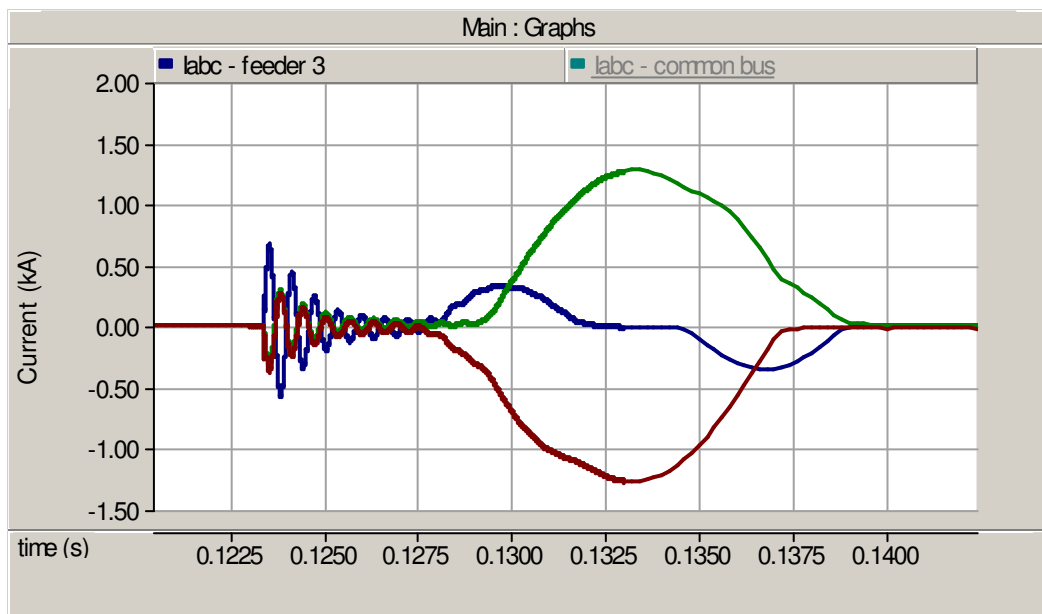


Fig 64: Energization of first feeder – currents through the breaker



5.4.2 Energization of the 5th feeder

The other interesting case is when the last feeder becomes energized. In this simulation, 4 feeders were connected at the beginning of the simulation and the VCB was used to energize the remaining feeder. The difference is that the feeders connected to the common bus already will provide a fairly stiff voltage source for the last cable to be energized, and hence the voltage drop will not be as high as in the first feeder. Fig 65 depicts the voltage across the breaker. Note here that the peaks are not nearly as sharp as in the first case due to the fact that the capacitance connected to the bus is significantly higher.

$$f = \frac{1}{2\pi \sqrt{L_{trafo} (C_{stray} + \sum_{n=1,2,4,5} C_{feed_n})}} \cong \frac{1}{2\pi \sqrt{L_{trafo} \sum_{n=1,2,4,5} C_{feed_n}}} \quad (21)$$



Fig 65: Energization of fifth feeder – voltage at the common bus

The voltage at the common bus is shown below in Fig 66, also expanded in Fig 67.

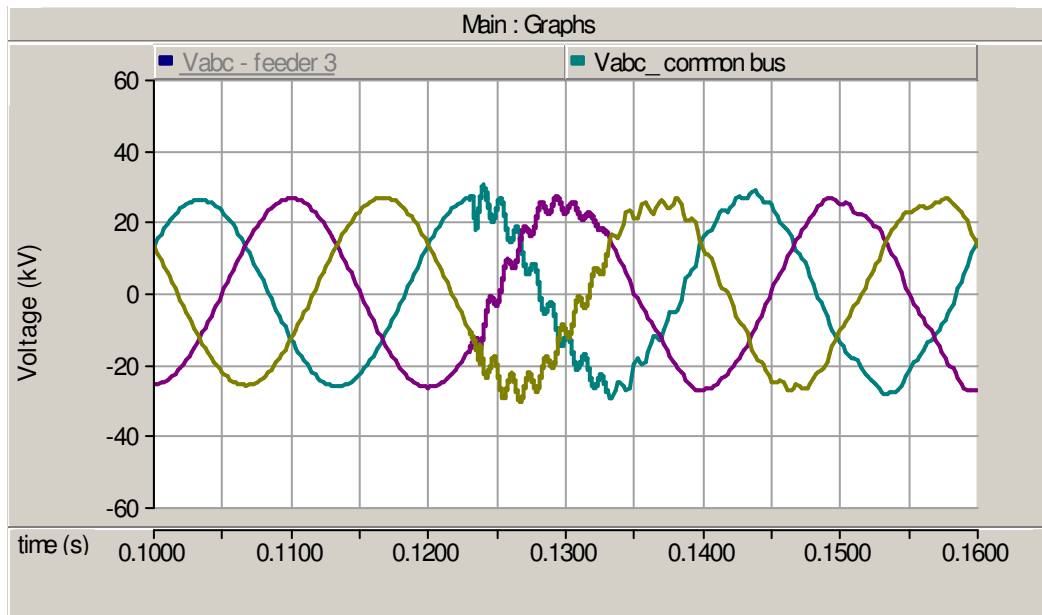


Fig 66: Energization of fifth feeder – voltage at the common bus

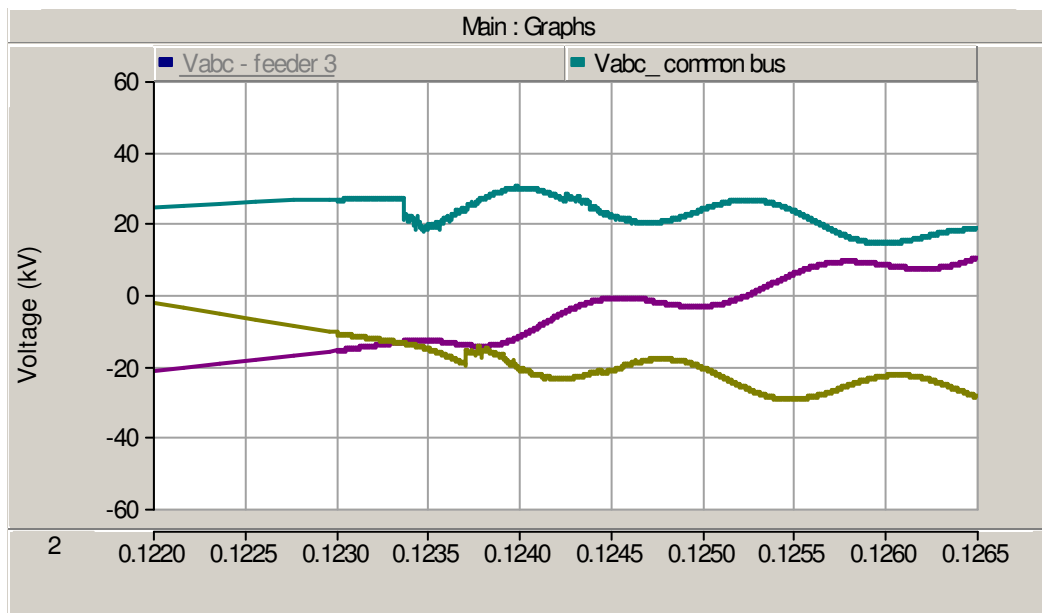


Fig 67: Energization of fifth feeder – voltage at the common bus

As expected, at the first pre-strike, the voltage only drops to 21KV, which corresponds to $4/5^{\text{th}}$ of the pre-strike voltage. Zooming in to the current through the breaker, one can see the extinction of the arc at high frequency zeros in Fig 68.

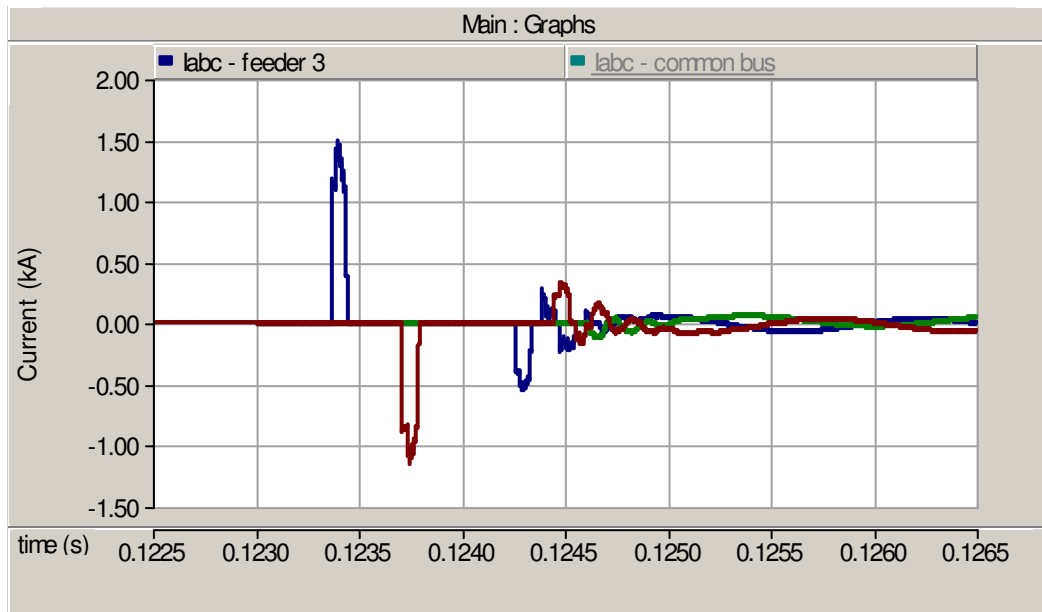


Fig 68: Energization of fifth feeder – current through feeder 3

Finally, the voltage present at each transformer terminal is analyzed. Due to the finite propagation of the wave along the feeder, each transformer in the chain will receive the voltage wave at a different time.

The first turbine's voltage is the black curve on the left in Fig 69, while the last turbine is the green curve which rises last. Each subsequent turbine is subjected to a slower rate of rise since the 640m long cable (which accounts for the time difference between voltage steps), will further dampen the wave as it travels. The last turbine, having no other turbines connected to the right, will be subjected to largest voltage step, roughly two times larger than the others. After that, the voltage is reflected back through the feeder, and the other turbines are affected by an additional voltage step (i.e. after 0.1234s)

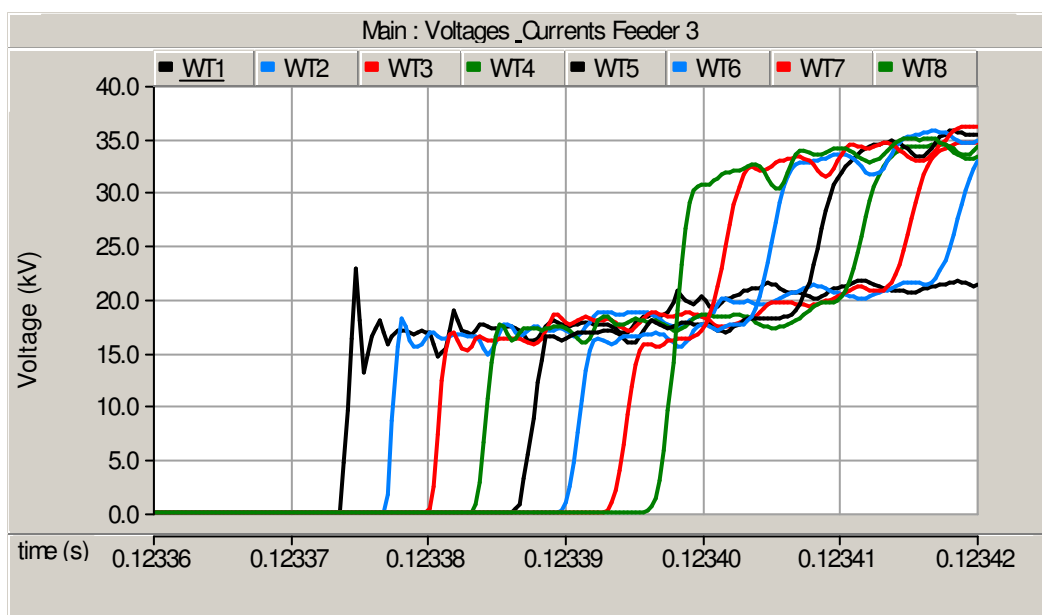


Fig 69: Energization of fifth feeder – voltage at each turbine



This result is to be expected, but the question remains if and what is the effect of such transients on the components in the wind farm. Minimizing the transient rise time and the voltage step size however would theoretically be better for components.

5.4.3 Energization of the 5th feeder under different topologies

Four different topologies shown in Fig 70 were studied to determine the transient properties under energization. The goal is to determine the transient overvoltages at the bus and at the transformers, while also drawing conclusions on the results.

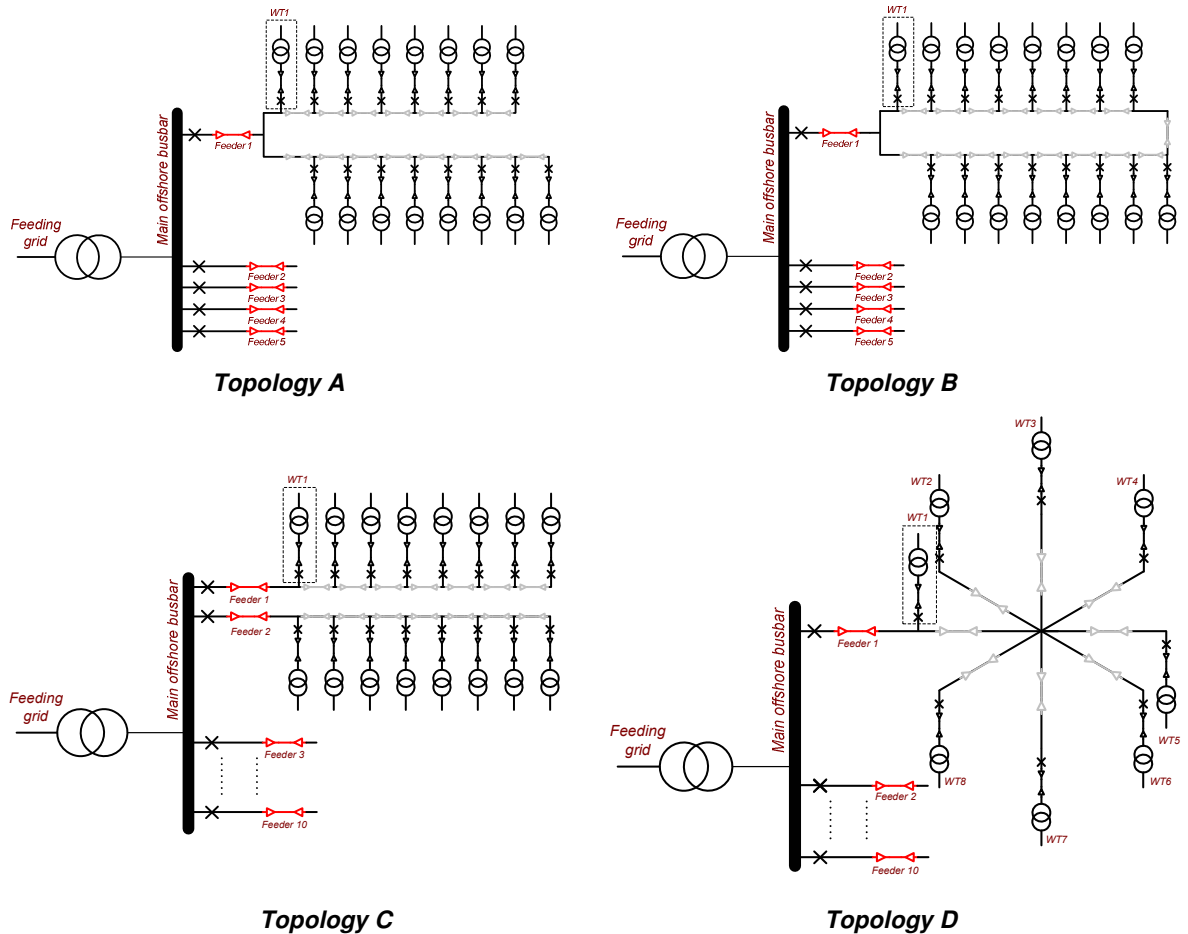


Fig 70: Topologies under study for energization of feeder

For further clarification, the red cables (↔↔) depict the feeder cables which have a 400mm^2 cross-section and varying length, valid for all topologies. The grey cables (↔↔) depict the 640m cables of either 95mm^2 or 150mm^2 cross-section depending on the amount of current. The turbine tower including the 25mm^2 cable is depicted by the following symbol (↔↔). The cross-sections of the cables between the turbines was the same as in the original configuration for topologies A and C. Topology B required that all cables have a 150mm^2 dimension (possibly even higher), while Topology C required that turbines WT2 through WT7 be fed through 95mm^2 cable since they hold as little current as the last turbines in the original configuration (topology A).



Note that there may be additional CBs along the line or variations in length when changing topologies. For example, topology D is created such that the cable lengths match those in the other topologies. However, this causes the turbines to have a separation of just 490m instead of 640m as before, thus affecting the amount of energy that can be withdrawn from the individual turbines due to the tower shadowing effect. Another issue is constructing the middle point somewhere in the sea between the turbines so one idea might be to put another turbine at the center. Other variations of this topology also exist, but a justification of choosing this specific topic for transient analysis is given. The focus is henceforth only from a transient propagation point of view, and no conclusions on the reliability or the costs will be drawn.

First, the voltages at the nacelle transformers are plotted and compared for the different topologies in Fig 71.

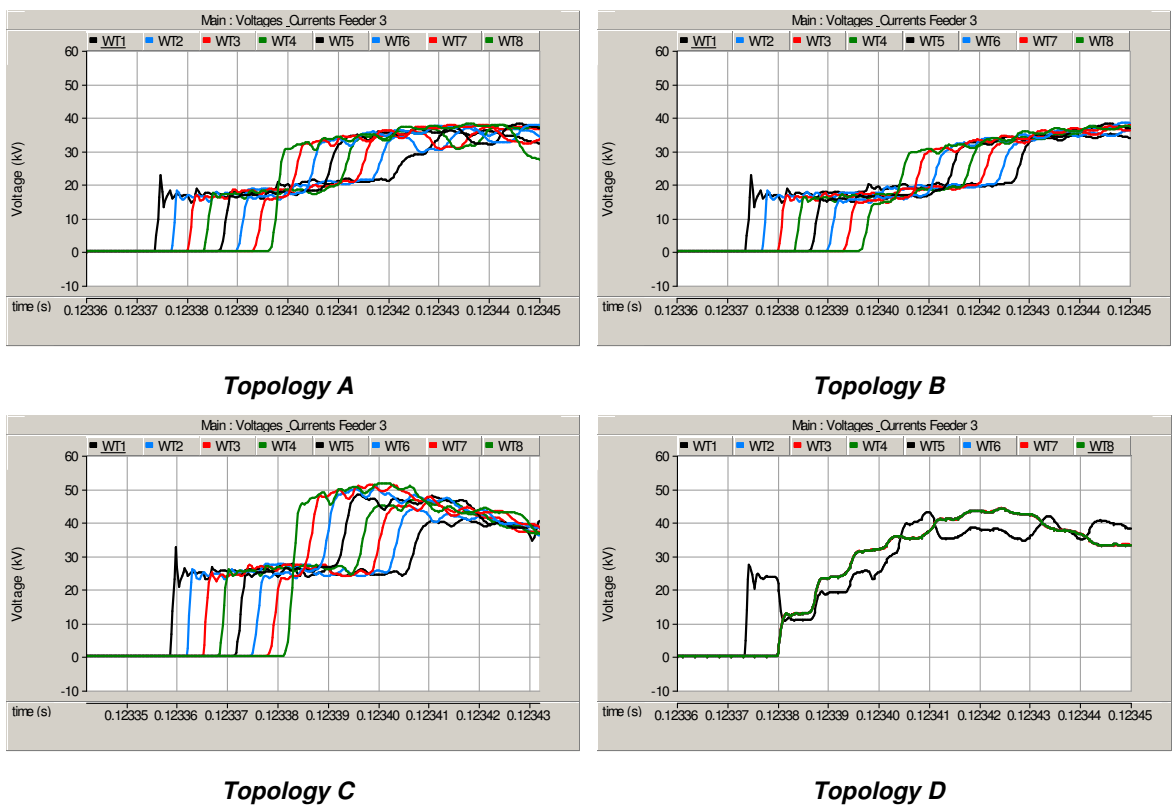


Fig 71: Voltage TOV under 4 different topologies



From a simplistic treatment of the problem, it is clear that topology C leads itself to the highest overvoltage, reaching up to 50kV as opposed to 30kV for the original topology of as seen at the last transformer. When a re-ignition occurs, a finite amount of time occurs before the wave reaches the first turbine. In topology A, right before the wave reaches the first turbine, it will encounter the surge impedance of two cables in parallel as opposed to the surge impedance of one cable as in topology C. This is illustrated in Fig 72 which shows how the initial surge of 19.13kV affects the system before and after it arrives at the node following the 2.33km long 400mm² cable. The subscript “1” denotes the initial wave, “2” denotes the reflected wave, and “3” denotes the transmitted wave. The graph shows how the wave that enters the 80m long 25mm² cable is 13.96kV in topology A, and 18.68kV in topology C. Once this transient wave reaches the transformer, it will almost be completely reflected back, producing twice the voltage at the transformer terminals. Specifically, the first transformer in topology A will be subjected to 27.9kV while topology C will receive a voltage of 37.36kV, about 1.3 times higher. Note that this refers solely to the very first voltage peak seen by the transformer.

The simulated results do not necessarily agree with the above analysis possibly because of the poor measuring resolution, not all parameters are known exactly, and damping is not taken into account using this theory. What it does demonstrate however is why topology C receives a higher voltage step than topology A.

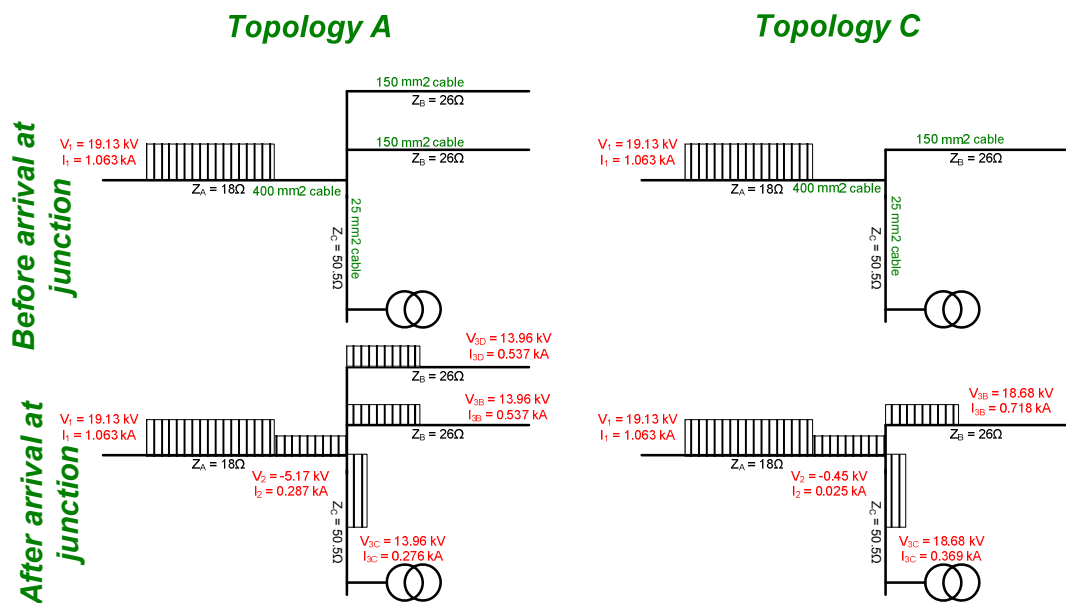


Fig 72: Explanation of wave propagation

Topology B is fairly similar to topology A except for the fact that the last cable has two voltage steps instead of one. This is due to the extra cable connected between the last turbine and the subsequent block of turbines connected to the same feeder.



Topology D is fairly promising in the sense of providing low TOVs in the system. The initial step for turbine 1 is just as high as in topology C, so in that sense turbine 1 suffers the highest voltage rise. Once the wave reaches the star point, it will encounter 7 surge impedances in parallel, causing most of the wave to be reflected back and hence producing a lower voltage on the last 7 turbines. Having more surge impedances connected to one node is hence better for transient conditions.

One way to avoid the initial step in the star-connection is to energize two or more star connections in parallel, possibly each extending equidistant on either side of the busbar. This idea is illustrated in Fig 73.

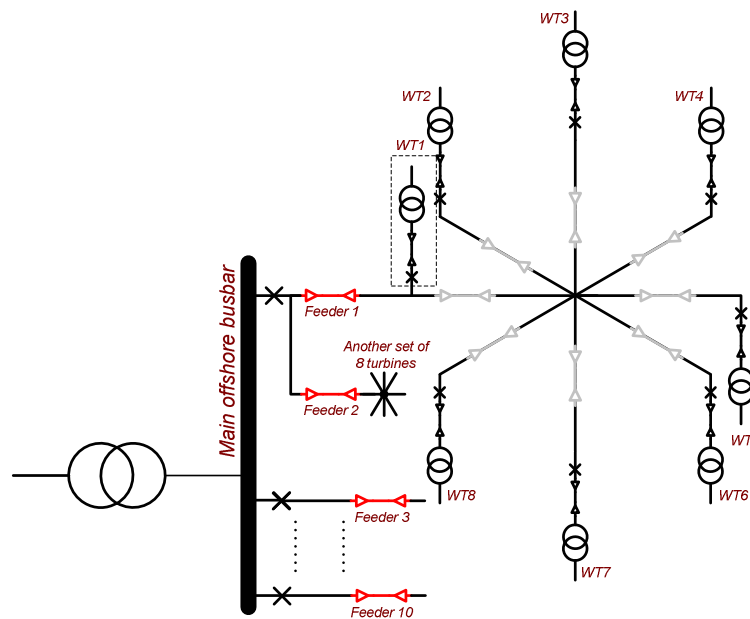


Fig 73: Alternate topology for topology D

In the figure below, the voltage profile at each of the transformers is shown with the same reference times as before. Note that the initial transient step for the 1st turbine is very small (about 9kV), which helps to solve the problem discussed above. The voltage then does not rise as abruptly, and because 7 of the 8 turbines are connected to a common point, they will each be subjected to the same TOV steps unlike in topology A where the last turbine bears the highest voltage step.

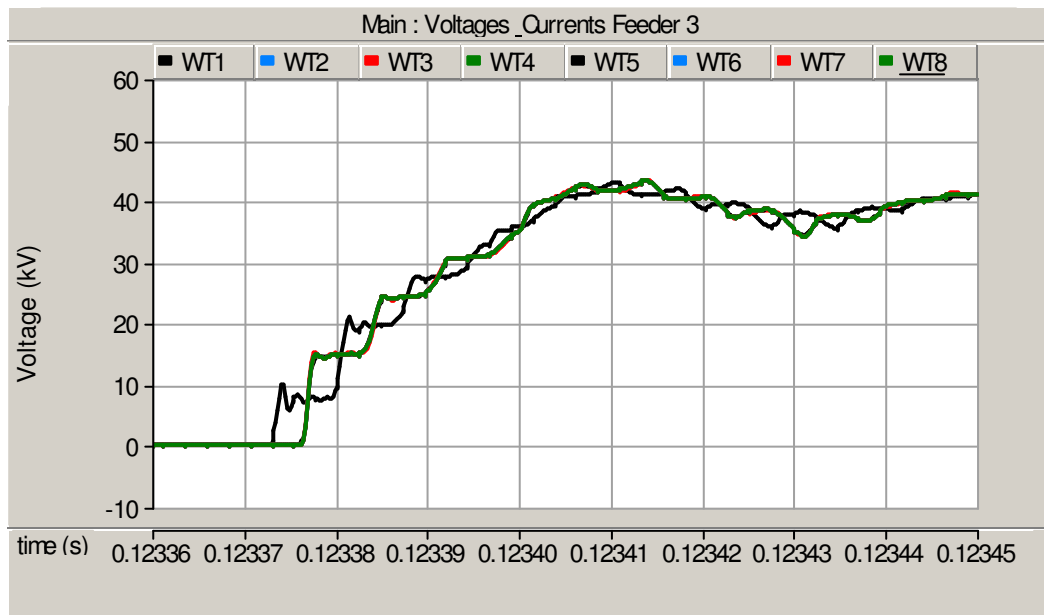


Fig 74: Voltage TOV for topology D, energizing two feeders at the same time

5.5 SLG fault and clearing fault at the feeder

The purpose of this section is to determine and characterize the TOV characteristics of the system when a single line-to-ground (SLG) fault is applied and subsequently cleared by the breaker before the incoming feeder. The fault could be applied anywhere, but for this example the location was chosen at the base of the first tower in the chain, right after the 2.33km long feeder ends. This is illustrated in Fig 75.

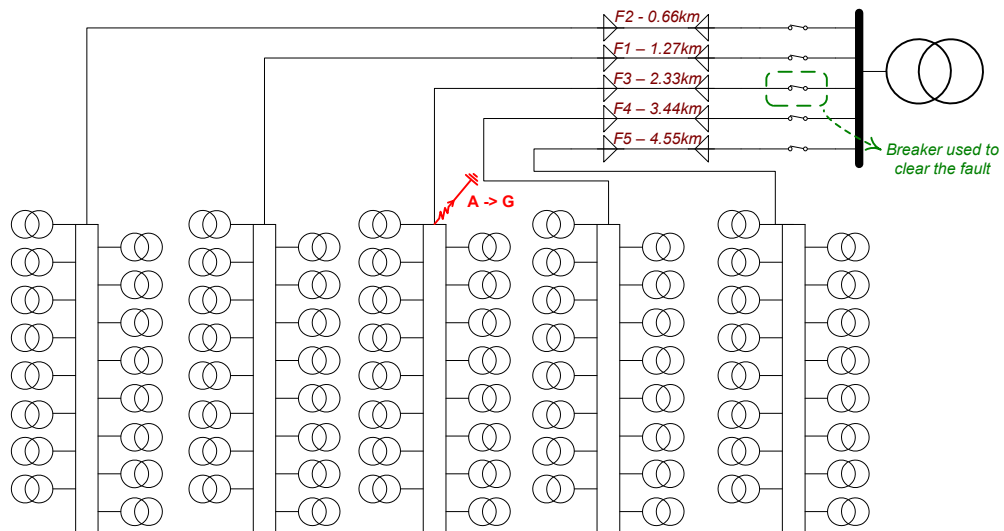


Fig 75: SLG fault location and point of clearing



5.5.1 Application of the SLG fault

The SLG fault applied at 0.08s is first analyzed in detail. Fig 76 shows the voltage profile at the common bus during the span of the fault, before the breaker has a chance to open. The results are as expected according to standard fault theory, whereby the voltages in the other two phases increase, as well as the current in phase A up to its fault level. Notice also the different between the case without generators on the left, and the case with generators on the right.

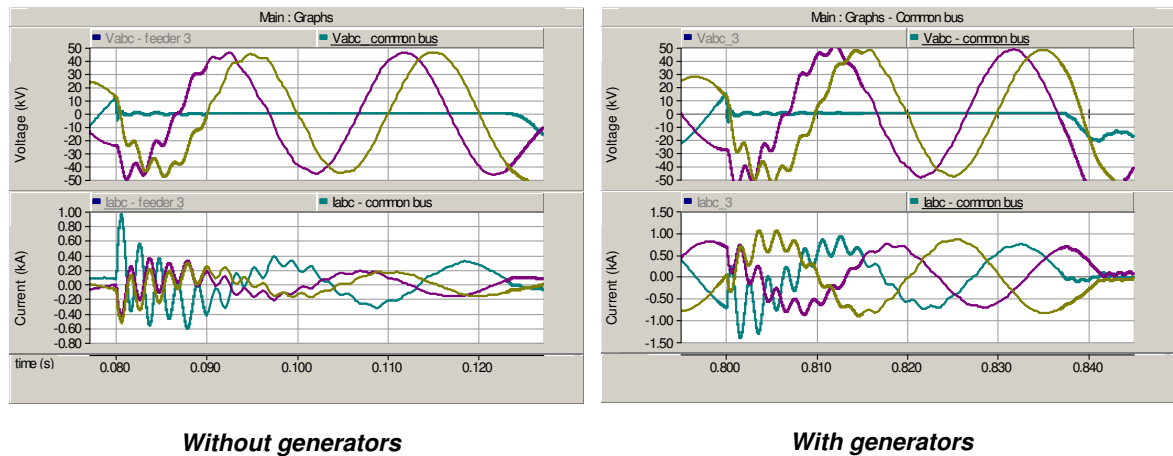


Fig 76: Voltage and current at the common bus during SLGF

Notice how in the case with generators, the currents during the fault are slightly higher because the generators are adding additional short-circuit capacity to the system. What is interesting also is that the fault current magnitudes during an SLGF fault are very close to the load current magnitudes as can be seen on the right side of Fig 76. For the left side of this figure, the pre-fault current is only at its no-load magnitude, which is much less than the load current.

What is interesting however is the propagation of the transient wave at the instant the fault is applied. Two extremes are interesting for investigation, mainly the voltages at transformers 1 (where the fault is applied) and 8 (the furthest transformer in the feeder from the fault). These two voltages are shown in Fig 77 below. The graph was analyzed for the case when simulating a fault with generators attached to the transformers. Under such a short time scale, the results are exactly the same, mainly because the short time required for cable reflections has no impact on the slow mechanical time constants of the generators. A comparison of both cases is henceforth not provided for such small time scales.

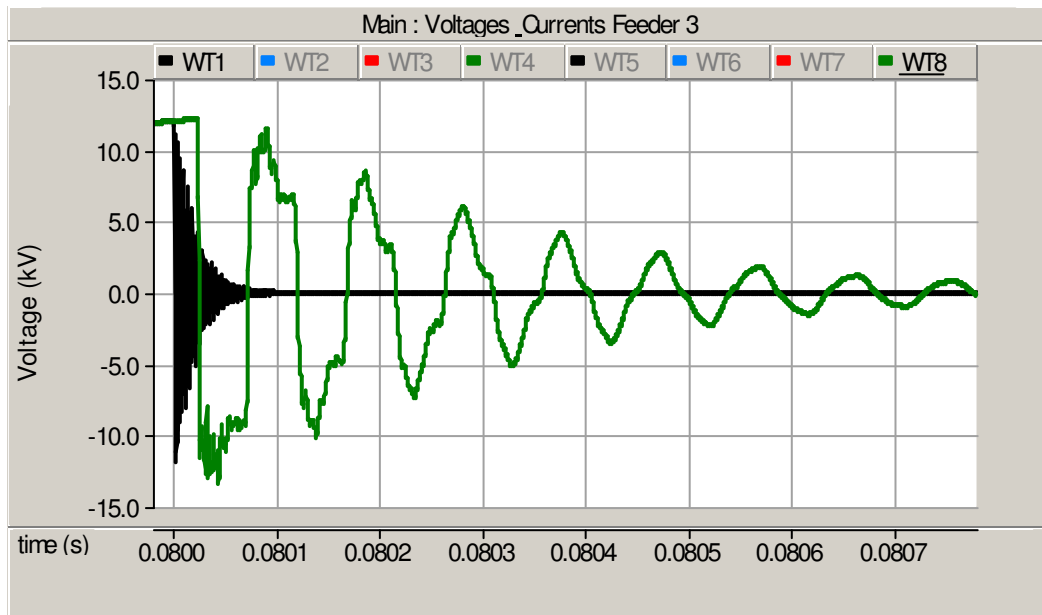


Fig 77: SLG fault location and point of clearing

The black curve showing the voltage at the transformer closest to the fault shows a high repetition frequency while the last transformer (shown in green) does not. The voltage profile at the first transformer can be analyzed with the help of Fig 78, showing the surge impedances at the point of connection of the SLGF. Refer to Fig 54 for further clarification. The measuring point for the voltage is between the 50.5Ω cable and the transformer, or more specifically on the high voltage side of the nacelle transformer.

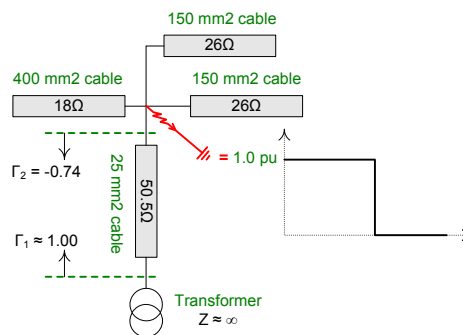


Fig 78: Surge impedances at the SLGF location

The fault application in phase A can be thought of as a simple voltage drop of magnitude 1.0pu or equivalently a voltage rise of magnitude -1.0pu. This voltage drop injects a travelling wave at the location of the fault which has 4 possible paths to take, one of which is the 25mm² cable which connects the transformer to the rest of the 34kV network (the 50.5Ω cable). Without going into much detail (see [21]), the reflections can be analyzed by using simple reflection theory. The travelling wave that arrives at the transformer after a time of $\tau=0.4\mu\text{s}$ will get reflected back into the line almost completely because of the very high surge impedance of the transformer (approaching infinity). The reflection coefficient is therefore 1, according to



$$\Gamma = \lim_{x \rightarrow \infty} \frac{x - 50.5}{x + 50.5} = 1 , \quad (22)$$

where x is defined as the impedance of the transformer which is very high.

Because of the unity reflection coefficient, the voltage step imposed on the transformer is double the surge voltage, mainly -2pu. If the initial voltage on the transformer was 1pu, then after τ , the voltage present at the terminals of the transformer would drop to -1pu, which is verified by the simulations.

At 2τ , the voltage reaches the point where the fault was initially applied. For this short time scale, the voltage wave sees 3 surge impedances in parallel: that of the 400mm² cable and two parallel cables of 150mm² cross-section. The equivalent surge impedance seen by the travelling wave is therefore

$$Z_B = 18 \parallel 26 \parallel 26 \Omega = 7.55 \Omega . \quad (23)$$

According to reflection theory, this creates a reflection coefficient as seen by the travelling wave of

$$\Gamma = \frac{7.55 - 50.5}{7.55 + 50.5} = -0.74 . \quad (24)$$

The voltage will therefore be reflected with a negative sign. At 3τ , the voltage wave which has been reflected from the common point once again reaches the transformer. The voltage now imposed on the transformer becomes roughly 0.48pu. This periodicity provides the necessary condition for the high frequency oscillations of 625kHz seen in the simulations at the first transformer. What it does show also is that the surge impedance values obtained might not be correct. It appears that the voltage magnitudes are higher in simulation than in theory, which implies that theory does not exactly predict the results.

The oscillations at the last transformer can be analyzed in a similar fashion except that the repetition frequency is due to the reflected wave which has travelled back and forth between the fault location and the end of the feeder (totalling a length of $l = 7 \times 0.640 = 4.48$ km). If this were true, the repetition frequency would be 11.2kHz, which is verified in simulations.

5.5.2 Clearing of the fault with the feeder breaker

The fault is now cleared with the help of the feeder breaker, located between the common bus and the 2.33km feeder cable. Fig 79 below shows the voltages and currents at the feeder 3 bus, right after the breaker.

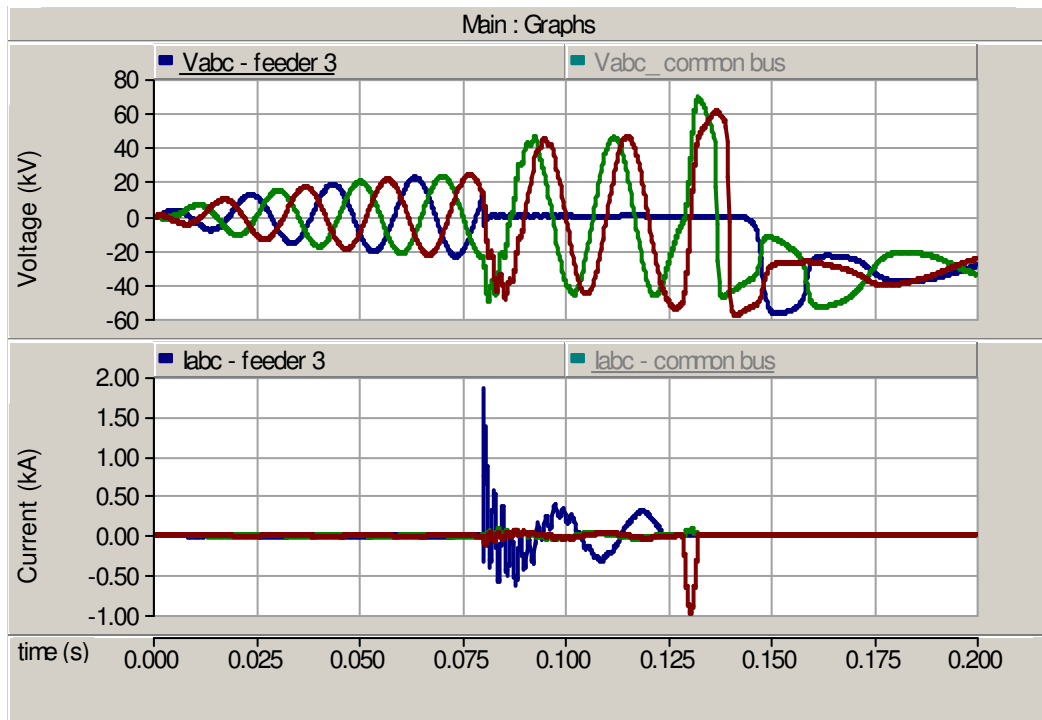


Fig 79: Voltages and currents at the feeder 3 bus

When the breaker operates, it first cuts off the fault current in phase A (shown in blue), followed shortly by the other phases. As the current is broken, the transformer saturates causing a high overvoltage at the feeder 3 bus, reaching values of up to 70kV in the non-faulted phases. This transient dies down eventually, but the large overvoltage supplemented by the high rate-of-rise in voltage has a distinct possibility to create re-ignitions, as can be seen in Fig 80 (the voltage across the breaker).

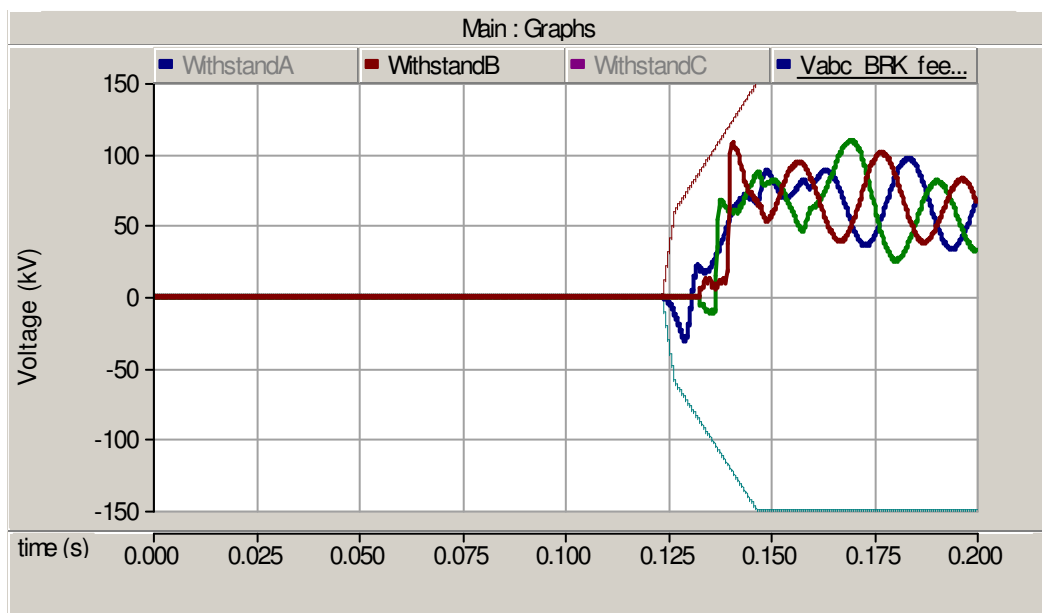


Fig 80: Voltages across the feeder breaker



For completeness, the voltage at the common bus is shown in Fig 81, depicting a decaying DC offset upon clearing of the fault.

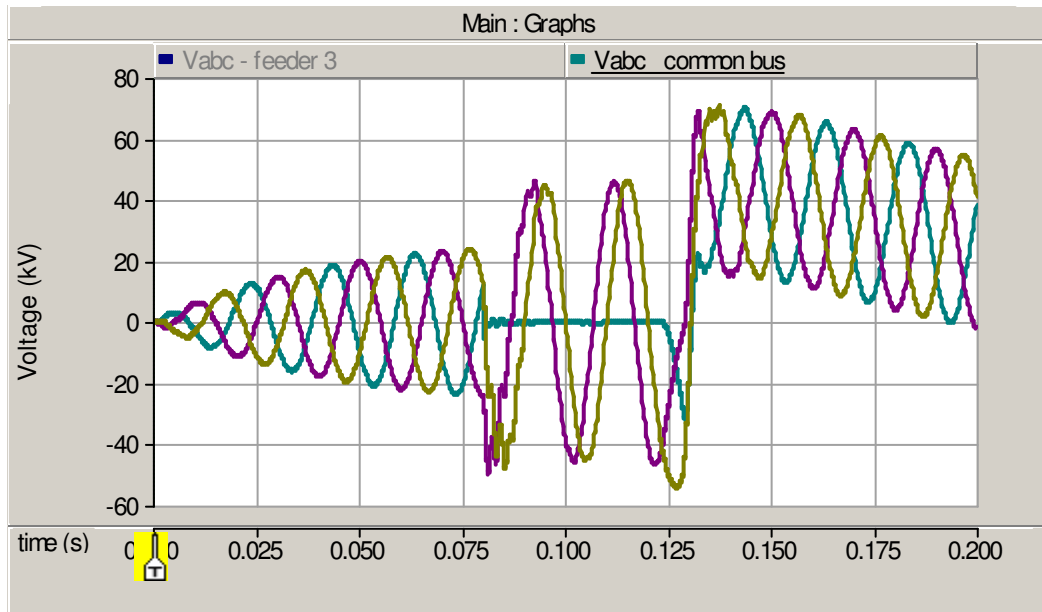
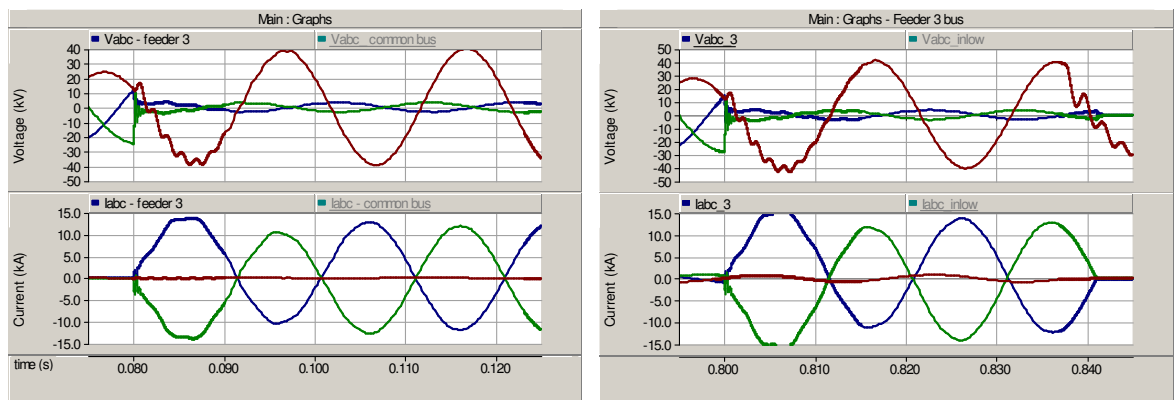


Fig 81: Voltage at the common bus during SLGF

5.6 DLG fault and clearing fault at the feeder

A double line-to-ground fault is now applied to the system at the exact same instant and place as in the SLGF. Again, as expected from fault theory, the voltage in phase C (assuming fault is in phases A and B) rises as well as the currents in phases A & B up to their fault levels. This is shown in Fig 82 for the case with and without generators. Note that in the case with generators, the fault is cleared at 0.84s, while it is not cleared in the case with no generators. However, what is demonstrated is that fault current is higher in the case with generators because the generators are providing some of the short circuit current to the fault as well.



Without generators

With generators

Fig 82: Voltage at the common bus during DLGF



What the above diagram shows is that in the case of clearing a fault at the feeder, a simulation without generators is fairly adequate. The short time scale necessary for cable reflections does by no means affect the slow mechanical time constants of the generators. Furthermore, because the system on land is able to provide a short circuit capacity far exceeding that of the wind farm, the contribution in the fault condition of the generators will therefore be minimal. What happens after the feeder is cleared is a different problem however since the generators will keep spinning and thus producing a voltage on the now isolated 34kV system. The initial application of the fault however, and during the fault, is not heavily impacted by the presence of generators.

Furthermore, the profile of the voltage across the breaker, shown in Fig 83, demonstrates that the transient voltage is not as sharp as it was in the SLGF case. However, what is apparent is that re-ignitions occur – only one in fact. Phase A & B voltages start to rise quickly right when current interruption occurs, causing it to surpass the breakdown strength of the gap. The current produced by the re-ignition will continue to conduct the arc until 0.143s, when the current once again reaches zero. This results is very similar to the case with the generators installed, and hence will not be shown again.

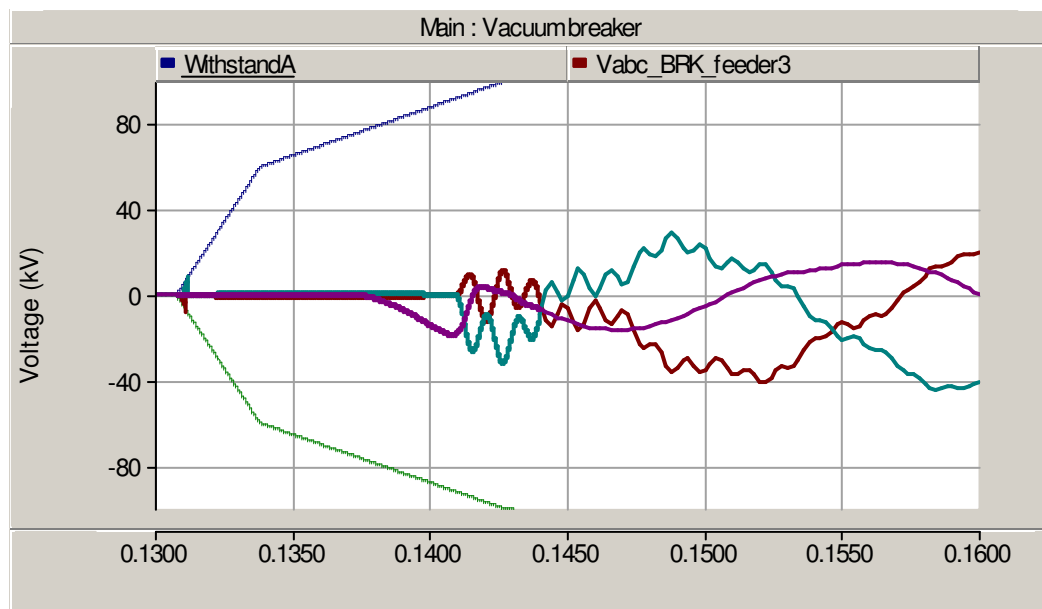


Fig 83: Voltage across the breaker during DLGF

5.7 Fault clearing with a fuse

5.7.1 Modelling the fuse

For the purpose of this work, the idea was to create a simple model of the fuse (preferably a current-limiting fuse) that could approximate as closely as possible the system response upon breaking of the fuse. The simplest method is to use a resistance that, upon arriving at the fault level in the circuit, would change its resistance such that a certain voltage is imposed across the resistance. This induced voltage would cause the current to drop to zero, signifying that the fuse has worked properly.

The idea is simple, and the model developed in PSCAD/EMTDC, using this method, is shown below. The initial resistance is chosen as 20m Ω , which is roughly the value given in ABB catalogs for the resistance under normal loading.

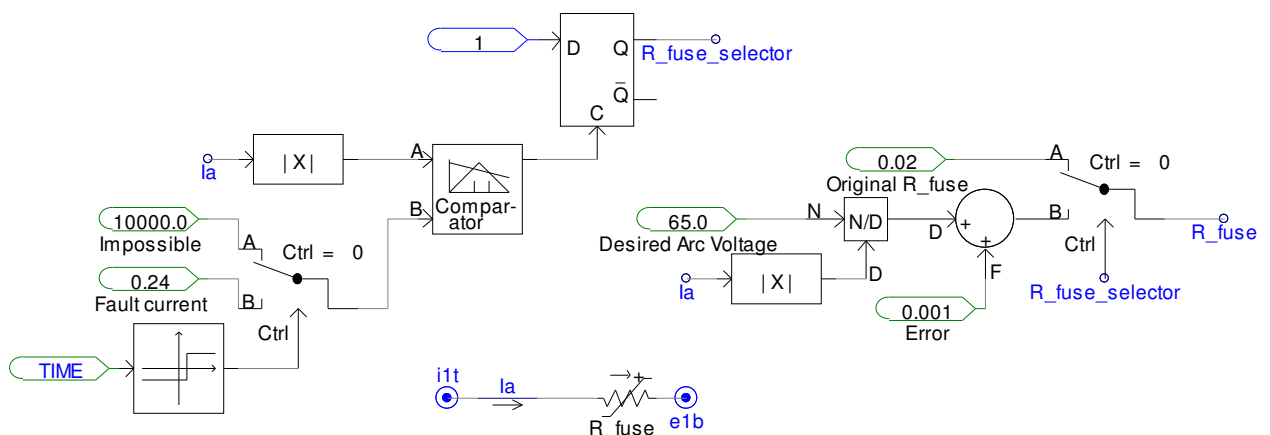


Fig 84: Modelling of the fuse in PSCAD.

To show that this model works, a very simple system with a fuse and a load in series is tested. Fig 85 shows the voltage and the current profile. The current is initially left to cross the peak of the fuse's breaking current for half a cycle for the purpose of illustrating the fault current's magnitude. Once the current reaches 1.0kA (the fault level of the fuse), the phase-to-ground voltage rises to about 1.5 times the system voltage to bring the current down to zero. After 0.23s, the fault is cleared as expected.

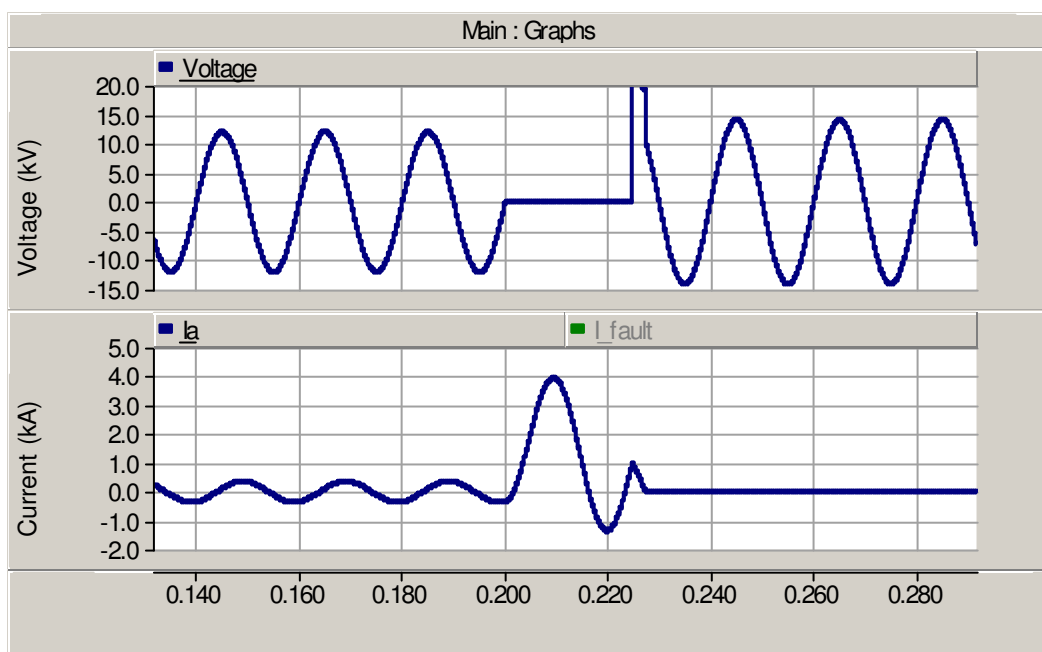


Fig 85: Phase voltage and current of a fused system

5.7.2 Clearing an actual fault

The modelled fuse is now applied to the actual wind farm system. The fuse is located, according to specifications for the wind farm, at the base of the tower. The importance of this report is to identify and simulate interesting scenarios, one of which is if the fuse in phase A breaks while the others do not. This is a niche case, but it demonstrates the situation when the turbine breakers do not operate and a fault stays present.



Fig 86 illustrates the setup. Following the node between the two 150mm² cables to the left, a fuse is situated, followed by an 80m cable to the transformer in the nacelle. The fault location is for example between the transformer and the 80m cable, but it could easily be at the base of the tower as well.

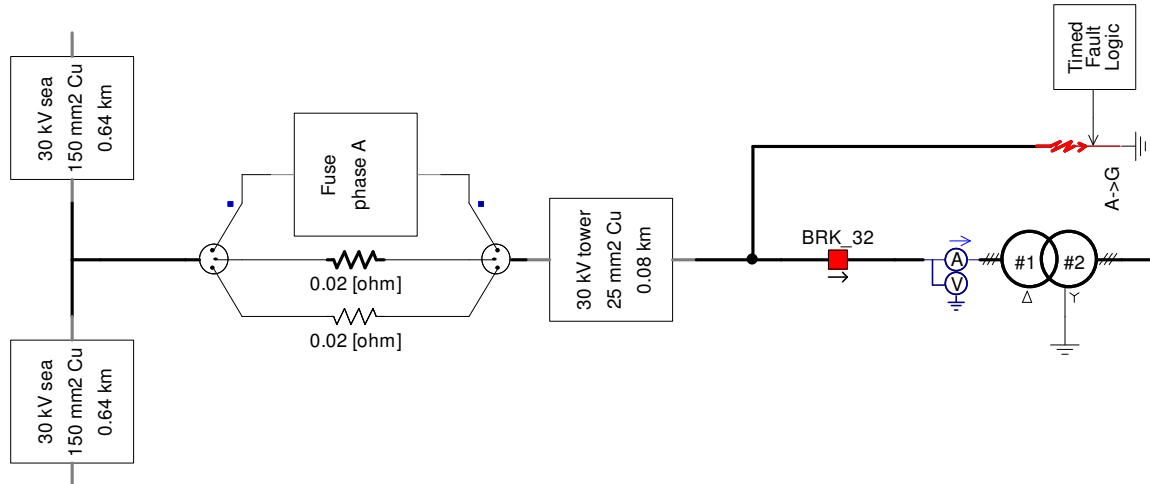


Fig 86: Diagram of the fused turbine

The 0.02Ω resistances simulate the nominal resistance of the fuse, while fuse A (top) is modelled as in Fig 84, also with the same nominal resistance. The voltage and current profile at the feeder 3 bus is shown in Fig 87. Phase A is faulted to ground at the location described in Fig 86, and after one cycle the fuse clears the fault in phase A. The voltage at bus 3 is then recovered in all 3 phases for at least the initial period.

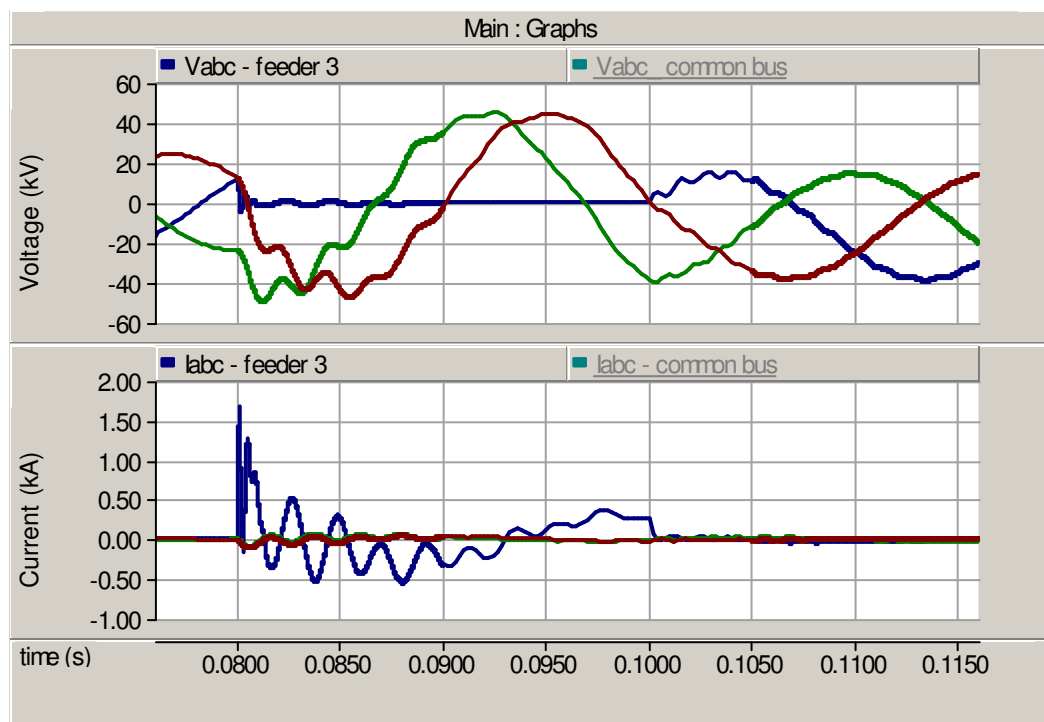


Fig 87: Voltage at feeder 3 bus



The voltage at feeder 3 describes the 34kV system voltage. It can be seen however that since phase A is disconnected, the transformer of the 2nd turbine will only be connected through phases B and C, causing an unbalanced situation. This unbalanced situation depicted in Fig 88 also shows that because of this unbalanced, the transformer in turbine 2 will become saturated, leading to large currents (above its load current rating) to flow.

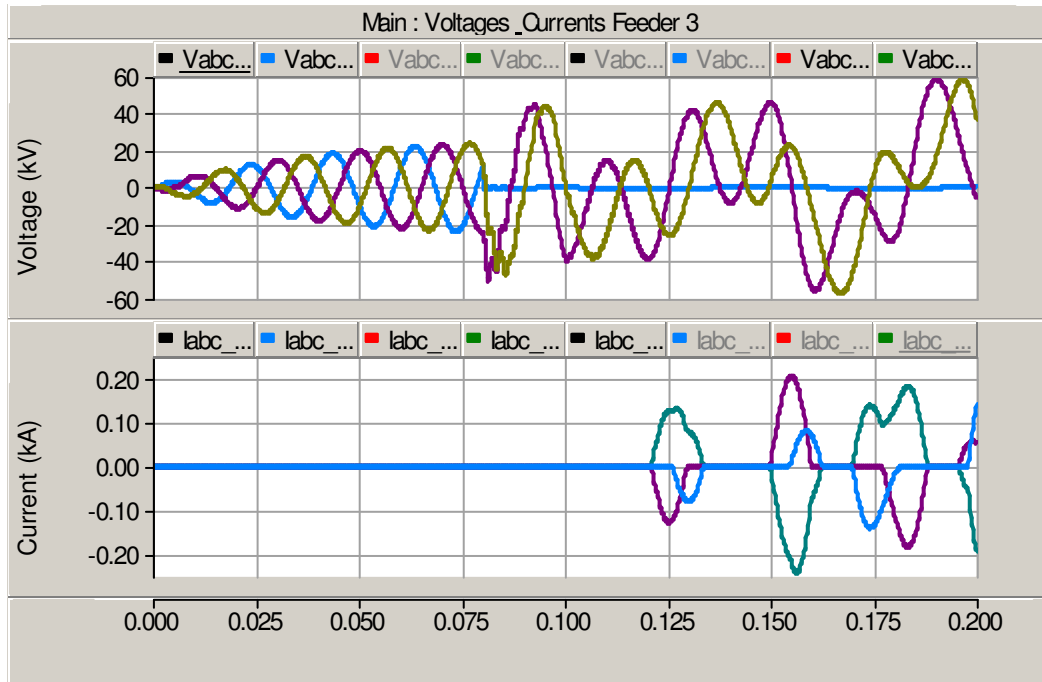


Fig 88: Voltage and current at terminals of turbine 2's transformer (the faulted turbine)

The neutral point of the voltage at the 34kV bus now begins to swing as can be seen in Fig 89 (voltages and currents at the common bus), eventually causing the breaker at the feeder to trip the whole feeder, or at least should be in a common protection scheme.

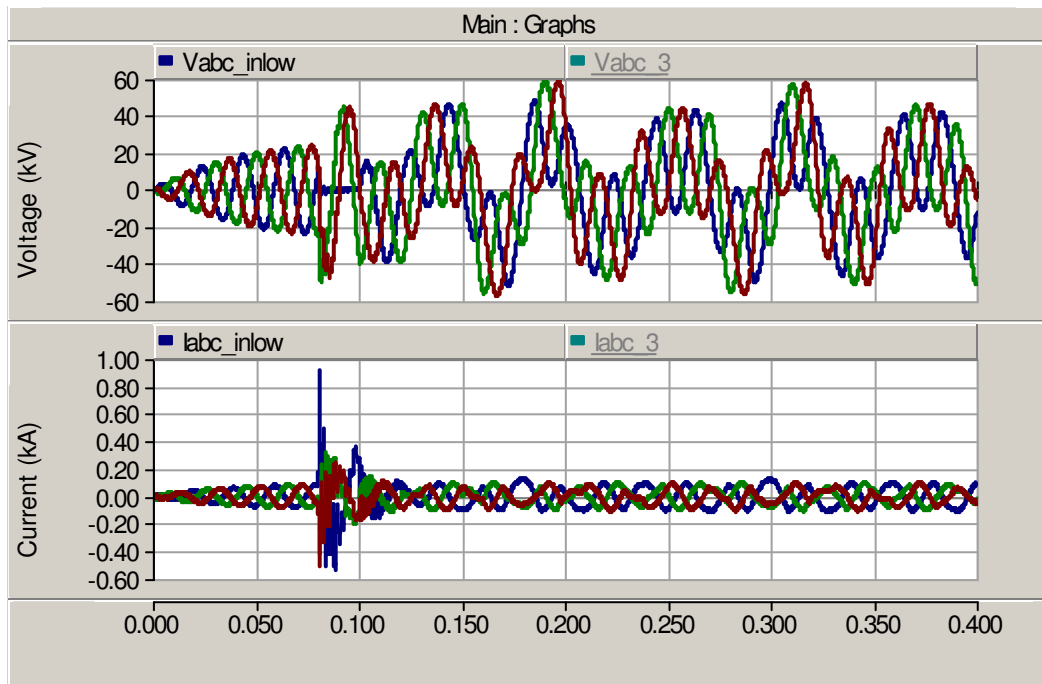


Fig 89: Voltage and current at the common bus

The problem with the above analysis however is that it is performed on a system with no generators connected to the turbines. The issue then becomes: Does adding the generators in the nacelle to the simulation change the situation, and will the unbalance still occur. For this purpose, a simple 2MW generator that would as closely as possible simulate a squirrel cage induction generator was added to the simulation.

The situation actually changes quite drastically when adding generators. The fault current values as well as the transient conditions will also change due to the new and slower mechanical constants added to the system. An induction generator will for the first few milliseconds keep its speed fairly constant which means that its voltage will also be kept fairly constant, and since only one turbine is faulted in phase A, the other 15 generators connected to the same feeder will help to keep the voltage fairly steady due to its slow mechanical constants, even after the initial transient period. This idea is illustrated in Fig 90, the voltage at the first turbine's transformer.

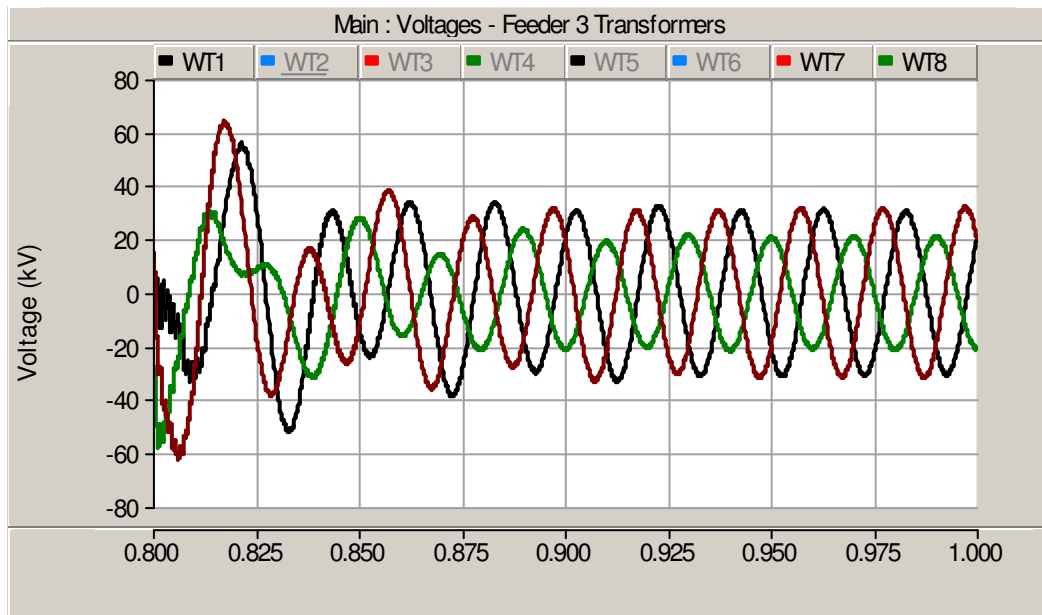


Fig 90: Voltage at transformer 1 – with generators installed

Phase A of transformer 2 having been faulted will have zero voltage, but the other generators will be able to keep the voltage at the other transformers high enough to provide power to the system and to keep the system in fair good balance and out of saturation. Looking at the current through transformer 2 on the high-voltage side in Fig 91, one can see that the current is far less volatile than in the case without generators previously shown in Fig 88. It rarely surpasses 100A after the initial 50ms.

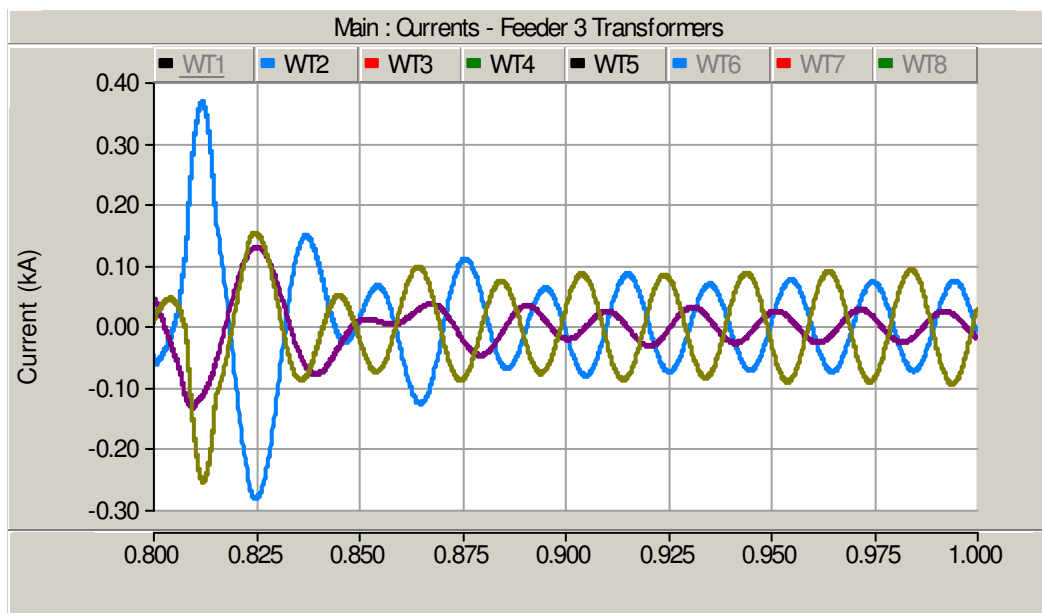


Fig 91: Currents through transformer 2 – with generators installed



The figures below, Fig 92 and Fig 93, also show what happens after the fault has cleared and the fuse has been burned (i.e. no more unnatural ground connections). The generator at turbine 2 is connected now through only two phases, but yet it is still rotating. The blue phase (the previously faulted phase) begins conducting again at 0.88s due to the fault clearing itself. The fault is applied at 0.8s at the location between the 80m tower cable and the transformer on the 34kV side.

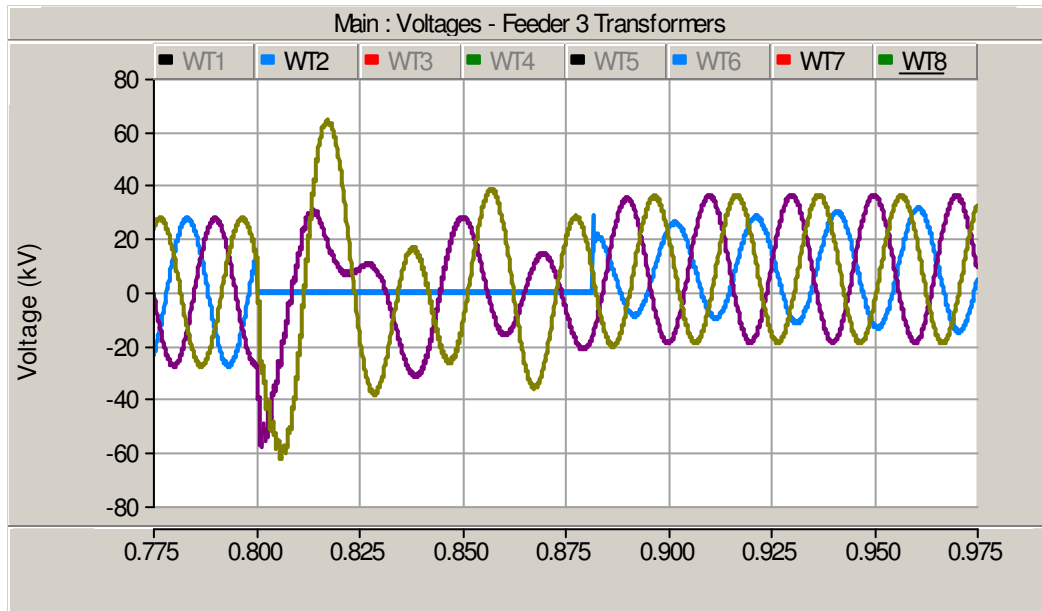


Fig 92: Voltage at transformer of the 2nd turbine

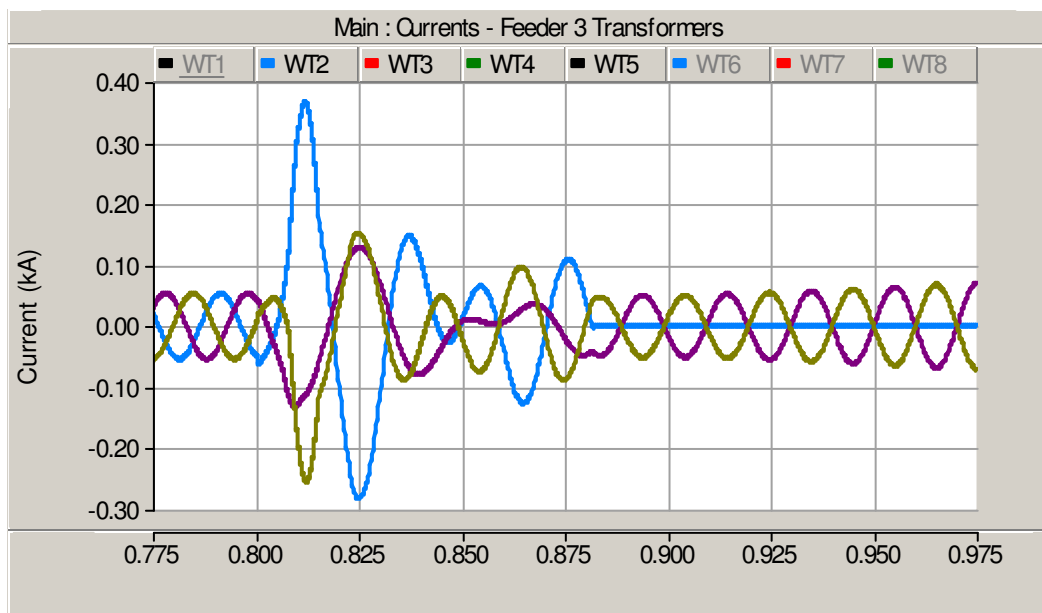


Fig 93: Current at transformer of the 2nd turbine



The generator is running unbalanced in turbine 2 as can be seen by the currents and voltages at the generator, even though the whole 34kV system is still fully operational as can be seen by the symmetrical voltage for turbine 1 in Fig 94 which stands right besides turbine 2. In this case, it would be ideal to trip the second generator because of the unbalance, but it shows that if the fault is cleared on a turbine, the system would still provide be fully operational, possibly minus a few kW due to the unbalance. This is in comparison to Fig 90 where the voltage at transformer 1 remains unbalanced.

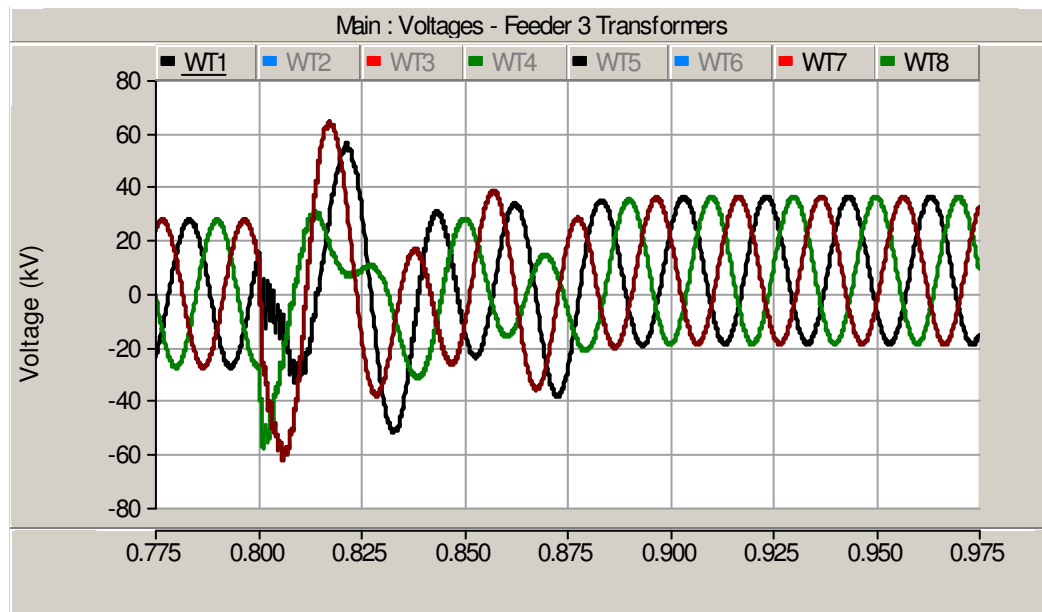


Fig 94: Voltage at transformer of the 1st turbine

5.8 Wind farm protection

In the industrial system, section 4, several protection devices were required to be installed due to the high amount of re-ignitions and the violent TOVs present. In this section of the report, it was also found that the wind farm can produce dangerous TOVs, but to what extent is not yet known. It is therefore only natural that one discusses protection schemes for wind farms as well, possibly using lessons from industrial systems to draw conclusions here.

There are several basic protection schemes that can be used, but only two are used for the purpose of illustration. The study will be qualitative and not quantitative to show the basic ideas.

5.8.1 Passive protection schemes

One passive protection scheme which will not be discussed in detail is the surge arrester. This device simply limits the voltage seen at a certain terminal through the use of a variable Zinc-Oxide resistance. The steel mill uses this protection scheme quite extensively to protect both the line-to-ground voltages and the line-to-line voltages from becoming too high. The conditions in the wind farm are not nearly as dangerous as in the steel mill, so this protection scheme is used more sparsely, and according to the simulations performed in the report, it can be seen that the voltage rarely surpasses 2pu in transient conditions.



What perhaps is more dangerous to the wind farm (i.e. insulation of the transformers) is the rate of rise. The rise time is defined as

$$t_{rise} = 2.2 \times \tau = 2.2 \times (Z_{surge} \times C_{transformer}) , \quad (25)$$

where Z_{surge} is the surge impedance seen by a travelling wave and $C_{transformer}$ is the equivalent capacitance seen at the terminals of a transformer. One very common solution to protect the transformer terminals is to increase the capacitance seen at the transformer.

The way to do this is to add a surge capacitor at the terminals which effectively provides a higher $C_{transformer}$ as required. For the purpose of illustration, the wind farm topology is simulated with a surge capacitor of 83nF, a common value used by ABB. The set-up is shown in Fig 95.

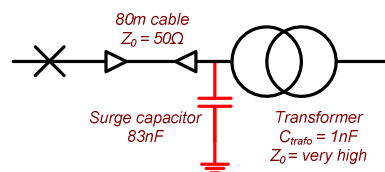
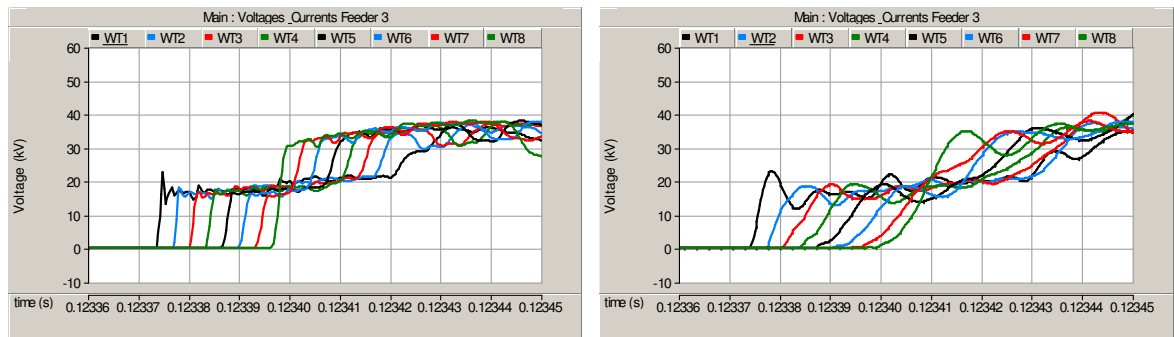


Fig 95: Surge capacitor protection scheme

The results below in Fig 96 show how the rate of rise changes when the surge capacitor is added. The left side is the original energization with the high rates of rise, and the right side shows the smoother rate of rise with a surge capacitance at the transformer terminals for comparison.



Without protection scheme

With surge capacitors

Fig 96: Surge capacitor protection scheme

As expected, the rate of rise as well as the rise time decreases when adding the capacitor. What is added to the waveform is an oscillatory component on the basis of this extra capacitance, but what it accomplishes outweighs the potential problems added by these oscillations. This appears then as a good solution for suppressing fast rise-times in wind farms.



Capacitors were also added in the industrial system as well but for a different reason all-together. The worry in that case was high frequency coupling between the high-voltage side and the low-voltage of the transformers side due to the inter-winding capacitances. A capacitor on the low-voltage side solved this problem by creating a high and well-defined capacitance, which will effectively overpower the stray capacitance on the low-voltage side. This is not necessarily a worry in wind farms since the low-voltage side is a generator which consists of slow mechanical time constants. The voltage cannot rise as quickly as in the industrial system since what is present on the low-voltage side is a load, changing the requirements quite drastically.

RC Protection was also used in industrial system used for the purpose of removing high frequency current zero crossings. The difference with wind farms is that re-ignitions are less of a problem since in the industrial system, the load was extremely large and inductive (roughly 80MVA for the arc furnace). The re-ignitions that could potentially occur are either due to switching of a transformer under no-load (producing saturation) or under certain cases of clearing a fault in the system. Take for example Fig 83 which describes a DLGF. What occurs in this diagram is one re-ignition at the beginning, after which the arc supports the current in those phases for another half cycle. This is precisely what one wishes to achieve with RC protection, and hence in this example of a wind farm, it is not required.

5.8.2 Active protection schemes

The above section has covered passive solutions, made up entirely of passive components. The active solution that is used most often when dealing with high frequency problems in a cable system is “Synchronized Closing” or “Synchronized Switching”. The idea is to basically ensure that for an opening operation, care is taken not to switch next to a current zero since this would risk re-ignitions.

Synchronized closing is used for example when energizing capacitor banks. Care should be taken to ensure that capacitors are energized at 0V in that phase, implying that each phase will have to be switched in separately. This ensures that there is no or little DC offset present in the current waveform [12]. Cables are similar to capacitors during energization, and hence this scheme could also apply. For the steel mill and industrial systems in general, reference [10] describes this process in more detail.

5.9 Conclusion

In this section of the report, some illustrative cases of the wind farm were simulated. Different test case scenarios were performed including among others energization, opening of a feeder and clearing of a fault with the feeder breaker or with a fuse at the turbine tower. An analysis of different possible topologies was also performed to show that the original topology presented is not necessarily the best for the purpose of transient propagation.



The goal of this section was also to perform some of the simulations with an actual generator connected in the tower to simulate as best as possible the real working conditions in the farm. Information from the previous sections was used to model the wind farm accurately, which was verified by comparison to papers already presenting similar topics. The case with generators was however not simulated in previous papers, and an attempt was also made to identify other interesting cases which were also not previously simulated.

Finally, a discussion on wind farm protection was carried out. The focus was to identify and simulate common protection schemes that were available previously for industrial systems and to apply this information to wind farms.



6 CONCLUSIONS

The report was divided into 4 main sections: cables, vacuum breaker, industrial system and wind farm. In the first section, modelling of cables in PSCAD was dealt with. It was found that parameters must be carefully entered into PSCAD for the purpose of simulating high frequency events along a cable system. Justifications were made as to how these geometric parameters are entered into PSCAD and why they produce the best results for a large frequency range.

The following section dealt with the modelling of VCBs, also in PSCAD. A physically realistic model was discovered and explained, after which several justified assumptions were made such as to model a VCB for the purpose of transient studies in large cable systems.

After the components necessary for transient studies were carefully simulated and tested, it was time to put them into operation as part of an industrial system. A steel mill was chosen since it provided a good body of knowledge on topics that will be important in wind farms and also because a myriad of experimental data was available. Accurately simulating this system by comparing to measured results was the key of this section, which was done with the aid of transient theory and general knowledge on industrial systems.

Finally, a wind farm was simulated. Information from the previous sections was used to draw conclusions for this section. Several cases were simulated in the wind farm and many lessons were learned as to how the system responds during these transient conditions. Accurate modelling was also crucial in this case, but since none or very little experimental data was available, not much could be done to verify the results. A lot was also learned on protection schemes for wind farms and how the differences and similarities between industrial systems could be used to protect the wind farm.

All in all, this has been an excellent learning experience on a topic which is for the most part not well developed for wind farms. A large part of the unknown failures of equipment could be resolved if more was known on high frequency transients, and it is the hope of this author that this work provided at least a good starting point.



7 FUTURE WORK

This project could easily be extended into a PhD project to look at the finer aspects in more detail. The VCB developed for this report is far from perfect since for example it cannot simulate current chopping well. A more well-defined VCB model, possibly simulated in EMTDC, and taking into account a lot of the other aspects that were not discussed in this report, could be produced.

The other major component of this report was the cables themselves. The report made several good approximations to accurately simulate the system in question. More work has to be done however as to the validity of these approximations, and possibly also develop much more complex and realistic approximations. The cables used in both systems in the report were accurate enough for their purpose, but fine-tuning a cable model could take months of work. The general idea would be to simulate as accurately as possible the high frequency effects in cable systems.

The steel mill used in this report provided good measurement data, but exactly matching the measured results to the simulated results was very difficult. Stray inductances, capacitances, and resistances in this system were determined to be extremely important in the correct modelling of the system, and hence more work is required to accurately simulate the real working conditions of the system.

As for the wind farm system, it was very hard to determine if the actual simulated results did in fact match any measured results. Mostly this was due to the poor quantity and quality of field measurements in wind farms, which is why industrial systems were used as a stepping stone for understanding the task at hand. Future work in this context would include the acquirement of real data to which simulations could be compared. Special measuring equipment would be required on-site since common measurement devices are only equipped to handle harmonics as defined by IEEE and IEC standards. Possible future work could also involve the inclusion of transient propagation studies into wind farm design, such as for example to determine necessity of protection equipment, or to determine which is the best topology for minimizing the negative effects of transients.

Finally then, the important issue with transient propagation comes down to the physical effect on the equipment. One can identify "dangerous" cases and mitigate the problem, but the question arises as to how necessary is the protection if any. The idea would then be to estimate the actual economic effect of transients on the system with respect to damaged insulation and lost opportunity costs. Ideally, the system designer could be provided with a set of tools to help him/her determine the dollar value of bad transients and to help component designers understand system conditions better.



8 REFERENCES

- [1] G. Mugala, R. Eriksson, U. Gafvert, "High Frequency Characterization of the Semi-Conducting Screens of Medium Voltage XLPE Cables," Annual Conference on Electrical Insulation and Dielectric Phenomena, 2002.
 - [2] S.S. Barnji, M. Kaufhold, A.T. Bulinski, "Electroluminescence Technique to Evaluate the Effect of Impulse Tests on High Voltage Cables," IEEE Transactions on Dielectrics and Electrical Insulation, vol.5, no.2, April 1998.
 - [3] "ABB XLPE Cable Guide rev. 2," from ABB Cables Karlskrona, available from <http://www.abb.com/product/us/9AAC710014.aspx> [last accessed Feb 1, 2007].
 - [4] L. Liljestrand, V. Scuka, "A 200KV Cable Generator with Nanoseconds Rise Time," Internal report no. UU:RIE:191:86, Uppsala Universitet, March 1986, Uppsala, Sweden.
 - [5] J. J. Grainger, W. D. Stevenson, 1994, *Power System Analysis*, McGraw-Hill, Inc.
 - [6] IEEE Std C37.012-2005, *IEEE Application Guide for Capacitance Current Switching for AC High-Voltage Circuit Breakers*, New York, IEEE Press.
 - [7] IEEE Std C37.04-1999, *IEEE Standard Rating Structure for AC High-Voltage Circuit Breakers*, New York, IEEE Press.
 - [8] J. Helmer, M. Lindmayer, "Mathematical Modelling of the High Frequency Behaviour of Vacuum Interrupters and Comparison with Measured Transients in Power Systems," in *Proc. of 17th International Symposium on Discharges and Electrical Insulation in Vacuum ISDEIV 1996*, vol.1, pp.323-331.
 - [9] S.M. Wong, L.A. Snider, E.W.C. Lo, "Overvoltages and Re-ignition Behaviour of Vacuum Circuit Breaker," in *Proc. Of 6th International Conference on Power System Transients IPST 2003*, New Orleans, USA, 28 Sept – 2 Oct 2003.
 - [10] L. Liljestrand, "Industrial Systems," Internal report no. SECRC/TR2004-PT/253, ABB AB Corporate Research, February 2005, Västerås, Sweden.
 - [11] L. Liljestrand, A. Sannino, H. Breder, S. Johansson, "Transients in Collection Grids of Large Offshore Wind Parks," in *Proc. of 3rd Nordic Wind Power Conference NWPC 2006*, Espoo, Finland, 22-23 May 2006.
 - [12] L. van der Sluis, A.L.J. Janssen, "Clearing Faults Near Shunt Capacitor Banks," IEEE Transactions on Power Delivery, vol.5, no.3, July 1990, pp.1346-1354.
 - [13] A. Greenwood, 1994, *Vacuum Switchgear*, Institution of Electrical Engineer, USA.
 - [14] IEC Std IEC62271-200:2003(E), High-Voltage Switchgear and Controlgear, Part 200 "AC Metal-Enclosed Switchgear and Controlgear for Rated Voltages Above 1kV and up to and Including 52kV," International Electrotechnical Commission, Genève, Switzerland.
 - [15] E. Kuffel, W.S. Zaengl, J. Kuffel, 2000, *High Voltage Engineering: Fundamentals 2nd ed.*, Newnes, England.
-



- [16] A.T. Roguski, "Experimental Investigation of the Dielectric Recovery Strength Between the Separating Contacts of Vacuum Circuit Breakers," IEEE Transactions on Power Delivery, vol.4, no.2, April 1989, pp. 1063-1069.
 - [17] A. Sannino, H. Breder, E.K. Nielsen, "Reliability of Collection Grids for Large Offshore Wind Parks," in *Proc. of 9th International Conference on Probabilistic Method Applied to Power Systems PMAPS 2006*, 11-15 June 2006, Stockholm, Sweden.
 - [18] B. Frankén, H. Breder, M. Dahlgren, E.K. Nielsen, "Collection Grid Topologies for Off-Shore Wind Parks," in *Proc. of 18th International Conference & Exhibition on Electricity Distribution CIRED 2005*, Turin, 6-9 June 2005.
 - [19] G. Quinonez-Varela, G.W. Ault, J.R. McDonald, "Steady-State Performance Analysis of Collector System Designs for Large-Scale Offshore Wind Farms," in *Proc. of 6th International Workshop on Large-Scale Integration of Wind Power and Transmission Networks for Offshore Wind Farms 2006*, Delft, The Netherlands, 26-29 Oct 2006.
 - [20] S. Lundberg, "Evaluation of Wind Farm Layouts," in *Proc. of 4th Nordic Workshop on Power & Industrial Electronics NORPIE 2004*, Trondheim, Norway, 14-16 June 2004.
 - [21] A. Greenwood, 1991, *Electrical Transients in Power Systems 2nd ed.*, Braun-Brumfield, Inc.
-